40204

National Library of Canada / Bibliothèque nationale du Canada

CANADIAN THESES ON MICROFICHE / THÈSES CANADIENNES SUR MICROFICHE

NAME OF AUTHOR/*NOM DE L'AUTEUR* Ru-San R. Ko

TITLE OF THESIS/*TITRE DE LA THÈSE* Laminar Free Convection In Periodic and Non-uniform Body Force Field

UNIVERSITY/*UNIVERSITÉ* Univ. of Alberta

DEGREE FOR WHICH THESIS WAS PRESENTED/ *GRADE POUR LEQUEL CETTE THÈSE FUT PRÉSENTÉE* Ph.D.

YEAR THIS DEGREE CONFERRED/*ANNÉE D'OBTENTION DE CE GRADE* 1978

NAME OF SUPERVISOR/*NOM DU DIRECTEUR DE THÈSE* G. S. H. Lock

Permission is hereby granted to the NATIONAL LIBRARY OF CANADA to microfilm this thesis and to lend or sell copies of the film.

The author reserves other publication rights, and neither the thesis nor extensive extracts from it may be printed or otherwise reproduced without the author's written permission.

L'autorisation est, par la présente, accordée à la BIBLIOTHÈQUE NATIONALE DU CANADA de microfilmer cette thèse et de prêter ou de vendre des exemplaires du film.

L'auteur se réserve les autres droits de publication; ni la thèse ni de longs extraits de celle-ci ne doivent être imprimés ou autrement reproduits sans l'autorisation écrite de l'auteur.

DATED/*DATÉ* October 12/78 SIGNED/*SIGNÉ* Ru-San Ko

PERMANENT ADDRESS/*RÉSIDENCE FIXÉ* 9540 Oakland Rd. S.W.
Calgary, Alberta, Canada

NL-91 (3-74)

National Library of Canada

Cataloguing Branch
Canadian Theses Division

Ottawa, Canada
K1A 0N4

Bibliothèque nationale du Canada

Direction du catalogage
Division des thèses canadiennes

NOTICE

The quality of this microfiche is heavily dependent upon the quality of the original thesis submitted for microfilming. Every effort has been made to ensure the highest quality of reproduction possible.

If pages are missing, contact the university which granted the degree.

Some pages may have indistinct print especially if the original pages were typed with a poor typewriter ribbon or if the university sent us a poor photocopy.

Previously copyrighted materials (journal articles, published tests, etc.) are not filmed.

Reproduction in full or in part of this film is governed by the Canadian Copyright Act, R.S.C. 1970, c. C-30. Please read the authorization forms which accompany this thesis.

THIS DISSERTATION
HAS BEEN MICROFILMED
EXACTLY AS RECEIVED

AVIS

La qualité de cette microfiche dépend grandement de la qualité de la thèse soumise au microfilmage. Nous avons tout fait pour assurer une qualité supérieure de reproduction.

S'il manque des pages, veuillez communiquer avec l'université qui a conféré le grade.

La qualité d'impression de certaines pages peut laisser à désirer, surtout si les pages originales ont été dactylographiées à l'aide d'un ruban usé ou si l'université nous a fait parvenir une photocopie de mauvaise qualité.

Les documents qui font déjà l'objet d'un droit d'auteur (articles de revue, examens publiés, etc.) ne sont pas microfilmés.

La reproduction, même partielle, de ce microfilm est soumise à la Loi canadienne sur le droit d'auteur, SRC 1970, c. C-30. Veuillez prendre connaissance des formules d'autorisation qui accompagnent cette thèse.

LA THÈSE A ÉTÉ
MICROFILMÉE TELLE QUE
NOUS L'AVONS REÇUE

THE UNIVERSITY OF ALBERTA

LAMINAR FREE CONVECTION IN PERIODIC AND NON-UNIFORM BODY FORCE FIELD

BY

RU-SAN R. KO

(C)

A THESIS

SUBMITTED TO THE FACULTY OF GRADUATE STUDIES AND RESEARCH

IN PARTIAL FULFILMENT OF THE REQUIREMENTS FOR THE DEGREE

OF DOCTOR OF PHILOSOPHY

DEPARTMENT OF MECHANICAL ENGINEERING

EDMONTON, ALBERTA

FALL, 1978

THE UNIVERSITY OF ALBERTA

FACULTY OF GRADUATE STUDIES AND RESEARCH

The undersigned certify that they have read, and recommend to the Faculty of Graduate Studies and Research, for acceptance, a thesis entitled LAMINAR FREE CONVECTION IN PERIODIC AND NON-UNIFORM BODY FORCE FIELD

submitted by RU-SAN R. KO

in partial fulfillment of the requirements for the degree of Doctor of Philosophy.

Gerald Lock
Supervisor

External Examiner 10/9/78

Date October 9, 1978

ABSTRACT

This study presents a theoretical investigation of the time-dependent, coupled conduction-convection heat transfer problem of a heated radial fin rotating simultaneously with its surroundings at a constant angular velocity about a horizontal axis. Mathematical formulation reveals that this is a periodic problem governed by a set of unsteady-state, nonlinear, partial differential equations which have neither initial conditions nor synchronous solutions.

Through an order-of-magnitude analysis, six parameters appear in the dimensionless governing equations and boundary conditions. The Prandtl number Pr is an indication of the relative importance of viscous dissipation and heat conduction in the fluid flow; the Froude number Fr is the ratio of the centrifugal acceleration to the gravitational acceleration; the geometric parameter γ is the ratio of the fin length to the distance between the fin tip and the center of rotation; the response parameters K_1 and K_2 are the measures of the transient responses in the fluid and solid, respectively; the sixth parameter C is an indication of the degree of coupling between the conduction and free convection heat transfer problems.

A Lefevre-type transformation is utilized to alleviate the effect of Prandtl number on the solutions. The Prandtl number of air, i.e. Pr=0.72, is then used throughout the analysis.

The fluctuating amplitude of the periodic solutions decreases inversely with the Froude number. In the limiting case of very large Froude number, the quasi-steady-state solutions, which are independent of the parameters K_1 and K_2, are obtained.

These quasi-steady-state solutions are presented over the range of $0.1 \leq \gamma \leq 0.5$ and $0.01 \leq C \leq 10$. The results are in good agreement with those of previous work.

Perturbation solutions are used to study the periodic heat transfer phenomena of small fluctuations. The investigation is conducted over the range of $10 \leq Fr \leq 100$, $0.01 \leq C \leq 10$, $0.1 \leq \gamma \leq 0.5$, $0.1 \leq K_1 \leq 100$, and $0.1 \leq K_2 \leq 1000$. In general, periodic fluctuation in the velocity solutions is appreciable when Fr=10, but negligible when Fr=100. On the other hand, no significant fluctuation is present in the temperature solutions.

The periodic solutions under small and moderate fluctuations are obtained by directly integrating the unsteady-state governing equations for this heat transfer problem. Because of the expensive numerical work required in the

approach of direct integration, solutions are only presented over the range of $2 \leq Fr \leq 10^5$ for $\gamma=0.1$, $C=0.01$, $K_1=1$, and $K_2=100$. The fluctuating amplitude of the solutions decreases inversely with the Froude number (Fr); however, the total heat transfer rate increases with the latter.

Analysis also shows that the cooling effect of a rotating fin is approximately $Fr^{1/4}$ times that of a conventional stationary fin. In other words, one can double the efficiency of a stationary cooling fin if it is technically and economically permissible to rotate the system to 16g (i.e. Fr=16).

Study of the solution applicability reveals that if the critical Rayleigh number for a stable laminar free convection flow is 10^8, the solutions presented in this work are applicable to a rotating system with the centrifugal acceleration not greater than 50g. Should the actural critical Rayleigh number obtained from the stability study of this periodic heat transfer problem be greater than 10^8, the presented solutions may have some application to the high speed turbines.

A rational approach has been developed to solve this periodic heat transfer problem governed by the diffusion-type, nonlinear partial differential equations, of which the initial conditions are missing and the synchronous

solutions under the finite-amplitude fluctuations are not obtainable. This approach can be used as a guideline to solve other periodic problems, which occur in the physical world but remain untouched because of the large fluctuations in the non-synchronous solutions or because of the missing initial conditions.

ACKNOWLEDGEMENTS

The author wishes to express the sincere appreciation to the following:

- Professor G.S.H. Lock for his patient supervision and assistance during the course of this thesis.
- Professors J.C. Mollendorf, L.W. Jackson, J.D. Dale, C.M. Rodkiewicz, and D.J. Wilson for their helpful criticism and invaluable suggestions on improving this thesis.
- the National Research Council for financial support under the Student Scholarship.
- my dear wife, Lily, for her understanding during my thesis writing and her patience and effort in typing this thesis.

TABLE OF CONTENTS

CHAPTER		PAGE
I.	INTRODUCTION	1
II.	THEORETICAL FORMULATION	6
	2.1 Boundary Layer Problem	6
	2.2 Conduction Problem	9
	2.3 Separation of Equations	11
	2.4 Normalized Equations	16
III.	NUMERICAL TECHNIQUES	22
	3.1 Quasi-Steady-State Solutions	23
	3.1.1 Boundary Layer Equations	24
	3.1.2 Fin Equation	26
	3.1.3 Matching	30
	3.2 Periodic Solutions	33
	3.2.1 Small Amplitude	34
	3.2.2 Moderate Amplitude	39
IV.	RESULTS AND DISCUSSION	54
	4.1 Quasi-Steady Results	55
	4.1.1 Solutions of Boundary Layer Problem	56
	4.1.2 Solutions of Conduction Problem	61
	4.1.3 Solutions of Overall Problem	67
	4.2 Perturbation Approximation	77

CHAPTER PAGE

4.2.1 Solution of Boundary Layer Problem 80

4.2.2 Solutions of Conduction Problem . 93

4.2.3 Solutions of Overall Problem 96

4.3 "Exact" Solutions 103

4.3.1 Solutions of Boundary Layer Problem 106

4.3.2 Solutions of Conduction Problem . 112

4.3.3 Solutions of Overall Problem 112

4.4 Limites of Applicability 121

V. CONCLUSIONS AND RECOMMENDATIONS 127

5.1 Conclusions 127

5.2 Recommendations for Future Work 139

***

REFERENCES 143

APPENDIX A. DERIVATION OF EQUATIONS 148

APPENDIX B. NORMALIZATION 153

B.1 Steady Equations 154

B.2 Periodic Equations 156

APPENDIX C. LOCAL SIMILARITY TRANSFORMATION 169

APPENDIX D. PERTURBATION EXPANSION 177

APPENDIX E. A SIMPLE TIME DEPENDENT SOLUTION 183

LIST OF TABLES

Table	Description	Page
4.1	Curve Fitting for Total Heat Transfer Rate Versus Parameter γ Plot with Different Slopes	70
4.2	Curve Fitting for Total Heat Transfer Rate Versus Parameter γ Plot with Commen Slope	71
4.3	Curve Fitting for Nusselt Number Versus Parameter γ Plot	75
4.4	Comparison of Least-Squares Fits	76

LIST OF FIGURES

Figure		Page
2.1	System of Radial Rotating Fin	7
2.2	Dimensions of Triangular Fin	10
3.1	Example No. 1	43
3.2	Example No. 2	45
3.3	Example No. 3	47
3.4	Example No. 4	48
3.5	Example No. 5	50
3.6	Example No. 6	52
4.1	Departure of Quasi-Steady Boundary Layer Solutions from Similarity	57
4.2	Effect of γ on Quasi-Steady Boundary Layer Solutions	59
4.3	Effect of C on Quasi-Steady Boundary Layer Solutions	60
4.4	Effect of C and γ on Quasi-Steady Interfacial Temperature	62
4.5	Quasi-Steady Interfacial Temperature Profiles for Checking the Possibility of Power Law Assumption	65
4.6	Quasi-Steady Interfacial Temperature Profiles for Checking the Possibility of Exponential Assumption	66
4.7	Effect of C on Quasi-Steady Heat Transfer Rate	68
4.8	Effect of γ on Quasi-Steady Heat Transfer Rate	69
4.9	Nusselt Number of Quasi-Steady-State Solutions	74

Figure		Page
4.10	Fin Effectiveness of Quasi-Steady Solutions	78
4.11	Even Part of the Perturbation Solutions for the Boundary Layer Problem	81
4.12	Odd Part of the Perturbation Solutions for the Boundary Layer Problem	83
4.13	Effect of γ on the Perturbed Boundary Layer Solutions	85
4.14	Effect of C on the Perturbed Boundary Layer Solutions	86
4.15	Perturbed Boundary Layer Solutions for Fr=10, C=1, K_1=1, K_2=1 and γ=0.1	87
4.16	Perturbed Boundary Layer Solutions for Fr=10, C=1, K_1=50, K_2=1 and γ=0.1	88
4.17	Perturbed Boundary Layer Solutions for Fr=10, C=1, K_1=1, K_2=100 and γ=0.1	89
4.18	Perturbed Boundary Layer Solutions for Fr=100, C=1, K_1=1, K_2=1 and γ=0.1	90
4.19	First-Order Perturbation Temperatures Along Solid Fin	95
4.20	Periodic Variation in Perturbed Heat Transfer Rate	98
4.21	Periodic Variation in Nusselt Number of Perturbation Result	100
4.22	Periodic Variation in Fin Effectiveness of Perturbation Result	102
4.23	Periodic Boundary Layer Solutions Obtained from Perturbation Approximation for Fr=10	107
4.24	Periodic Boundary Layer Solutions Obtained by the Direct Integration Method for Fr=10	108
4.25	Periodic Boundary Layer Solutions Obtained by the Direct Integration Method for Fr=2	110

Figure		Page
4.26	Periodic Fin Temperature ... the Direct Integration Metho...	113
4.27	Periodic Variation in the ... Transfer Rate of Exact Sol...	114
4.28	Periodic Variation in the N... ...ber of Exact Solution	115
4.29	Periodic Variation in Fin E... ...ss of Exact Solution	116
4.30	Limits of Solution Applicab...	125

NOMENCLATURE

A	dimensionless group, $DRa^{1/2}$
A(X)	cross sectional area of fin
B	dimensionless period for the solid, $2\pi\kappa_s/\omega L^2$
Bi	Biot number, hW/K_s
C	dimensionless group, $(LK_f/WK_\xi)Ra^{1/4}$
$\underline{D}$	dimensionless period for the fluid, $2\pi\kappa_f/\omega L^2$
D	span of fin
f	stream function
$\hat{f},\tilde{f}$	odd and even perturbation solutions of the stream function
Fr	Froude number, $R\omega^2/g$
g	gravitational acceleration
Gr	Grashof number
h	convective heat transfer coefficient
k,K	thermal conductivity
K_1	dimensionless group, $\frac{2\pi}{A}(\frac{4}{3}\frac{1+Pr}{Pr}\gamma^{-1})^{1/2}$
K_2	dimensionless group, $2\pi/B\gamma^2$
K_3	dimensionless group, $(\frac{3}{4}\frac{Pr}{1+Pr}\gamma^{-3})^{1/4}C$
L	fin length (radially)
Nu	Nusselt number, hL/K_f
Os	Ostrach number, $\beta R\omega^2 L/c_p$
p,P,$\underline{P}$	pressure
Q	total heat transfer rate
Ek	Ekman Number, $\nu/\omega L^2$

Pr	Prandtl number, ν/κ_f
R	distance between fin tip and axis of rotation
Ra	Rayleigh number, $\beta\omega^2 R\theta_r L^3/\nu\kappa_f$
S	dimensionless group, $\frac{1}{2}(\frac{\gamma}{Pr\beta\theta_r})^{1/2}$
t	time
T	temperature
u,U	radial velocity
v,V	circumferential velocity
W	root half-width
x,X	radial displacement from fin tip
y,Y	lateral displacement from fin surface
α	position angle of fin
β	thermal-expansion coefficient
ψ	stream function
ϕ,Φ	dimensionless temperature
$\hat{\Phi},\tilde{\Phi}$	odd and even perturbation solutions for temperature
ε	fin effectiveness
λ	sign variable
η	similarity variable
κ	thermal diffusivity
ω	angular velocity
μ	viscosity
ν	momentum diffusivity (kinematic viscosity)
ρ	density

γ	length-radius ratio, L/R
θ	temperature, $T-T_\infty$
τ	dimensionless time, $\omega t/2\pi$
ξ	dimensionless radial displacement from fin tip, γx

SUBSCRIPTS

o	fin
c	characteristic value
r,t	fin root, tip
∞	outside boundary layer
f,s	fluid, solid
x,y,X,Y	differentiation with respect to x,y,X,Y
ξ,η,t,τ	differentiation with respect to ξ,η,t,τ

SUPERSCRIPTS

p	periodic or time-dependent
s	quasi-steady

CHAPTER I

INTRODUCTION

Free convection phenomena occur in a non-isothermal fluid under the influence of body force. For example when a vertical metal fin is heated in an originally quiescent fluid, heat is conducted into the surrounding fluid to cause temperature difference, which in turn generates the density variations in the fluid; a boundary layer flow adjacent to the fin is then formed as a result of the density variations and the body force field, and consequently more heat is transferred from the fin to the fluid.

In practical application, stationary fins have been frequently employed to increase the total heat transfer rate between a solid body and its surrounding fluid of different temperature by increasing the area of the contact surface. The free convection phenomena associated with these stationary fins are normally subject to the uniform gravitational force field.

In this thesis, the heat transfer problem of a heated radial fin rotating simultaneously with ambient air about a horizontal axis is studied. The fin is located at a certain distance from the center of rotation so that the centrifugal acceleration at the fin root can always be set

greater than the periodically changing effect of gravitational force by adjusting the rotating speed. Formulation of this problem shows that periodic terms correlated to the gravitational acceleration appear in the derived governing equations and the solutions may have finite fluctuating amplitudes.

During recent years considerable interest has been shown in periodic phenomena associated with fluid flow and convection heat transfer [1-25]*. In most of these studies, the periodicity with respect to time normally originates from a given oscillating boundary condition [1-15]; for example, oscillation of a solid wall or its temperature, fluctuation of the free stream fluid velocity or temperature. Very few works [16-25] have dealt with problems in which the periodicity appears solely in the governing equations. In general, it is very difficult to solve the complete set of governing equations of these periodic problems directly. Because of this, several particular techniques have been developed.

The method of successive approximation consists of splitting the solutions into two ro more time-dependent components, each of which satisfies a different set of equations simplified from the original governing equations after careful, physical reasoning. Usually, these simplified

---

* Numbers designate references given on page 143

equations are much easier to solve; for instance, they may consist of synchronous solutions which can be obtained by means of separation of variables or Laplace transformation. However, this method demands artistically intuitive skill on separating the equations and their solutions. Such technique becomes very complicated and tedious if higher-order approximations are required to produce more accurate results.

The best-known method for solving unsteady problems with small fluctuations is the perturbation expansion in powers of the oscillation amplitude which has first been normalized with respect to the mean amplitude. The zeroth-order equations of the expansion are related to the steady basic flow while the higher-order perturbation equations are associated with the superimposed fluctuations. The accuracy of the solutions obtained can easily be estimated from the order of perturbation been used. In other words, this method is powerful only when the oscillation amplitude is small; otherwise work may increase considerably in order to include higher-order perturbations for more accurate solutions. It is also very likely that the method will fail completely if the normalized oscillation amplitude is not much less than unity.

A powerful technique to handle problems with finite amplitude oscillations has been introduced by C.C. Lin [26]

who divides the governing equations, as well as their solutions, into time-average and time-dependent parts. The complete set of time-average equations describing the mean flow is retained; the time-dependent equations, usually linear and uncoupled from each other, are simplified to such convenient forms that their solutions can be obtained analytically. These approximate, time-dependent results are then substituted into time-average equations to get mean-flow solutions. Hence, the accuracy of the overall solutions depends strongly upon the proper simplification of the time-dependent equations. This simplification generally requires a condition of very high oscillating frequency if the oscillating amplitude is relatively large in comparison with the mean value. This requirement becomes a severe limitation on Lin's method. It appears that no formulation using Lin's method can be successfully applied to periodic problems under low-frequency, finite-amplitude oscillations [11, 12, 15].

In this study, the periodic heat transfer problem are governed by a set of time-dependent, nonlinear partial differential equations, and none of the three methods above is considered to be proper for seeking the solutions under low frequency, moderate-amplitude fluctuations.

Benefiting from the availability of high-speed electronic computers numerical methods provide a good possibility

for solving such a periodic problem. A consequent challenge is the numerical instability of the governing equations heightened by the need for unknown initial solutions at an undetermined time of the period; a poorly chosen initial time level, or an inaccurately guessed initial result can easily lead to solution divergence or numerical overflow. A proper approach is developed in this study to alleviate such difficulties in starting the numerical integration.

At each time level, the governing equations express a distinct, coupled conduction-convection heat transfer problem, and solution matching at the solid-fluid interface is necessary. The transformation developed in a similar work [29] is applied so that the coupled governing equations can be solved numerically with a "local similarity" technique [27-30]. As a result, not only the matching problem of interfacial temperature and heat flux at each time level is resolved spatially in a few iterative loops, but also the periodic conditions of temperature, velocity, and their derivatives with respect to either time or any base vector are successfully satisfied at every time step through a couple of timewise iterations.

CHAPTER II

THEORETICAL FORMULATION

The system under consideration is illustrated schematically in Figure 2.1 which indicates a triangular fin in a surrounding fluid rotating at constant speed about a horizontal axis. Heat is supplied at the root of the fin and conducted into the fluid from the fin surface. As a result, a free convection problem induced by a periodic gravitational force and a spatially varying centrifugal force takes place.

2.1 BOUNDARY LAYER PROBLEM

It is assumed that:

(1) The fluid is Newtonian.

(2) The flow is laminar.

(3) The flow is two dimensional in space.

(4) Fluid properties are constant, with the exception of fluid density to which the Oberback-Boussinesq approximation can be applied.

(5) There is no heat generation in the fluid.

(6) Wall effect and the trailing-edge effect are insignificant.

(7) Radiation is insignificant.

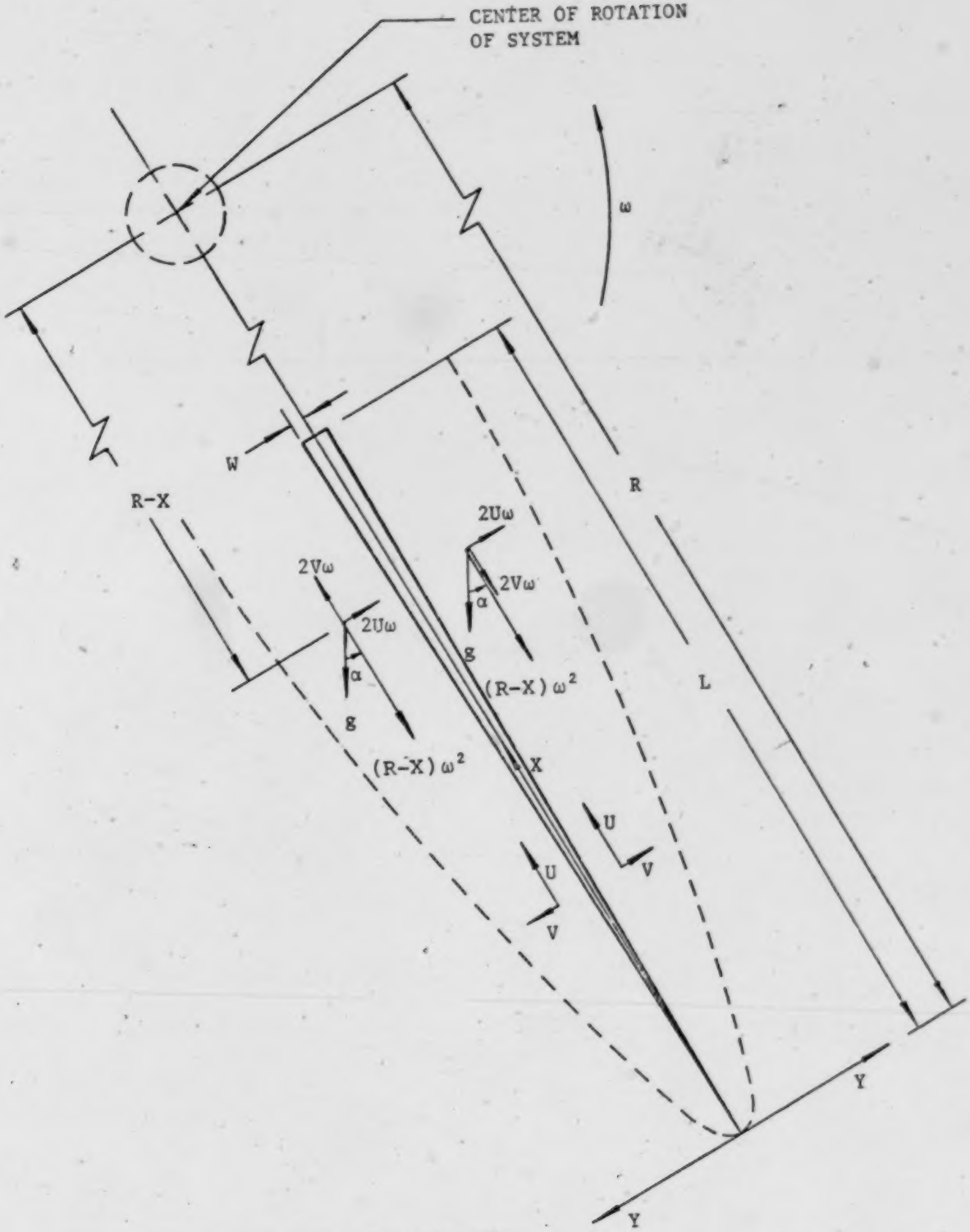

Figure 2.1 System of Radial Rotating Fin

(8) The mechanical work against the body force field is insignificant.

(9) The fin slenderness is large and the effect of inclination and curvature become negligible [44]

(10) The rotation of the system is so fast that the centrifugal acceleration is always greater than the gravitational acceleration.

The governing equations of this periodic free-convection problem have been derived in Appendix A. Referring to equations (A.14)-(A.17) in Appendix A, one can easily obtain the following unsteady boundary layer equations (see also Appendix B):

$$U_X + V_Y = 0, \tag{2.1}$$

$$U_t + UU_X + VU_Y = -\frac{1}{\rho_\infty}\underline{P}_X + \nu U_{YY} - 2\lambda\omega V + \beta[(R-X)\omega^2 + g\cos(\omega t)](T-T_\infty), \tag{2.2}$$

$$V_t + UV_X + VV_Y = -\frac{1}{\rho_\infty}\underline{P}_Y + \nu V_{YY} + 2\lambda\omega U - \beta[Y\omega^2 - \lambda g\sin(\omega t)](T-T_\infty), \tag{2.3}$$

and

$$T_t + UT_X + VT_Y = \kappa_f T_{YY} \tag{2.4}$$

where λ=1 or -1 for the leading and trailing faces, respectively. The imposed boundary conditions are:

$$\begin{aligned} &X = 0: && U = 0 \quad T = T_\infty \\ &Y = 0 (L \geq X \geq 0): && U = V = 0 \quad T = T_0^*(X,t) \\ &Y = \infty: && U = 0 \quad T = T_\infty \quad \underline{P} = 0 \end{aligned} \tag{2.5}$$

where $T_o(X,t)$ is the interfacial temperature distribution of the solid fin and the adjacent fluid.

2.2 CONDUCTION PROBLEM

The basic notation and the coordinates of the conduction heat transfer problem in the fin are illustrated in figure (2.2). It has been shown in previous work [27] that if the Biot number (Bi) is much less than order one, this conduction problem becomes spatially quasi-one-dimensional, i.e. the lateral temperature gradient across the fin is comparatively small. A tacit implication of this small, lateral temperature variation is that the thermal boundary layers on both sides of the fin are symmetric about the X-axis. It is known that this symmetry holds when the whole system is spinning at very high angular velocity [27,28], and the convective heat transfer coefficients $h_1(X,t)$ and $h_2(X,t)$, shown in figure (2.2), are identical and equal to

$$h_1(X,t) = h_2(X,t) = \frac{-K_f T_Y(X,0,t)}{T_o(X,t) - T_\infty} \qquad (2.6)$$

Moreover, if there is no heat generation within the fin and the properties of the fin are constant, the temperature $T_o(X,t)$ of this high-speed rotating fin satisfies the following unsteady, quasi-one-dimensional conduction equation:

$$\frac{X}{\kappa_s}\frac{\partial T_o}{\partial t} + X\frac{\partial^2 T}{\partial X^2} + \frac{\partial T_o}{\partial X} + \frac{L}{W}\frac{K_f}{K_s}\frac{\partial T(X,0,t)}{\partial Y} = 0 \qquad (2.7)$$

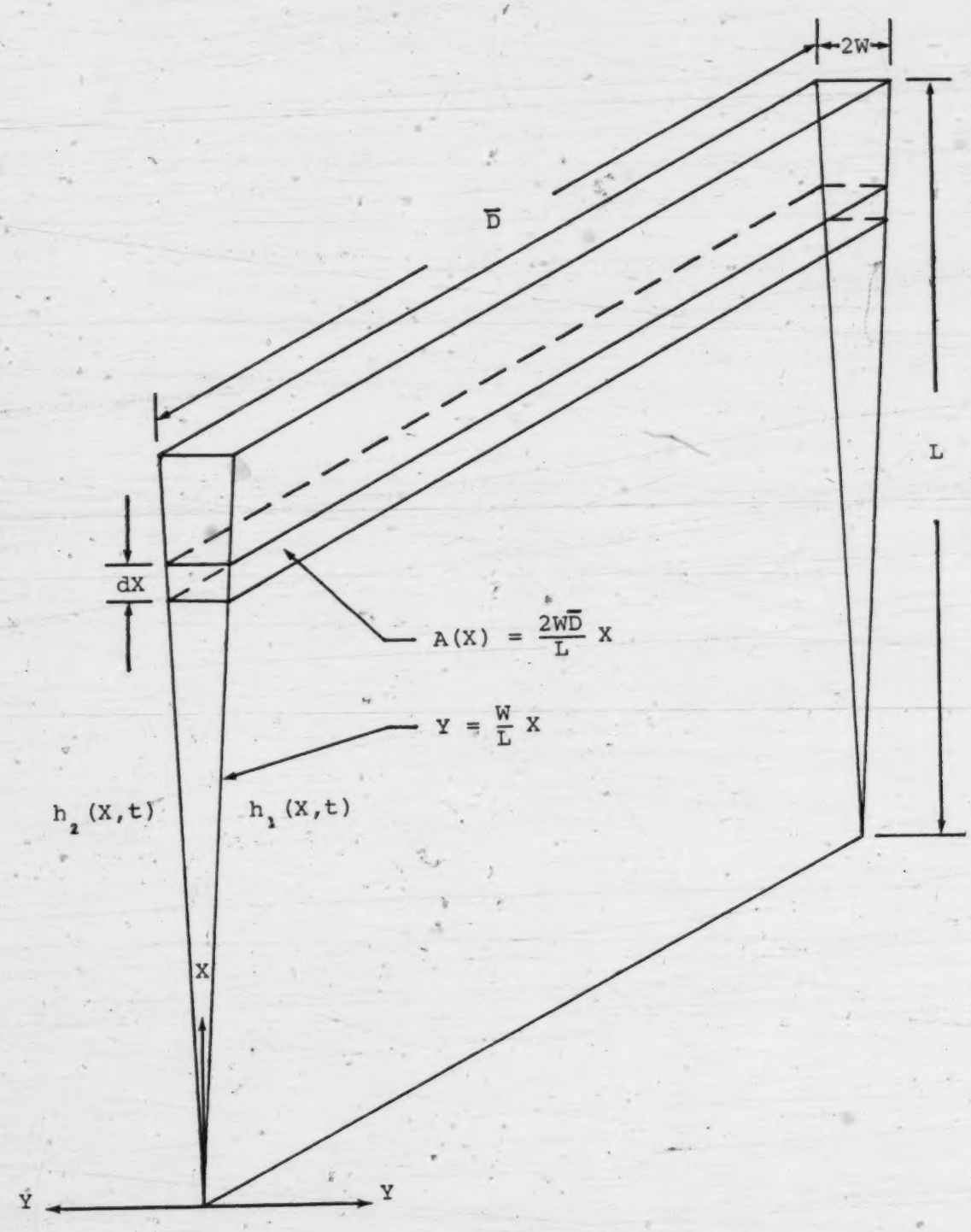

Figure 2.2 Dimensions of Triangular Fin

In this study, the rotation speed of the system is not very high and $h_1(X,t)$ may not equal $h_2(X,t)$ unless thermal boundary-layer on both sides of the fin are symmetric. Further study of the boundary layer equations (2.1)-(2.4) is required before the validity of the quasi-one-dimensional equation (2.7) can be confirmed.

2.3 SEPARATION OF EQUATIONS

A lack of initial conditions is a unique challenge in the present problem. The governing equations (2.1)-(2.4) are a set of strongly coupled, nonlinear partial differential equations with periodic coefficients. The physical conditions imposed on the solutions indicate that this is a two dimensional, boundary value problem varying periodically with time. In principle, a periodic problem like this does not necessitate any initial conditions; this substantial difference from the ordinary transient-type unsteady problem can lead to great difficulty in obtaining a solution. Only in some special cases when the periodic solutions are synchronous, i.e. in the product forms of a time-dependent and a time-independent functions, does such an absence of initial conditions not cause any technical problem. Unfortunately, synchronous solutions are not obtainable in the present problem, and the powerful method of similarity transformations can neither remove the time

dependency from the governing equations as well as their boundary conditions, nor simplify the problem by mapping it onto a two-dimensional domain. It is thus imperative to overcome the difficulty in obtaining proper initial conditions so that a successful method ensuring accurate solutions can be applied.

A perturbation method can provide the first degree approximation to the solutions. When the centrifugal acceleration is very large [27, 28], the problem reaches quasi-steady state and does not need any initial condition, it is logical to start with problems under the influence of relatively large centrifugal force field. The solutions are first expanded into a series of linearly independent, synchronous functions. Second, the quasi-steady-state solutions can be used as the first terms of these series expansions. Although in principle, the accuracy of each approximate solution can be improved by including more synchronous terms in the series, this method is regarded as neither reliable nor economical if the rotating speed is reduced considerably. Direct integration of the governing equations (2.1)-(2.4) by means of a numerical technique is certainly a rational alternative for handling such moderate rotating-speed problem. In order to directly

integrate equations (2.1)-(2.4), all the missing initial conditions have to be guessed at every point on the X-Y plane. These guessed values should be accurate enough so that after reasonable timewise iterations, not only all the dependent variables but also their derivatives have to be matched at each point throughout the two dimensional domain. Otherwise, all the effort may only lead to long computation, solution oscillation and, very possibly, numerical overflow. Apparently, the high rotating speed solutions, if available, may be a suitable approximation to these guessed initial conditions.

Although product-form solutions are not obtainable in this problem, one can easily split the solutions into steady and periodic parts denoted respectively by superscripts s and p. If $\Theta=T-T_\infty$, substitutions of

$$\begin{aligned} \Theta(X,Y,t) &= \Theta^s(X,Y) + \Theta^p(X,Y,t) \\ U(X,Y,t) &= U^s(X,Y) + U^p(X,Y,t) \\ V(X,Y,t) &= V^s)X,Y) + V^p(X,Y,t) \\ \underline{P}(X,Y,t) &= P^s(X,Y) + P^p(X,Y,t) \end{aligned} \qquad (2.8)$$

and

into equations (2.1)-(2.4), and separations of these equations into time-dependent and time-independent parts lead to

$$U^s_X + V^s_Y = U^p_X + V^p_Y \tag{2.9}$$

$$U^s U^s_X + V^s U^s_Y + \frac{1}{\rho_\infty} P^s_X - \nu U^s_{YY} + 2\lambda\omega V^s - \beta\omega^2 (R-X)\theta^s$$

$$= -\Big[U^p_t + U^s U^p_X + U^p U^s_X + V^s U^p_y + V^p U^s_y + U^p U^p_x + V^p U^p_y + \frac{1}{\rho_\infty} P^p_X$$

$$- \nu U^p_{yy} + 2\lambda\omega V^p - [\beta g\cos(\omega t)]\theta^s - \beta\omega^2 (R-X)\theta^p$$

$$- [\beta g\cos(\omega t)]\theta^p\Big] \tag{2.10}$$

$$U^s V^s_X + V^s V^s_y + \frac{1}{\rho_\infty} P^s_y - \nu V^s_{yy} - 2\lambda\omega U^s + \beta\omega^2 Y\theta^s \tag{2.11}$$

$$= -\Big[V^p_t + U^s V^p_X + V^s V^p_y + U^p V^s_X + V^p V^s_Y + U^p V^p_X + V^p V^p_y + \frac{1}{\rho_\infty} P^p_Y$$

$$- \nu V^p_{YY} - 2\lambda\omega U^p - [\lambda\beta g\sin(\omega t)]\theta^s + \beta\omega^2 Y\theta^p - [\lambda\beta g\sin(\omega t)]\theta^p\Big]$$

and

$$U^s\theta^s_X + V^s\theta^s_Y - \kappa_f\theta^s_{YY} = -\Big[\theta^p_t + U^s\theta^p_X + V^s\theta^p_y + U^p\theta^s_X + V^p\theta^s_Y$$

$$+ U^p\theta^p_X + V^p\theta^p_Y - \kappa_f\theta^p_{YY}\Big]. \tag{2.12}$$

The right-hand-sides of these equations are functions of time and, individually, become zero in the steady case. In other words, the steady solutions θ^s, U^s, V^s, and P^s satisfy the equations

$$U^s_X + V^s_y = 0 \tag{2.13}$$

$$U^s U^s_X + V^s U^s_Y = \frac{-1}{\rho_\infty} P^s_X + \nu U^s_{YY} - 2\lambda\omega V^s + \beta\omega^2 (R-X)\theta^s \tag{2.14}$$

$$U^s V^s_X + V^s V^s_Y = \frac{-1}{\rho_\infty} P^s_Y + \nu V^s_{YY} + 2\lambda\omega U^s - \beta\omega^2 Y\theta^s \tag{2.15}$$

$$U^S \Theta^S_X + U^S \Theta^S_Y = \kappa_f \Theta^S_{YY} \tag{2.16}$$

and the boundary conditions

$$\begin{aligned} &X = 0 \; ; \quad U^S = 0 \quad \Theta^S = 0 \\ &Y = 0 \; (L \geq X \geq 0) : \quad U^S = V^S = 0 \quad \Theta^S = \Theta^S_o(X) \\ &Y = \infty \; ; \quad U^S = 0 \quad \Theta^S = 0 \quad P^S = 0 \end{aligned} \tag{2.17}$$

This satisfication is always found because of the way the steady solutions are defined. Consequently, the periodic part of the boundary layer problem is governed by equations

$$U^P_X + V^P_Y = 0 \tag{2.18}$$

$$\begin{aligned} &U^P_t + U^S U^P_X + V^S U^P_Y + U^P U^S_X + V^P U^S_Y + U^P U^P_X + V^P U^P_Y \\ &= \frac{-1}{\rho_\infty} P^P_X + \nu U^P_{YY} - 2\lambda\omega V^P + [\beta g \cos(\omega t)]\Theta^S + \beta\omega^2(R-X)\Theta^P \\ &\quad + [\beta g \cos(\omega t)]\Theta^P, \end{aligned} \tag{2.19}$$

$$\begin{aligned} &V^P_t + U^S V^P_X + V^S V^P_Y + U^P V^S_X + V^P V^S_y + U^P V^P_X + V^P V^P_Y \\ &= \frac{-1}{\rho_\infty} P^P_Y + \nu V^P_{yy} + 2\lambda\omega U^P + [\lambda\beta g \sin(\omega t)]\Theta^S - \beta\omega^2 Y\Theta^P \\ &\quad + [\lambda\beta g \sin(\omega t)]\Theta^P, \end{aligned} \tag{2.20}$$

and

$$\Theta^P_t + U^S \Theta^P_X + V^S \Theta^P_Y + U^P \Theta^S_X + V^P \Theta^S_y + U^P \Theta^P_X + V^P \Theta^P_Y = \kappa_f \Theta^P_{YY}. \tag{2.21}$$

The associated boundary conditions are

$$X = 0 : \quad U^P = 0 \quad \Theta^P = 0$$

$$Y = 0 (L \geq X \geq 0) : \quad U^P = V^P = 0, \quad \Theta^P = \Theta_o^P(X,t) \qquad (2.22)$$

$$Y = \infty : \quad U^P = 0 \quad \Theta^P = 0 \quad P^P = 0$$

Solutions of equations (2.13)-(2.16) and boundary conditions (2.17) have been studied in previous work [27,28] where the conduction problem in the fin is found to be also quasi-one-dimensional. As mentioned in section 2.2, one of the necessary conditions for a quasi-one-dimensional fin equations is the symmetry of the two thermal boundary layers adjacent to this solid fin. In the study, there is a need for further investigation of the separate boundary layer equations (2.13)-(2.16) and (2.18)-(2.21).

2.4 NORMALIZED EQUATIONS

Upon using the normalized variables [27]

$$x = X/L \qquad y = Y\, Ra^{1/4}/L$$

$$u^S = U^S L/\kappa_f\, Ra^{1/2} \qquad v^S = V^S L/\kappa_f\, Ra^{1/4} \qquad (2.23)$$

$$p^S = P^S/\rho_\infty \kappa_f\, \omega Ra^{1/4} \qquad \phi^S = \Theta^S/\Theta_r \ ,$$

it has been shown in Appendix B that for air, the quasi-steady boundary layer equations (2.13)-(2.16) can be simplified through the processes of normalization and ordering. By referring to equations (B.14)-(B.17) in

section B.1, these simplified boundary layer equations in the normalized form are

$$u^s_x + v^s_y = 0, \tag{2.24}$$

$$\frac{1}{Pr}\,(u^s u^s_x + v^s u^s_y) = u^s_{yy} + (1 - \gamma x)\phi^s, \tag{2.25}$$

$$p^s_y = 2\lambda u^s, \tag{2.26}$$

and

$$u^s \phi^s_x + v^s \phi^s_y = \phi^s_{yy}. \tag{2.27}$$

Equation (2.26) indicates that the Coriolis force merely induces the lateral pressure gradient in this quasi-steady part of the problem. Having suppressed the pressure term from equation (2.25), one can find the pressure distribution p^s without any difficulty once the solution u^s is at hand. Hence equation (2.26) can be ignored in this quasi-steady problem unless one is interested in the pressure profile. Hereinafter, the steady problem becomes that of solving the other three partial differential equations with the associated boundary conditions:

$$\begin{array}{lll} x = 0: & u^s = 0 & \phi^s = 0 \\ y = 0 \ (1 \geq x \geq 0): & u^s = v^s = 0 & \phi^s = \phi^s_o(x) \\ y = \infty: & u^s = 0 & \phi^s = 0 \end{array} \tag{2.28}$$

Similarly, the periodic boundary layer equations (2.18)-(2.21) can be simplified after the following normalized variables, obtained in section B.2 , have been introduced:

$$x = X/L \qquad y = YRa^{1/4}/L \qquad \tau = \omega t/2\pi$$

$$u^p = U^p LFr/\kappa_f Ra^{1/2} \qquad v^p = V^p LFr/\kappa_f Ra^{1/4} \qquad \phi^p = (\theta^p/\theta_r)Fr$$

and

$$p^p = P^p Ra^{1/4}\rho_\infty \beta\theta_r gL \qquad \text{if } S \leq O[1],$$

or

$$p^p = 2\pi P^p Fr/\rho_\infty \kappa_f \omega Ra^{1/4} \qquad \text{if } S \geq O[1],$$

where parameter

$$S = \frac{1}{2\pi}\left(\frac{\gamma}{Pr\beta\theta_r}\right)^{1/2}$$

is the magnitude ratio of the Coriolis force term, $2\omega U^p$, to the buoyance force term, $\beta g\theta^s \sin(\omega t)$, in equation (2.20). Physically, this parameter S indicates whether the $2\omega U^p$ or $\beta g\theta^s \sin(\omega t)$ term gives rise to the pressure fluctuation p^p of this periodic problem.

With reference to equations (B.20b), (B.21b), and (B.23b) in Appendix B, the simplified forms of equations (2.18)-(2.20) are

$$u^p_x + v^p_y = 0, \tag{2.29}$$

$$\frac{1}{Pr}\{[\frac{1}{A}]u^p_\tau + u^s u^p_x + u^p u^s_x + v^s u^p_y + v^p u^s_y + [\frac{1}{Fr}](u^p u^p_x + v^p u^p_y)\}$$

$$= u^p_{yy} + \phi^s \cos(2\pi\tau) + (1 - \gamma x)\phi^p = [\frac{1}{Fr}]\phi^p \cos(2\pi\tau), \tag{2.30}$$

and

$$[\frac{1}{A}]\phi^p_\tau + u^s\phi^p_x + v^s\phi^p_y + u^p\phi^s_x + v^p\phi^s_y + [\frac{1}{Fr}](u^p\phi^p_x + v^p\phi^p_y) = \phi^p_{yy}, \quad (2.31)$$

subject to the associated boundary conditions:

$$\begin{aligned} x = 0 &: \quad u^p = 0 \quad \phi^p = 0 \\ y = 0 \ (1 \geq x \geq 0) &: \quad u^p = v^p = 0 \quad \phi^p = \phi^p_o(x,\tau) \\ y = \infty &: \quad u^p = 0 \quad \phi^p = 0 \end{aligned} \quad (2.32)$$

As described in section B.1, the reciprocal of the parameter A, i.e.

$$\frac{1}{A} = \frac{1}{2\pi}(\frac{Pr\ \gamma}{\beta\theta_r})^{1/2},$$

indicates how intensively transient behavior is induced by the periodic effect of the gravitational force.

The lateral equation of motion is, again, "de-coupled" from the other boundary layer equations (2.29)-(2.31), and the pressure fluctuation can be calculated either from

$$p^p_y = 2\lambda u^p + [\frac{1}{S}]\lambda\phi^s \sin(2\pi\tau) \quad (2.33)$$

if $S \geq O[1]$, or from

$$p^p_y = [S]2\lambda u^p + \lambda\phi^s \sin(2\pi\tau) \quad (2.33a)$$

if $S \leq O[1]$. In other words, this periodic portion of the problem is governed by equations (2.29)-(2.31) and the boundary condition (2.32) if one is not interested in the pressure distribution at all.

Equations (2.29)-(2.31) show that the periodic thermal boundary layers on either side of the fin are

symmetric to each other. This is consistent with the possibility that the periodic conduction in the solid fin may be quasi-one-dimensional in space.

Reunion of the split, steady and periodic solutions generates the normalized solutions of the overall problem:

$$\begin{aligned} u(x,y,\tau) &= u^s(x,y) + [\tfrac{1}{Fr}]\, u^p(x,y,\tau) \\ v(x,y,\tau) &= v^s(x,y) + [\tfrac{1}{Fr}]\, v^p(x,y,\tau) \\ \phi(x,y,\tau) &= \phi^s(x,y) + [\tfrac{1}{Fr}]\, \phi^p(x,y,\tau) \end{aligned} \tag{2.34}$$

These solutions satisfy the combined governing equations of the boundary layer problem:

$$u_x + v_y = 0, \tag{2.35}$$

$$\tfrac{1}{Pr}\{[\tfrac{1}{A}]u_\tau + uu_x + vu_y\} = u_{yy} + (1-\gamma x)\phi + [\tfrac{1}{Fr}]\phi\cos(2\pi\tau), \tag{2.36}$$

$$[\tfrac{1}{A}]\phi_\tau + u\phi_x + v\phi_y = \phi_{yy}\ , \tag{2.37}$$

and the boundary conditions:

$$\begin{array}{lll} x = 0: & u = 0 & \phi = 0 \\ y = 0\ (0 \le x \le 1): & u = v = 0 & \phi = \phi_o(x,\tau) \\ y = \infty: & u = 0 & \phi = 0 \end{array} \tag{2.38}$$

Again, equations (2.35)-(2.37) indicate the symmetry of the two thermal boundary layers; hence the quasi-one-dimensional, unsteady fin equation (2.7) may be employed providing, of course, the Biot number (Bi) of the problem

is small. By using the dimensionless variables

$$x = X/L \qquad y = Y\, Ra^{1/4}/L$$

and

$$\phi = (T-T_\infty)/(T_r-T_\infty),$$

equation (2.7) can be written as

$$[\frac{1}{B}]x\frac{\partial \phi_o}{\partial \tau} + x\frac{\partial^2 \phi_o}{\partial x^2} + \frac{\partial \phi_o}{\partial x} + [C]\phi_y(x,0) = 0 \qquad (2.39)$$

where

$$B = 2\pi\kappa_s/\omega L^2$$

and

$$C = \frac{L}{W}\frac{K_f}{K_s} Ra^{1/4}.$$

CHAPTER III

NUMERICAL TECHNIQUES

In equations (2.36) and (2.37), if the transient term are expressed by

$$u_\tau = [\frac{1}{Fr}]\ u_\tau^p \quad \text{and} \quad \phi_\tau = [\frac{1}{Fr}]\ \phi_\tau^p \tag{3.1}$$

where u_τ^p and θ_τ^p are normalized quantities, the boundary layer equations (2.35)-(2.37) can be written into

$$u_x + v_y = 0, \tag{3.2}$$

$$\frac{1}{Pr}\{[\frac{1}{AFr}]\ u_\tau^p + uu_x + vu_y\} = u_{yy} + (1-\gamma x)\phi + [\frac{1}{Fr}]\ \phi\cos(2\pi\tau), \tag{3.3}$$

and

$$[\frac{1}{AFr}]\ \phi_\tau^p + u\phi_x + v\phi_y = \phi_{yy}\ , \tag{3.4}$$

The first approach is to solve these equations for large Fr values. It can be seen from the above equations that the fluctuation is introduced into the problem through the gravitational force term, $\phi\cos(2\pi\tau)$, the magnitude of which is controlled by the parameter 1/Fr. When the angular velocity ω of the system is extremely high,

$$Fr = \frac{R\omega^2}{g} \to \infty$$

implies that the problem becomes quasi-steady [27,28].

In general, the Fr value is finite and the problem becomes periodic and much more difficult to solve. Hence, it is natural to seek solutions for very large values of Fr in the first place and then progress to cases when Fr is of order one.

3.1 QUASI-STEADY-STATE SOLUTIONS

It is imperative to develop an efficient method of obtaining the high speed solutions. As described in reference [27], this is a steady, two-dimensional, free convection problem coupled with another quasi-one-dimensional conduction problem through their interfacial boundary conditions; the numerical solutions are obtainable through the iterative matchings of both temperature and heat flux at the solid-fluid interface. Although use of the local similarity transformation and the numerical technique employed in previous work [27,28] has assured this solution matching, an improved scheme to provide faster numerical integration as well as solution convergence is still necessary because in solving the low rotating speed problems, numerical computation may increase enormously in seeking the periodic solution through timewise iterations. The development of a faster scheme in obtaining solution at each time step can drastically reduce the computation time. To this end, a slightly different method is described below.

3.1.1 BOUNDARY LAYER EQUATIONS

It is convenient to transform the governing equations (2.24), (2.25), and (2.27) into another set of partial differential equations by putting [29]

$$\xi = \gamma x \qquad \eta = \left(\frac{Pr}{1+Pr}\right)^{1/4}\left(\frac{4x}{3}\right)^{-1/4} y$$

$$\psi^s(x,y) = \left(\frac{Pr}{1+Pr}\right)^{1/4}\left(\frac{4\xi}{3\gamma}\right)^{3/4} f^s(\xi,\eta) \tag{3.5}$$

and $$\phi^s(x,y) = \Phi^s(\xi,\eta)$$

where $\psi^s(x,y)$ is a stream function, defined by

$$u^s = \psi^s_y \qquad \text{and} \qquad v^s = -\psi^s_x \tag{3.6}$$

such that equation (2.24) is automatically satisfied. The newly transformed equations are

$$Pr\, f^s_{\eta\eta\eta} + f^s f^s_{\eta\eta} - \frac{2}{3}(f^s_\eta)^2 + (1+Pr)\Phi^s$$

$$= \xi\left[\frac{4}{3}(f^s_\eta f^s_{\eta\xi} - f^s_{\eta\eta} f^s_\xi) + (1+Pr)\Phi^s\right] \tag{3.7}$$

$$\Phi^s_{\eta\eta} + f^s \Phi^s_\eta = \frac{4}{3}\xi(f^s_\eta \Phi^s_\xi - \Phi^s_\eta f^s_\xi) \tag{3.8}$$

subject to the associated boundary conditions.

$$\eta = 0 \ (0 \le \xi \le \gamma): \qquad f^s_\eta = f^s = 0, \qquad \Phi^s = \Phi^s_o(\xi)$$

$$\eta = \infty: \qquad f^s_\eta = 0, \qquad \Phi^s = 0. \tag{3.9}$$

It is worthwhile mentioning that transformation (3.5) is a combination of the Lefevre type [31] and the Blasius-Howarth type [32-34] transformations. The Blasius-Howarth transformation stretches the coordinates [45] in such

a way that the ξ-directional dependency of the problem is greatly reduced, and hence all the ξ-derivatives of the solutions can be replaced more accurately by finite difference approximations. The transformation of Lefevre serves the purpose of reducing the effect of the Prandtl number on the obtained results [35] and thus removing the need to determine separate solutions for a large range of fluids.

The integrating scheme of this problem is very similar to that of the previous work [27-29]. First, the whole region is discretized along the ξ-direction into parallel ξ-levels. Second, the discrete values of the unknown interfacial temperature $\phi_o^s(\xi)$ are guessed at each ξ-level. Physically, this set of guessed values must increase monotonically from the tip of the fin. Third, by use of a fourth-order Runge-Kutta method equations (3.7) and (3.8) are integrated in η-direction at the first ξ-level, where the right hand sides of these equations have been suppressed because of $\xi=0$. Fourth, the integration at each subsequent ξ-level is carried out laterally across the boundary after the ξ-directional derivatives in equations (3.7) and (3.8) have been replaced by finite difference approximations. Finally, the discrete values of interfacial heat flux, corresponding to the guessed interfacial temperature $\phi_o(\xi)$, are obtained.

An initial-value technique was used in combination with the Runge-Kutta method to integrate equations (3.7) and (3.8) in η-direction. Experience showed that numerical integration of these boundary layer equations was very sensitive to the missing initial values of $f^s_{\eta\eta}$ and ϕ^s_η at $\eta=0$; an inaccurate initial guess could easily lead to solution overflow. This numerical instability was overcome by the continuation method [36] with a least-squares convergence criterion on satisfying the asymptotic boundary conditions at the edge of the boundary layer [37].

Numerical experiment was conducted to determine the step size $\Delta\eta$ for the above integration. By varying $\Delta\eta$ from 0.5 to 0.005, integrated solutions were obtained and compared; it is found that as $\Delta\eta$ reduced to 0.005, both $f^s_{\eta\eta}(\xi,0)$ and $\phi^s_\eta(\xi,0)$ converged asymptotically to two corresponding values. A step size of $\Delta\eta=0.04$ was then used in the integration so that the accuracies of $f^s_{\eta\eta}(\xi,0)$ and $\phi^s_\eta(\xi,0)$ were within one percent of their asymptotic values.

3.1.2 FIN EQUATION

Equations (2.24)-(2.27) shows that the steady thermal boundary layers on both sides of the fin are symmetric with each other; hence, the conduction problem becomes quasi-one-dimensional when the Biot number (Bi) is much less than one.

Introducing the normalized variables of the boundary layer problem:

$$x = X/L, \qquad y = YRa^{1/4}/L, \qquad \tau = \omega t/2\pi$$

and $$\phi = \theta/\theta_r = (T-T_\infty)/(T_r-T_\infty),$$

into equation (2.7) and separating the resulting dimensionless equation after the substitution of

$$\phi(x,y,\tau) = \phi^s(x,y) + [\frac{1}{Fr}]\phi^p(x,y,\tau),$$

and

$$\phi_o(x,\tau) = \phi_o^s(x) + [\frac{1}{Fr}]\phi_o^p(x,\tau),$$

one obtains the quasi-steady fin equation:

$$x\frac{d^2\phi_o^s}{dx^2} + \frac{d\phi_o^s}{dx} + [C]\phi_y^s(x,0) = 0 \qquad (3.10)$$

and the periodic fin equation:

$$[\frac{1}{B}]x\frac{\partial\phi_o^p}{\partial\tau} + x\frac{\partial^2\phi_o^p}{\partial x^2} + \frac{\partial\phi_o^p}{\partial x} + [C]\phi_y^p(x,0,\tau) = 0, \qquad (3.11)$$

The parameter C, already defined in previous work [27] as

$$C = \frac{L}{W}\frac{K_f}{K_s}Ra^{1/4},$$

is a determining factor of the coupling between conduction and convection systems; the new parameter B defined by

$$B = 2\pi\kappa_s/\omega L^2$$

indicates the insensitivity of the fin temperature in response to the heat flux fluctuation imposed on the fin surface.

By virtue of the transformation (3.5), equation (3.10) can be written as

$$\xi \frac{d^2\phi_o^s}{d\xi^2} + \frac{d\phi_o^s}{d\xi} + K_3 \xi^{-1/4} \phi_\eta^s(\xi,0) = 0 \qquad (3.12)$$

or

$$\frac{d}{d\xi}\left(\xi \frac{d\phi_o^s}{d\xi}\right) + K_3 \xi^{-1/4} \phi_\eta^s(\xi,0) = 0 \qquad (3.13)$$

subject to the boundary conditions

$$\xi = \gamma: \qquad \phi_o^s = 1$$

$$\xi = 0: \qquad \xi \frac{d\phi_o^s}{d\xi} = 0. \qquad (3.14)$$

Since the fin equation, either in the form of (3.12) or (3.13), is singular at $\xi=0$, difficulty occurs during its numerical integration. To accommodate this, one may use the following approach.

If the functions $F(\xi)$ and $H(\xi)$ are defined, respectively, as

$$F(\xi) = \frac{d}{d\xi}\left(\xi \frac{d\phi_o^s}{d\xi}\right) \quad \text{and} \quad H(\xi) = \xi \frac{d\phi_o^s}{d\xi},$$

equation (3.13) can be integrated from $\xi=\gamma$ to $\xi=\Delta\xi$ with a fourth-order Runge-Kutta method after the missing boundary condition $H(\gamma)$ is guessed. Once the discrete values of $F(\xi)$ and $H(\xi)$ at each ξ level other than $\xi=0$ are at hand, one can calculate $H(0)$ with the aid of the extropolation formula

[46]:

$$H(0) = H(\Delta\xi) - \frac{\Delta\xi}{24}\left[55F(\Delta\xi) - 59F(2\Delta\xi) + 37F(3\Delta\xi) - 9F(4\Delta\xi)\right] + O[\Delta\xi^5],$$

and then modify $H(\gamma)$ so that the boundary condition $H(0)=0$ is satisfied. The evaluation of $F(\xi)$ in the above formula is simple since equation (3.13) indicates that $F(\xi)$ is a function of neither $H(\xi)$ nor $\Phi_o^s(\xi)$. Consequently, the integral of this $F(\xi)$, i.e. $H(\xi)$, is also nothing more than a function of ξ and the known function $\Phi_\eta^s(\xi,0)$. The value of $H(0)$ calculated from formula above is directly related to the initial guess $H(\gamma)$; the exact value of $H(\gamma)$, which leads to the satisfication of $H(0)=0$, can then be found from $H(\gamma)-H(0)$. With $\Delta\xi<\xi<\gamma$, $\dfrac{d\Phi_o^s}{d\xi} = \dfrac{H(\xi)}{\xi}$

are obviously obtainable; further integration gives a new set of discrete temperatures Φ_o^s, among which the value of $\Phi_o^s(0)$ is again obtained through extropolation. That is,

$$\Phi_o^s(0) = \Phi_o^s(\Delta\xi) - \frac{\Delta\xi}{24}\left[55\frac{d\Phi_o^s(\Delta\xi)}{d\xi} - 59\frac{d\Phi_o^s(2\Delta\xi)}{d\xi} + 37\frac{d\Phi_o^s(3\Delta\xi)}{d\xi} - 9\frac{d\Phi_o^s(4\Delta\xi)}{d\xi}\right]$$

$$= \Phi_o^s(\Delta\xi) - \frac{1}{24}\left[55H(\Delta\xi) - \frac{59}{2}H(2\Delta\xi) + \frac{37}{3}H(3\Delta\xi) - \frac{9}{4}H(4\Delta\xi)\right].$$

3.1.3 MATCHING

The whole problem of this steady heat transfer model has been shown to consist of two sub-problems coupled together through their interfacial temperature and interfacial heat flux. The two-dimensional free-convection problem is governed by two boundary layer equations (3.7) and (3.8); the quasi-one-dimensional conduction problem is described by the fin equation (3.12) or (3.13). The matching of the interfacial heat flux has been considered in the formulation of equations (3.12) and (3.13); hence, the only interfacial matching left to be done is on the temperature. In other words, the assumed wall temperature $\phi_o^s(\xi)$ of the boundary layer problem must satisfy the conduction equation of the fin and its associated boundary conditions.

An iteration method is applied to obtain the interfacial temperature profile $\phi^s(\xi,0)$. At first, $\phi^s(\xi,0)$ is guessed and treated as a known boundary condition of the boundary layer equations; the integration of these equations can, in turn, provide the unknown interfacial heat flux $\phi_\eta^s(\xi,0)$ corresponding to the guessed $\phi^s(\xi,0)$. In distinction to previous work [27,28], only the obtained $\phi_\eta^s(\xi,0)$ is fed into the fin equation to generate a new interfacial temperature distribution $\phi_o^s(\xi)$. The guessed

$\Phi^s(\xi,0)$ is then compared with this $\Phi^s_o(\xi)$ and modification of the former is required whenever a difference greater than 10^{-5} is detected. With the newly modified $\Phi^s(\xi,0)$, the procedure is repeated in the hope that a new $\Phi^s_o(\xi)$ can match this $\Phi^s(\xi,0)$ to a better degree. Hence, this interfacial matching problem technically becomes a matter of finding an efficient way to improve the initial guess $\Phi^s(\xi,0)$.

Practical experience indicates that if the parameter C of equation (3.11) is less than one, the average value of the previous $\Phi^s(\xi,0)$ and the calculated $\Phi^s_o(\xi)$ is a good initial guess of $\Phi^s(\xi,0)$ for the next iteration loop; generally, the interfacial matching is achievable in a few iterations. This is not true, however, when the parameter C is greater than one. On the contrary, this modification method by averaging may sometimes lead to the oscillation or even divergence of the interfacial temperature. To accommodate this, this averaging method can only be used in the first iteration loop and after that, a linear or nonlinear optimisation technique [38] should be employed in getting the improved initial guess $\Phi^s(\xi,0)$. It has been found that in this way the convergent criterion of the interfacial temperature profile can be satisfied to an accuracy of 10^{-5} within 3-10 iteration loops.

The result of previous work [27,28] can provide good initial guess for $\phi^s(\xi,0)$. Although the local similarity transformations of the present and previous studies are different, a closer inspection of these transformations discloses that the interfacial temperature profile is a function of the same ξ variable in both cases and, hence, does not vary with the transformation. For this reason, it is a great advantage to use the existing interfacial temperature of previous work as the initial guess in the present study so that the converged solution can be obtained almost immediately. Another advantage which stems from previous observations is that in the non-dimensionalized domain (x,y), the converged interfacial temperature profiles are insensitive to the variation of parameter γ. In other words, once the interfacial temperature corresponding to a small γ value is obtained, it can be used as a good initial guess for problems of the same parameter C but larger γ values. Both advantages are very favourable as far as the computing time is concerned.

Several numerical experiments had been carried out before the present computer program was thoroughly applied to this study. A linear interfacial temperature was chosen as the initially guessed input profile to a testing case of γ=0.3, C=1.0, and Pr=0.72. Excellent agreement between the obtained solution and the previous result [27,28] was

obtained. Stepsizes of 0.05 and 0.025 were chosen for the ξ variable when γ=0.5 which was the greatest γ values used in this study. Comparison of the results showed that not only the individual values of two solutions but also their total heat transfer rates did not differ by more than 0.5% from each other. To save computer time and storage, eleven ξ-steps corresponding to $\Delta\xi$=0.05 were used for γ=0.5. For convenience, same number of ξ-levels was used throughout the study even for the cases of smaller γ values.

3.2 PERIODIC SOLUTIONS

Two methods can be used to solve this periodic problem pending on the fluctuating magnitude of the solutions. The boundary layer equation (2.36) indicates that the periodic source of this problem comes from the gravitational force term, $\phi\cos(2\pi\tau)$, which increases its effect with the parameter 1/Fr. If this parameter is much less than unity, a perturbation-type series expansion is a proper method of simplifying the governing equations before the use of the numerical integration technique. If this parameter 1/Fr is not much less than unity, the perturbation method becomes tedious and uneconomical because of the necessary inclusion of more series terms; a direct approach of solving the unsteady problem is then inevitable. In other words, the periodic solutions are divided into two categories: those of small amplitudes and those of moderate amplitudes.

3.2.1 SMALL AMPLITUDE

Referring to transformation (3.5), one can introduce a local similarity transformation [29]

$$\xi = \gamma x, \qquad \eta = \left(\frac{Pr}{1+Pr}\right)^{1/4}\left(\frac{4x}{3}\right)^{-1/4} y$$

$$\psi(x,y) = \left(\frac{Pr}{1+Pr}\right)^{1/4}\left(\frac{4\xi}{3\gamma}\right)^{3/4} f(\xi,\eta) \tag{3.15}$$

$$\phi(x,y) = \Phi(\xi,\eta),$$

where $\psi(x,y)$ is the stream function defined by

$$u = \psi_y \qquad \text{and} \qquad v = -\psi_x, \tag{3.16}$$

into the boundary layer equations (2.35)-(2.37). The continuity equation (2.35) is then satisfied completely by definition (3.16); the other two boundary layer equations (2.36) and (2.37) are respectively converted into

$$Pr f_{\eta\eta\eta} + f f_{\eta\eta} - \frac{2}{3} f_\eta^2 + (1+Pr)[1+\cos(2\pi\tau)/Fr]\Phi \tag{3.17}$$
$$= \xi\left[\frac{4}{3}(f_\eta f_{\eta\xi} - f_{\eta\eta} f_\xi) + (1+Pr)\Phi\right] + (K_1/2\pi)\xi^{1/2} f_{\eta\tau}$$

and

$$\Phi_{\eta\eta} + f\Phi_\eta = \frac{4}{3}\xi(f_\eta \Phi_\xi - \Phi_\eta f_\xi) + (K_1/2\pi)\xi^{1/2}\Phi_\tau \tag{3.18}$$

where $K_1 = \frac{2\pi}{A}\left(\frac{4}{3}\frac{1+Pr}{Pr}\gamma^{-1}\right)^{1/2}$.

Similarly, the conduction equation (2.39) of the fin can be transformed into

$$(K_2/2\pi)\xi\frac{\partial \Phi_o}{\partial \tau} + \xi\frac{\partial^2 \Phi_o}{\partial \xi^2} + \frac{\partial \Phi_o}{\partial \xi} + K_3\xi^{-1/4}\Phi_\eta(\xi,0,\tau) = 0 \tag{3.19}$$

where $K_2 = 2\pi/B\gamma^2$ and $K_3 = \left(\frac{3}{4}\frac{Pr}{1+Pr}\gamma^{-3}\right)^{1/4} C$.

Response parameters K_1 and K_2 represent, respectively, the significance of the transient responses in the fluid and solid to the periodic effect imposed on the system, while parameter K_3 indicates the degree of coupling between conduction and free convection. Transformation of the boundary conditions (2.38) leads to

$$\begin{aligned} &\eta = 0\,(0 \le \xi \le \gamma): && f_\eta = f = 0, && \Phi(\xi,0,\tau) = \Phi_o(\xi,\tau) \\ &\eta = \infty: && f_\eta = 0, && \Phi = 0. \end{aligned} \tag{3.20}$$

The associated boundary conditions of equation (3.19) are

$$\begin{aligned} &\xi = 0: && \xi\frac{\partial \Phi_o}{\partial \xi} = 0 \\ &\xi = \gamma: && \Phi_o = 1 \end{aligned} \tag{3.21}$$

If 1/Fr is small the solutions may be written in the perturbation series of the form (Appendix D):

$$\begin{aligned} f(\xi,\eta,\tau) &= f^s(\xi,\eta) + \frac{1}{Fr}[\tilde{f}(\xi,\eta)\cos(2\pi\tau) \\ &\quad + \hat{f}(\xi,\eta)\sin(2\pi\tau)] + O\left[\frac{1}{Fr^2}\right] \\ \Phi(\xi,\eta,\tau) &= \Phi^s(\xi,\eta) + \frac{1}{Fr}[\tilde{\Phi}(\xi,\eta)\cos(2\pi\tau) \\ &\quad + \hat{\Phi}(\xi,\eta)\sin(2\pi\tau)] + O\left[\frac{1}{Fr^2}\right] \end{aligned} \tag{3.22}$$

where $f^s(\xi,\eta)$ and $\Phi^s(\xi,\eta)$ are the quasi-steady solutions obtained in section 3.1.

The first order perturbation solutions $\tilde{f}$, $\hat{f}$, $\tilde{\Phi}$, and $\hat{\Phi}$ etc. satisfy the simultaneous equations:

$$Pr\tilde{f}_{\eta\eta\eta} + (1+Pr)(\tilde{\Phi}+\Phi^s) - \frac{4}{3} f^s_\eta \tilde{f}_\eta + f^s_{\eta\eta}\tilde{f} + f^s\tilde{f}_{\eta\eta}$$
$$= K_1\xi^{1/2}\hat{f} + \frac{4}{3}\xi(f^s_{\eta\xi}\tilde{f}_\eta - f^s_\xi\tilde{f}_{\eta\eta} - f^s_{\eta\eta}\tilde{f}_\xi + f^s_\eta\tilde{f}_{\eta\xi}) + (1+Pr)\xi\tilde{\Phi}, \tag{3.23}$$

$$\tilde{\Phi}_{\eta\eta} + f^s\tilde{\Phi}_\eta + \Phi^s\tilde{f}_\eta = K_1\xi^{1/2}\hat{\Phi} + \frac{4}{3}\xi(\Phi^s_\xi\tilde{f}_\eta + f^s_\eta\tilde{\Phi}_\xi - \Phi^s_\eta\tilde{f}_\xi - f^s_\xi\tilde{\Phi}_\eta), \tag{3.24}$$

$$Pr\hat{f}_{\eta\eta\eta} + (1+Pr)\hat{\Phi} - \frac{4}{3} f^s_\eta\hat{f}_\eta + f^s_{\eta\eta}\hat{f} + f^s\hat{f}_{\eta\eta}$$
$$= -K_1\xi^{1/2}\tilde{f}_\eta + \frac{4}{3}\xi(f^s_{\eta\xi}\hat{f} + f^s_\eta\hat{f}_{\eta\xi} - f^s_{\eta\eta}\hat{f}_\xi - f^s_\xi\hat{f}_{\eta\eta})$$
$$+ (1+Pr)\xi\hat{\Phi}, \tag{3.25}$$

$$\hat{\Phi}_{\eta\eta} + \Phi^s\hat{f}_\eta + f^s\hat{\Phi}_\eta = -K_1\xi^{1/2}\tilde{\Phi} + \frac{4}{3}\xi(\Phi^s_\xi\hat{f}_\eta + f^s_\eta\hat{\Phi}_\xi - \Phi^s_\eta\hat{f}_\xi - f^s_\xi\hat{\Phi}_\eta) \tag{3.26}$$

$$K_2\xi\hat{\Phi}_o + \xi\frac{d^2\tilde{\Phi}_o}{d\xi^2} + \frac{d\tilde{\Phi}_o}{d\xi} + K_3\xi^{-1/4}\tilde{\Phi}_\eta(\xi,0) = 0, \tag{3.27}$$

$$-K_2\xi\tilde{\Phi}_o + \xi\frac{d^2\hat{\Phi}_o}{d\xi^2} + \frac{d\hat{\Phi}_o}{d\xi} + K_3\xi^{-1/4}\hat{\Phi}\eta(\xi,0) = 0 \tag{3.28}$$

and the associated boundary conditions:

$\eta = 0$: $\tilde{f} = \hat{f} = \tilde{f}_\eta = \hat{f}_\eta = 0$

$\tilde{\Phi} = \tilde{\Phi}_o(\xi)$, $\hat{\Phi} = \hat{\Phi}_o(\xi)$

$\eta = \infty$: $\tilde{f}_\eta = \hat{f}_\eta = \tilde{\Phi} = \hat{\Phi} = 0$

$\xi = 0$: $\xi\frac{d\tilde{\Phi}_o}{d\xi} = \xi\frac{d\hat{\Phi}_o}{d\xi} = 0$

$\xi = \gamma$: $\tilde{\Phi} = \hat{\Phi} = 0$.

Higher order corrections can be obtained in a similar manner (Appendix D) but are not considered here.

Periodic solutions of large amplitudes ($1/Fr \geq 1$) excluded from this study due to the fact that a different physical problem can be expected if the periodic, gravitational force term $\phi\cos(2\pi\tau)/Fr$ prevails over the centrifugal force term $(1-\gamma x)\phi$ in equation (2.36). This may be explained by considering a typical case of Fr=1. At the moment the rotating fin is in its vertically downward ($\tau=0$) position, aforesaid two forces act in the same direction and promote a boundary layer flow with its leading edge located at the fin tip; however when the fin rotates to its vertically upward position ($\tau=1/2$), these two body forces act against each other and the prevailing gravitational force tends to develop a backward flow with a new leading edge located at the fin root. This alternating leading edge problem is discussed further as a topic for future research in section 5.2.

New difficulty in solving equations (3.23)-(3.28) is encountered after the domain (ξ,η) is discretized into eleven ξ-levels. Comparison between the quasi-steady and perturbation problems indicates that not only the number of governing equations but also the number of unknown interfacial boundary conditions is doubled in the latter.

That is, the integration of boundary layer equations (3.23)-(3.26) at each ξ-level requires the surmise of four eigenvalues: $\tilde{f}_{\eta\eta}(\xi,0)$, $\hat{f}_{\eta\eta}(\xi,0)$, $\tilde{\Phi}_{\eta}(\xi,0)$, and $\hat{\Phi}_{\eta}(\xi,0)$. Most of all, the doubling of the interfacial matching requirements between two conduction and four convection equations is the main source of new difficulty.

Owing to the linearity of the perturbation equations (3.23)-(3.26), the search for the four eigenvalues at each ξ-level was accomplished within one iteration by using the method of adjoints [36].

The overall problem was successfully solved by means of an iterative scheme. At first, two interfacial temperature profiles $\tilde{\Phi}_o$ and $\hat{\Phi}_o$ which satisfied the perturbed boundary conditions of the fin equation were assumed. Based on these temperatures, equations (3.23)-(3.26) were integrated simultaneously at each ξ-level to yield two temperature gradients $\tilde{\Phi}_{\eta}$ and $\hat{\Phi}_{\eta}$ at the solid-fluid interface. These temperature gradients were then used in the integration of the coupled conductive fin equations (3.27) and (3.28) to give two new interfacial temperature profiles. If these newly obtained temperatures did not agree with their previously assumed values to 10^{-5}, their mean values were then used as refined values. The whole procedure was repeated until the convergence criterion of 10^{-5} for both interfacial temperatures had been fulfilled.

3.2.2 MODERATE AMPLITUDE

A direct numerical approach is used to solve the problems of the Froude number being not much greater than one. Reconsideration is given to the following governing equations:

$$Pr f_{\eta\eta\eta} + f f_{\eta\eta} - \frac{2}{3} f_{\eta}^2 + (1+Pr)[1 + \cos(2\pi\tau)/Fr]\Phi$$
$$= \xi[\frac{4}{3}(f_{\eta} f_{\eta\xi} - f_{\eta\eta} f_{\xi}) + (1+Pr)\Phi] + (K_1/2\pi)\xi^{1/2} f_{\eta\tau} \quad (3.17)$$

$$\Phi_{\eta\eta} + f\Phi_{\eta} = \frac{4}{3}\xi(f_{\eta}\Phi_{\xi} - \Phi_{\eta} f_{\xi}) + (K_1/2\pi)\xi^{1/2}\Phi_{\tau} \quad (3.18)$$

$$(K_2/2\pi)\xi\frac{\partial\Phi_o}{\partial\tau} + \xi\frac{\partial^2\Phi_o}{\partial\xi^2} + \frac{\partial\Phi_o}{\partial\xi} + K_3\xi^{-1/4}\Phi_{\eta}(\xi,0,\tau) = 0 \quad (3.19)$$

and their boundary conditions:

$\xi = 0$: $\quad \xi\frac{\partial\Phi_o}{\partial\xi} = 0$

$\xi = \gamma$: $\quad \Phi_o = 1$

$\eta = 0$: $\quad f = 0, \quad f_{\eta} = 0, \quad \Phi(\xi,0,\tau) = \Phi_o(\xi,\tau)$

$\eta = \infty$: $\quad f_{\eta} = 0, \quad \Phi = 0.$

Now, if one knows the exact values of time-derivatives $f_{\eta\tau}$ and Φ_{τ} at every point (ξ,η) and at a specific time τ_i, these equations pose a two dimensional problem which is much easier to solve. Once the solutions at this initial time level have been obtained, the time-derivatives $f_{\eta\tau}$ and Φ_{τ} at the second time level can be approximated by backward

finite differences. Again, a two-dimensional problem is produced. Similar approximations can be conducted in the successive levels over a whole period of time.

The main difficulty of this approach is in the judicious choice of the initial time derivatives $f_{\eta\tau}$ and Φ_τ at every point (ξ,η). This choice should avoid causing any numerical instability during follow-up integration, and should lead to fast convergence of the solutions. A consequent problem is to determine the proper time level for τ_i so that higher accuracy in approximating those transient terms $f_{\eta\tau}$ and Φ_τ may be achieved at least at this initial level, and even better if it can also be done at subsequent time levels.

When the Froude number is moderate and much greater than one, previously obtained perturbation solutions are relatively reliable and hence provide good approximations to the initial values of $f_{\eta\tau}$ and Φ_τ. The remaining problem is to determine a proper initial time so that good approximations can also be obtained at subsequent time levels.

At the second time level, the accuracy of the two-point finite difference formula in approximating those time derivatives depends strongly upon the product of the time interval $\Delta\tau$ and the magnitude of the second order time-derivatives. Because of the long computation required

in solving the two-dimensional problem at each τ level, the time interval $\Delta\tau$ should be as large as possible. Hence, the only alternative to obtain higher accuracy in using the two-point finite difference approximation is to start solving the problem at the specific time level, after which the perturbation method detects the minimum magnitudes in the second order time-derivatives.

Owing to the fact that the total heat transfer rate reflects the overall features of the problem, the time level where the total heat transfer rate of perturbation result indicates a straight line, or a point of inflexion with respect to time, is an appropriate point for the second time level if Fr is slightly greater than order one. In other words, the appropriate initial time level is just the level one time interval ahead of this point.

When Fr is not much greater than unity, the perturbation results are unreliable; indiscriminate use of them in either approximating initial transient terms or determining the initial time level can easily lead to numerical overflow. However, a proper decision may be deduced from careful comparison of various manifestations among:

(1) the perturbation result P1 of the larger Fr case,

(2) the predicted solution S1 of P1, where S1 is obtained through the direct integration of periodic equations (3.17)-(3.19), and

(3) the perturbation result P2 of the present (small Fr) problem.

The total heat transfer rate Q can be used in selecting the initial time level. It is logical to assume that variation in the value of Q is in phase with the overall changing trends of system temperature and velocity. A zero variation in Q indicates a momentarily unchanged system which, in turn, corresponds to zero or extremely small transient terms in equations (3.17)-(3.19). If comparison among solutions P1, P2, and S1 does not reveal severe or irregular phase shifts, it is reasonable to choose initial time level from those of maximum or minimum Q values so that the inevitable errors in approximating transient terms become less effective because of their comparatively small magnitudes in the equations. Several most typical cases are illustrated in the following paragraphs and the guideline on determination of initial time level will be reinforced by these examples as the discussion proceeds.

Figure (3.1) shows one of the most favorable cases. The perturbation result P1 for a large Froude number is in phase with its predicted solution S1; in addition, the perturbation result P2 for a moderate Froude number does not reveal significant phase-shift from either P1 or S1. In this case, the solution S2 predicted by P2 for the moderate Froude number can be expected, with more confidence,

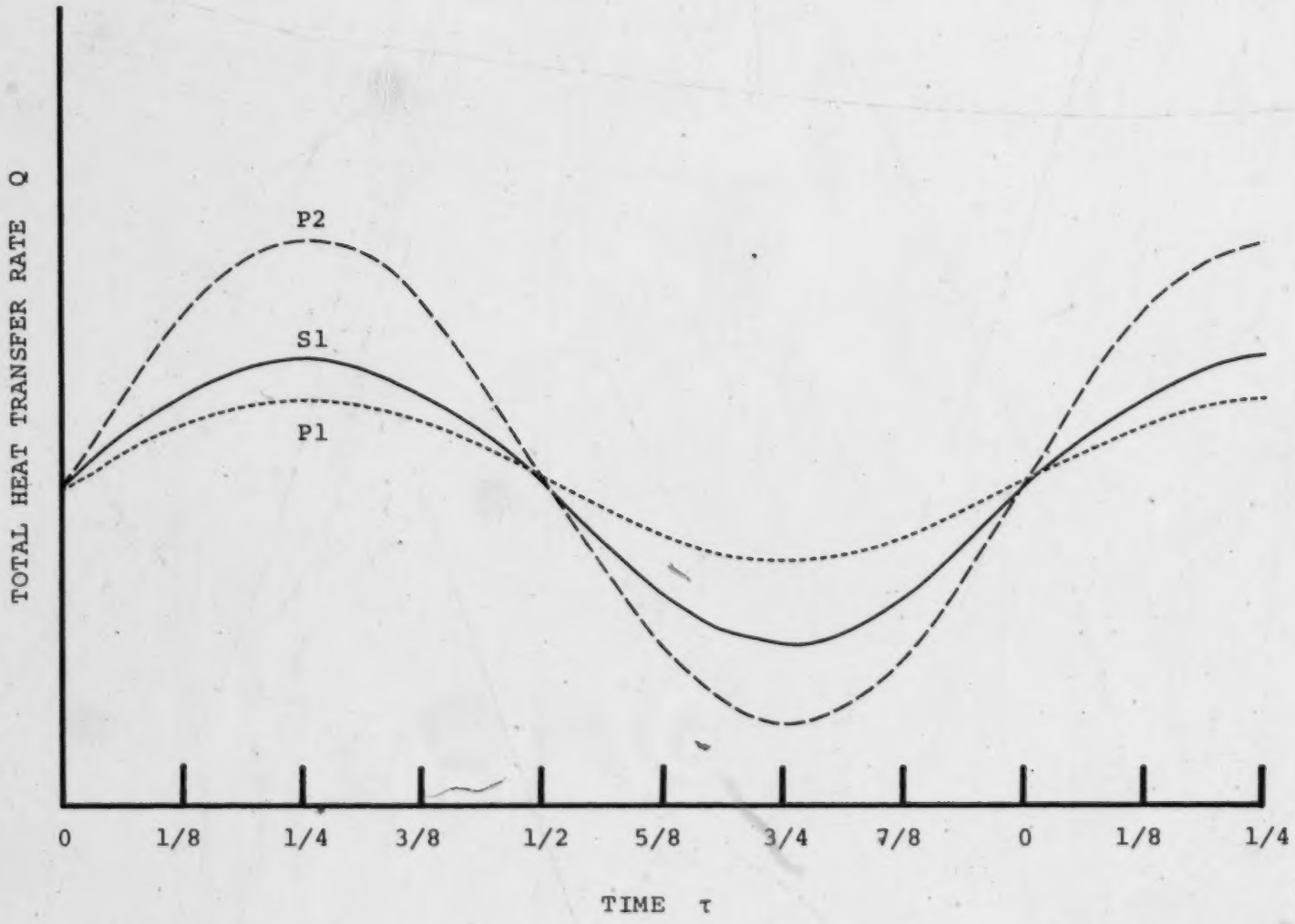

Figure 3.1 Example No.1

to be in phase with all the solutions in Figure (3.1). More specifically, both levels of $\tau=1/4$ and $\tau=3/4$ can be chosen as τ_i. However, the $\tau=1/4$ level is considered to be proper because of its smaller magnitude-difference between P1 and S1. Once this initial time level has been determined, the transient terms in equations (3.17)-(3.19) can be approximated by using its perturbation solution P2. On the other hand, one can choose $\tau=0$ or $1/2$ as τ_i and use S1 for the initial solutions if higher accuracy in the initial finite difference approximation is more desirable.

Sometimes, the phase of the solution may be sensitive to the variation of Froude number, as is shown in Figure (3.2). Although the perturbation result P1 for a large Froude number is in phase with its corresponding solution S1, it is significantly out of phase from P2. Since there is no phase-shift between S1 and P1, it is plausible to expect that no phase-shift between P2 and S2, and both $\tau=0$ and $\tau=1/2$ can be the candidates for τ_i. However, $\tau=0$ is properer because of its smaller curvature. The reason behind this is that when the curvature of the selected extreme point is small, the error in approximating those transient term of governing equations (3.17)-(3.19) with P2 becomes less susceptible to any unpredeicted, but possible, phase-shift between P2 and S2. In addition, the

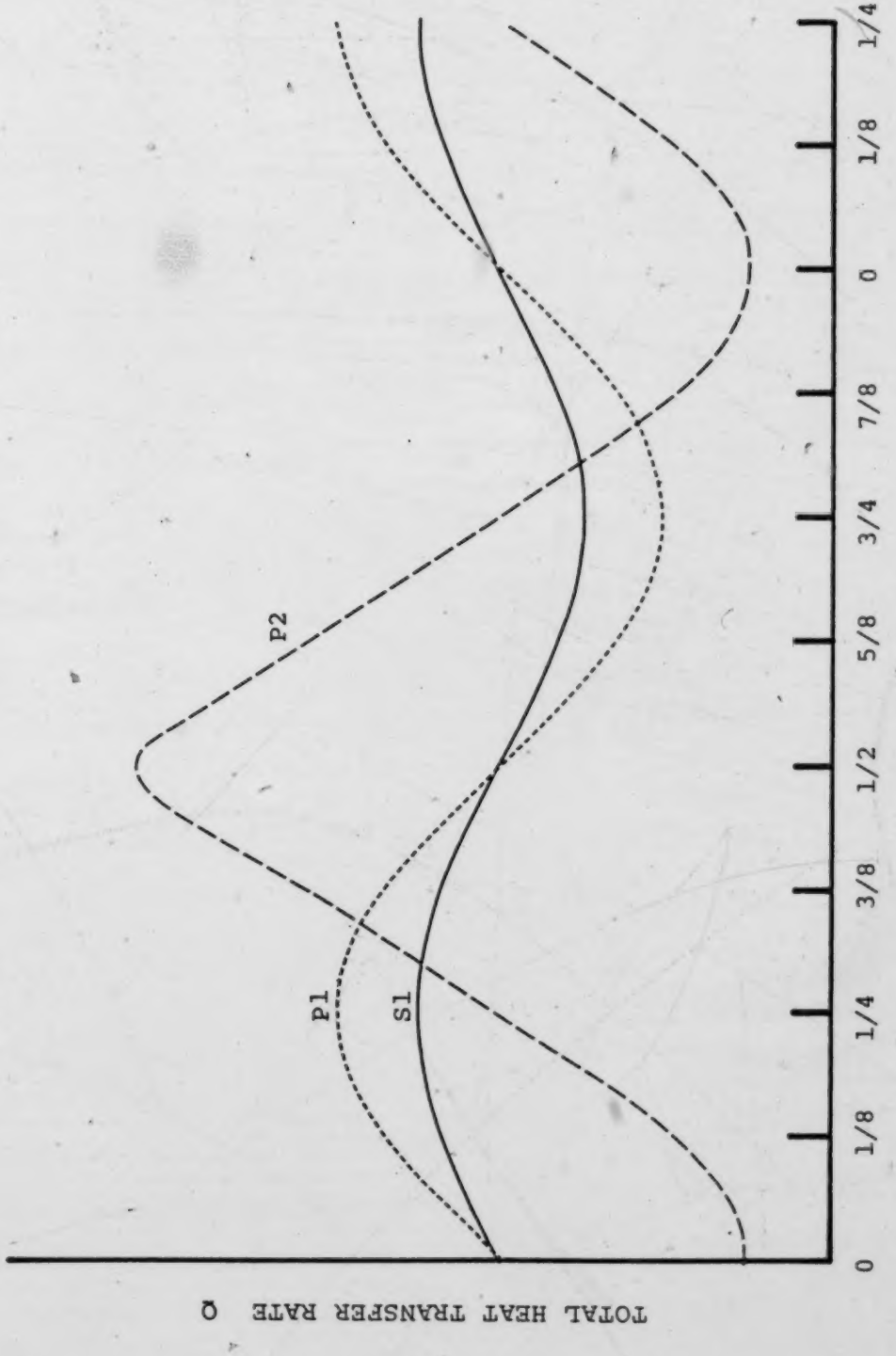

Figure 3.2 Example No.2

second order time-derivatives are proportional to the curvature and a smaller curvature means the possibility of smaller truncation errors in the use of two-point finite-difference approximation at the second time-level.

Concerning the example of Figure (3.3), the perturbation approximation P1 is about one-eighth of a period out of phase from its predicted solution S1. Fortunately, this P1 curve is in phase with the perturbation solution P2. If P1 and P2 are not very far apart in their magnitudes of Froude number, one can assume that the Froude number does not have a significant phase-shift effect to the solutions either. In contrast with two previous examples, S1 in lieu of P2 is more suitable for determining the initial time level as well as for approximating all the transient terms of the governing equations (3.17)-(3.19). Again, the level of $\tau=3/8$ rather than $\tau=7/8$ is a better choice for τ_i because of its smaller curvature.

A more difficult case is illustrated in Figure (3.4), where the perturbation solution P1 is in phase with neither its precicted result S1 nor the perturbation solution P2 corresponding to a smaller Fr. However, comaprison between S1 and P1 shows that the extreme points of the former locate about one-eiththh of the period behind their

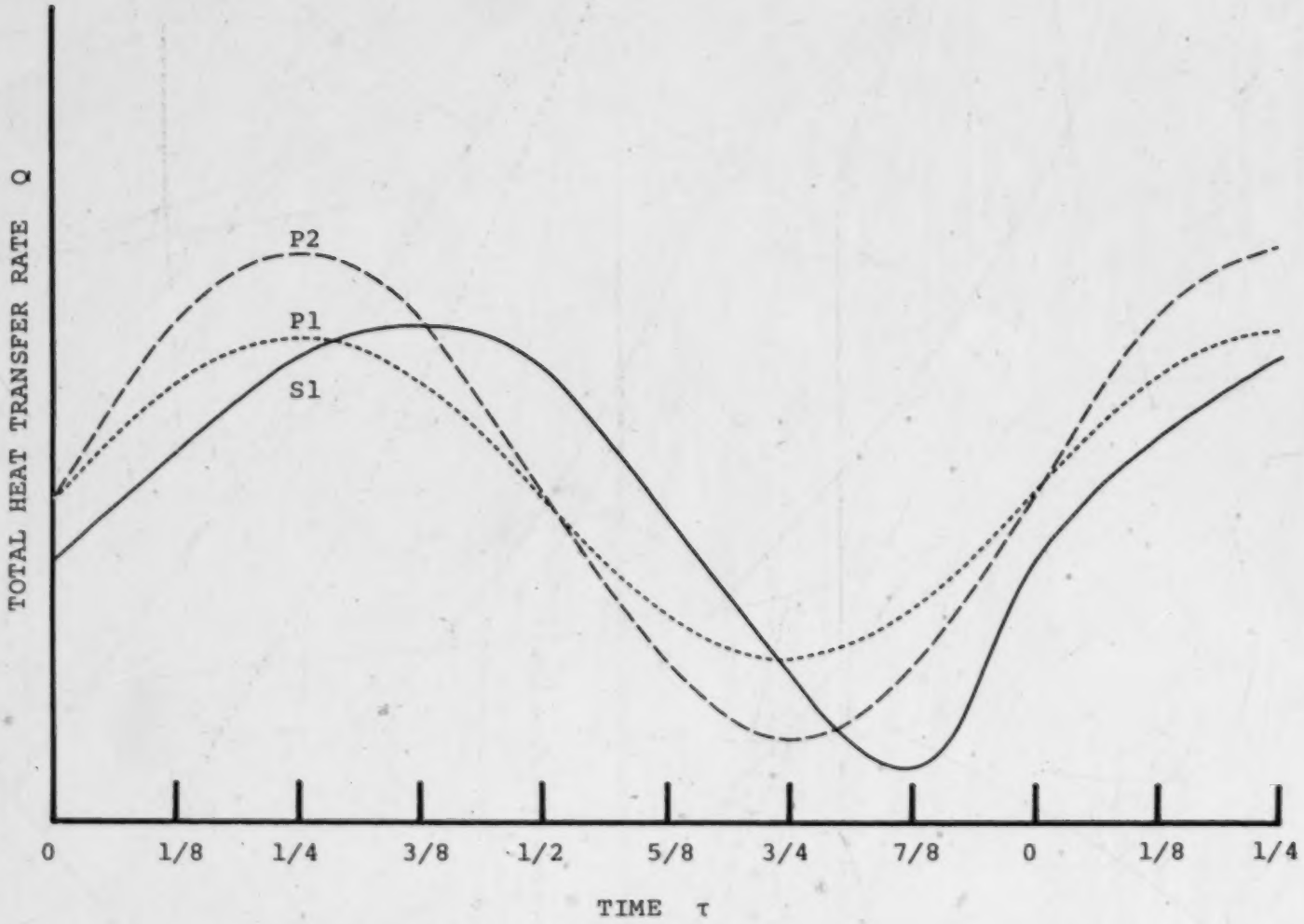

Figure 3.3 Example No.3

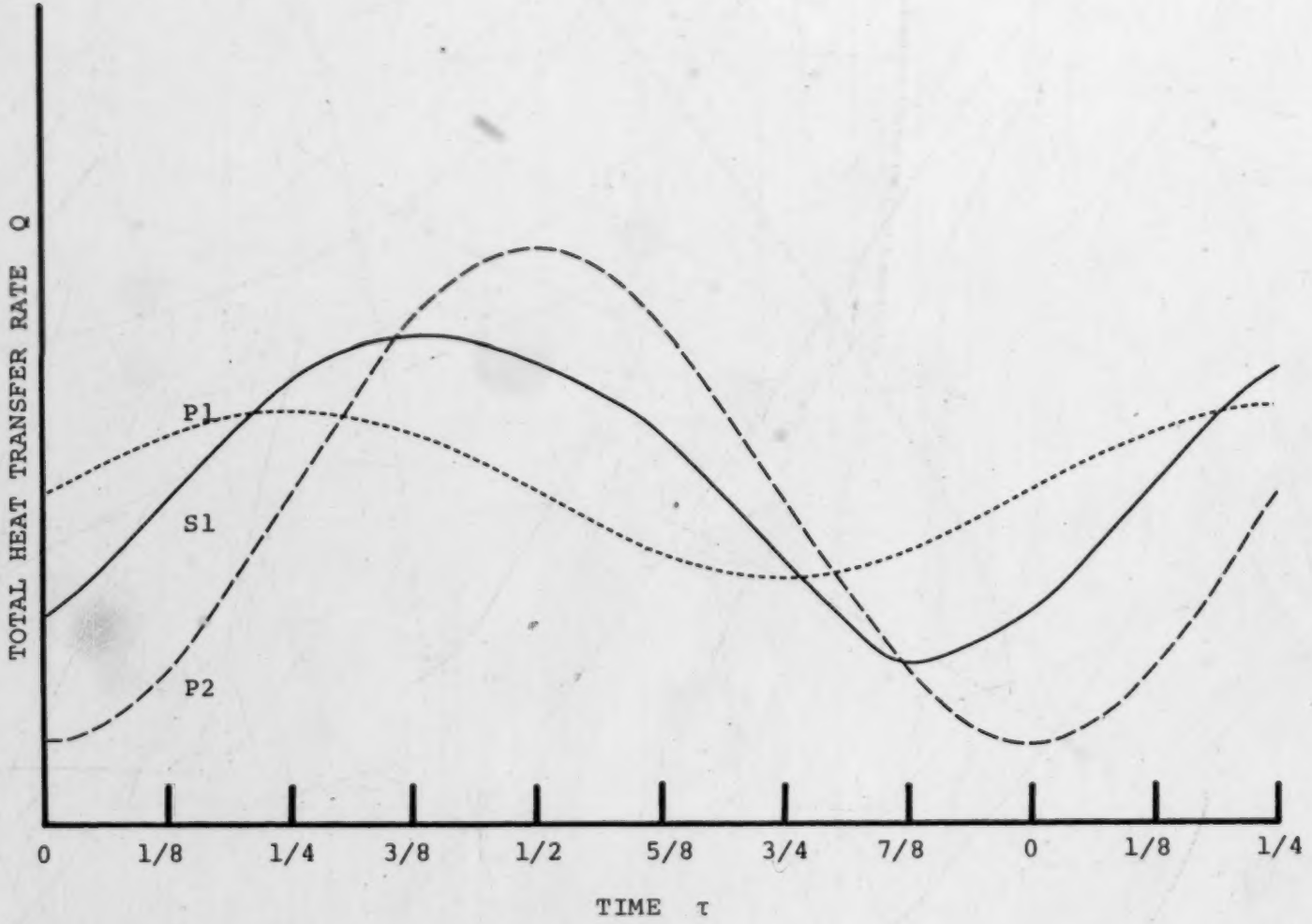

Figure 3.4 Example No.4

corresponding points of the latter. Assuming the same correlation also exists between P2 and its predicted solution S2 for a small Froude number, one can choose the level of $\tau=5/8$ as τ_i and start solving equations (3.17)-(3.19) by approximating all the transient terms with P2.

Sometimes, the change of Froude number can cause a different phase-shift in the solutions. The discussion of the four examples above is based on the assumption that the correlation observed between solution S1 and its approximation P1 corresponding to a large Froude number also holds for smaller Froude numbers. This is not always true and the correlation may vary with the Froude number. As depicted in Figure (3.5), the solution S1 corresponding to a large Froude number has a time-lag of L1 behind its perturbation approximation P1, whereas the unknown solution S2 for a small Froude number may have a double time-lag of L2 behind its perturbation approximation P2. Apparently this is a good example of poor accuracy in perturbation solution when the Froude number is not large. If one wrongly chooses τ_i-level to be $\tau=3/8$ instead of $\tau=1/2$, the numerical integration may eventually lead to divergence of the solution. To overcome this, a proper correlation between the solution phase-shift and the variation of Froude number should be established by observing additional

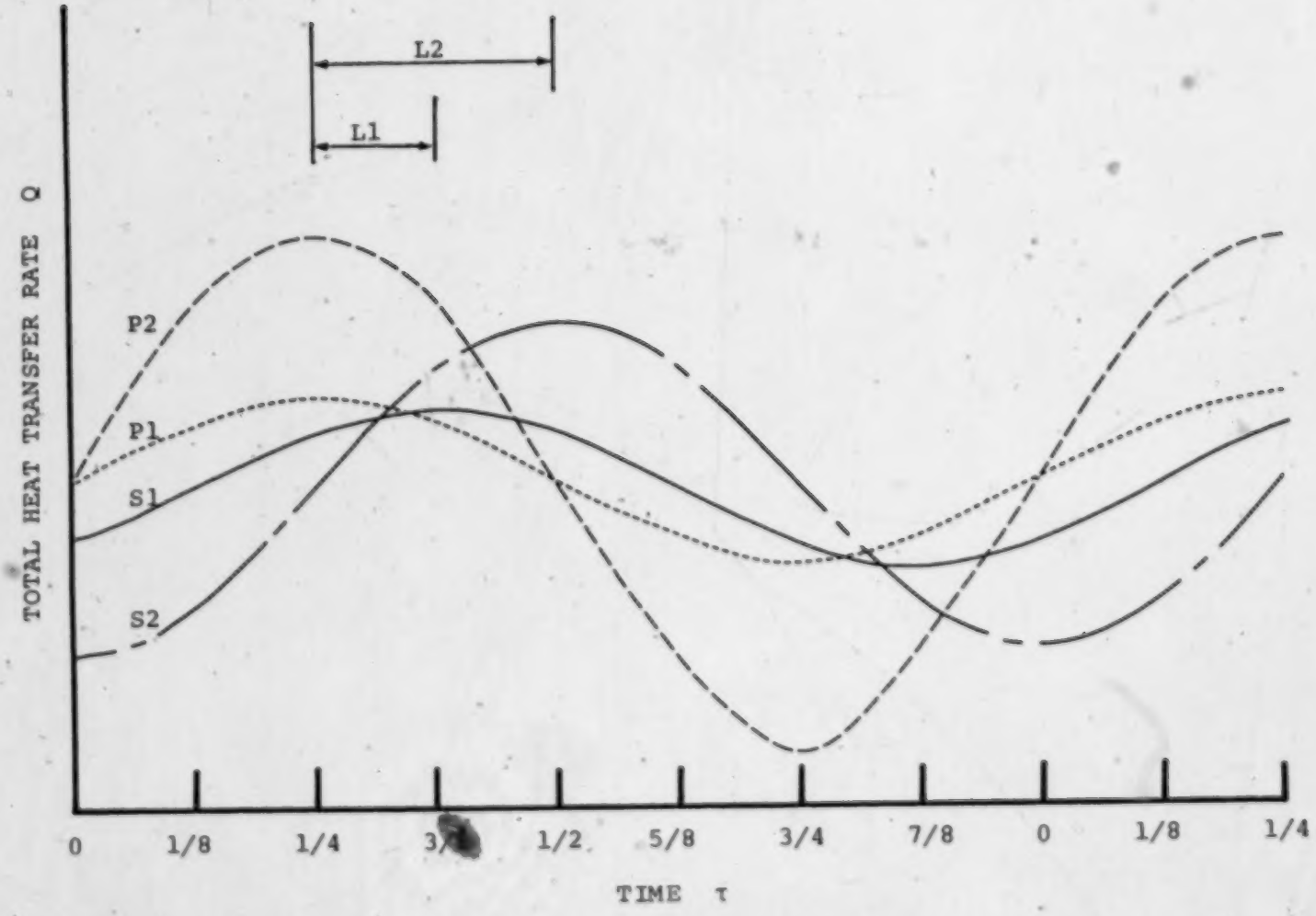

Figure 3.5 Example No.5

solutions corresponding to one or two intermediate Froude numbers.

Figure (3.6) indicates a severe case where not only the perturbation result P1 corresponding to a large Froude number deviates significantly in magnitude from its approximated solution S1, but also no correlation exists between extreme points of P1 and S1. Moreover, comparing P1 with the perturbation solution P2 corresponding to a smaller Froude number, one notices that no consistent phase-shift holds between their extreme points. That is, the maximum point of P2 is one-eighth of a period behind its corresponding point (at $\tau=1/4$) of P1 while the minimum point of P2 is one quarter of a period behind its corresponding point (at $\tau=3/4$) of P1. It is recommended that a series of problem with gradually decreasing Froude number be solved. Owing to the lack of accuracy in the perturbation approximation, one should use S1 instead of P2 in determining the initial time level, as well as in approximating those transient terms of equations (3.17)-(3.19) corresponding to the new but slightly smaller Froude number. In addition, the time level of $\tau=3/4$ in Figure (3.6) is an appropriate choice for τ_i because of its smallest curvature among all the extreme points of the S1 curve.

Once the initial time level τ_i and its associated

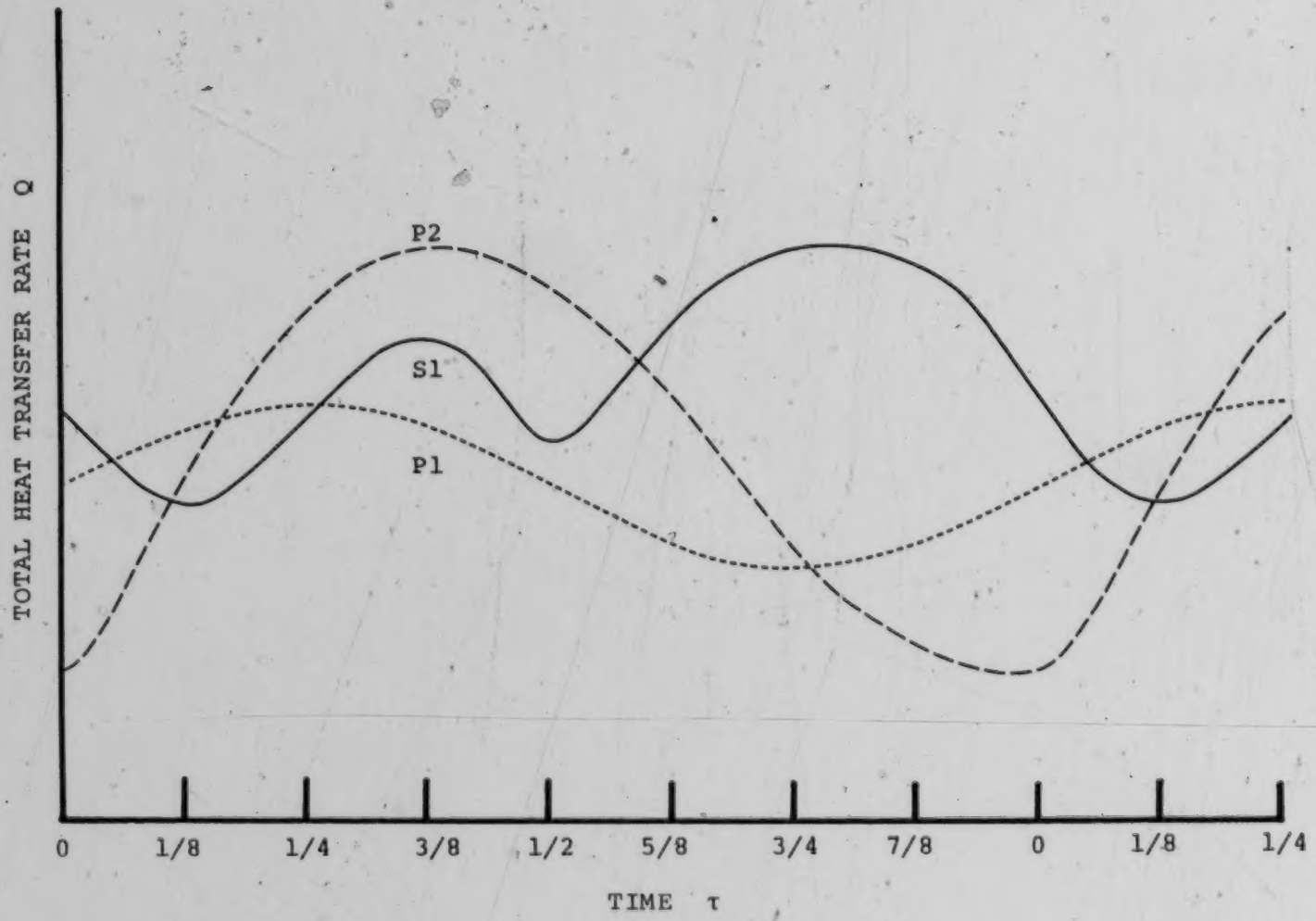

Figure 3.6 Example No.6

time-derivatives $f_{\eta\tau}$ and Φ_τ are properly determined, integration of the governing equations at this initial and subsequent time levels can be carried out without any difficulty. At the end of one time period, the timewise convergence of solutions is checked. Theoretically, this convergence can be checked at each time level after the first timewise iteration, provided that the solutions obtained at each time level have been previously stored. However, the immense size of computer memory required for storing such not-yet-converged solutions makes it impractical to check the convergence of the solutions at every time level. In this work, the check was performed only at the end of each period and the timewise convergence was achieved within 3 iterations to an accuracy of 10^{-4}.

CHAPTER IV

RESULTS AND DISCUSSION

As demonstrated in the previous chapter, the results of this periodic heat transfer problem can be divided into quasi-steady solutions, perturbation approximations, and "exact" solutions obtained from the direct integration of the governing equations (3.17)-(3.19). These equations and their associated boundary conditions indicate that the problem contains six parameters: Pr, Fr, γ, K_1, K_2, and C (or K_3). Among them, the effect of Prandtl number (Pr) on the solutions is removed by use of the Lefevre-type transformation (Appendix C); hence a fixed value of 0.72 is used (as the Prandtl number of air) throughout this study, and the number of parameters is therefore reduced to five.

The Froude number Fr is the most important parameter in this study. Since solving this coupled convection-conduction heat transfer problem with the necessity of additional time-wise iterations requires expensive numerical work even for one set of parameter values, it is uneconomical to study the effect of all the remaining five parameters; only the parameter of greatest interest in the present study should be considered. One of the main objectives of the present work is the development of a technique for handling periodic problems of

moderated fluctuating amplitude, which strictly depends on the magnitude of Fr. For this reason, although some attention is also given to the study of other parameters, the investigation is mostly centered around the Froude number.

4.1 QUASI-STEADY RESULTS

The quasi-steady results can provide the basic information to the problem. Although this quasi-steady case has been previously investigated [27,28], the present results are obtained in a new coordinate system using different transformations. In addition, these quasi-steady solutions are the base in constructing perturbation approximation which, in turn, may be the key to the solutions of the periodic equations (3.17)-(3.19). Thus, presentation of these new quasi-steady results is not only for the purpose of comparison but also for the sake of completeness. For convenience, these quasi-steady solutions are divided into three parts.

In order that the present results can be compared with those of previous work, parameter C rather than K_3 is used here. This is certainly acceptable because for a fixed Prandtl number of 0.72, parameter K_3 expressed by

$$K_3 = \left(\frac{3}{4}\,\frac{Pr}{1+Pr}\,\gamma^{-3}\right)^{1/4} C \qquad (4.1)$$

is, in fact, a function of parameters C and γ. In this study, investigation into the effect of these two parameters

is carried out with six values of C (0.01, 0.1, 1.0, 3.0 5.0 and 10.0) and five values of γ (0.1, 0.2, 0.3, 0.4 and 0.5).

4.1.1 SOLUTIONS OF BOUNDARY LAYER PROBLEM

As far as the study of this free convection problem is concerned, the investigation encompasses the solutions within the momentum and thermal boundary layers. The shapes of these boundary layers are sketched as dashed lines in figure (2.1); namely, the boundary layer thickness increases from zero at the fin tip (x=0) to finite value at the fin root (x=1). However the definition of new coordinate variable η of transformation (3.5) indicates that in the transformed coordinates (ξ,η), the closer the fluid flow to the fin tip the greater the stretch of boundary layer in η-direction. A proper transformation should therefore stretch the boundary layer in such a way that its thicknesses at different ξ-levels are of the same order of magnitude. These boundary layer thicknesses become independent of ξ only if similarity solutions exist. The possible existence of similarity solutions for this boundary layer problem is certainly worth considering.

4.1.1-1 DEPARTURE FROM SIMILARITY

Figure (4.1) shows the velocity and temperature profiles at three ξ levels along a high-speed fin with parameters C and γ respectively equal to 5.0 and 0.5;

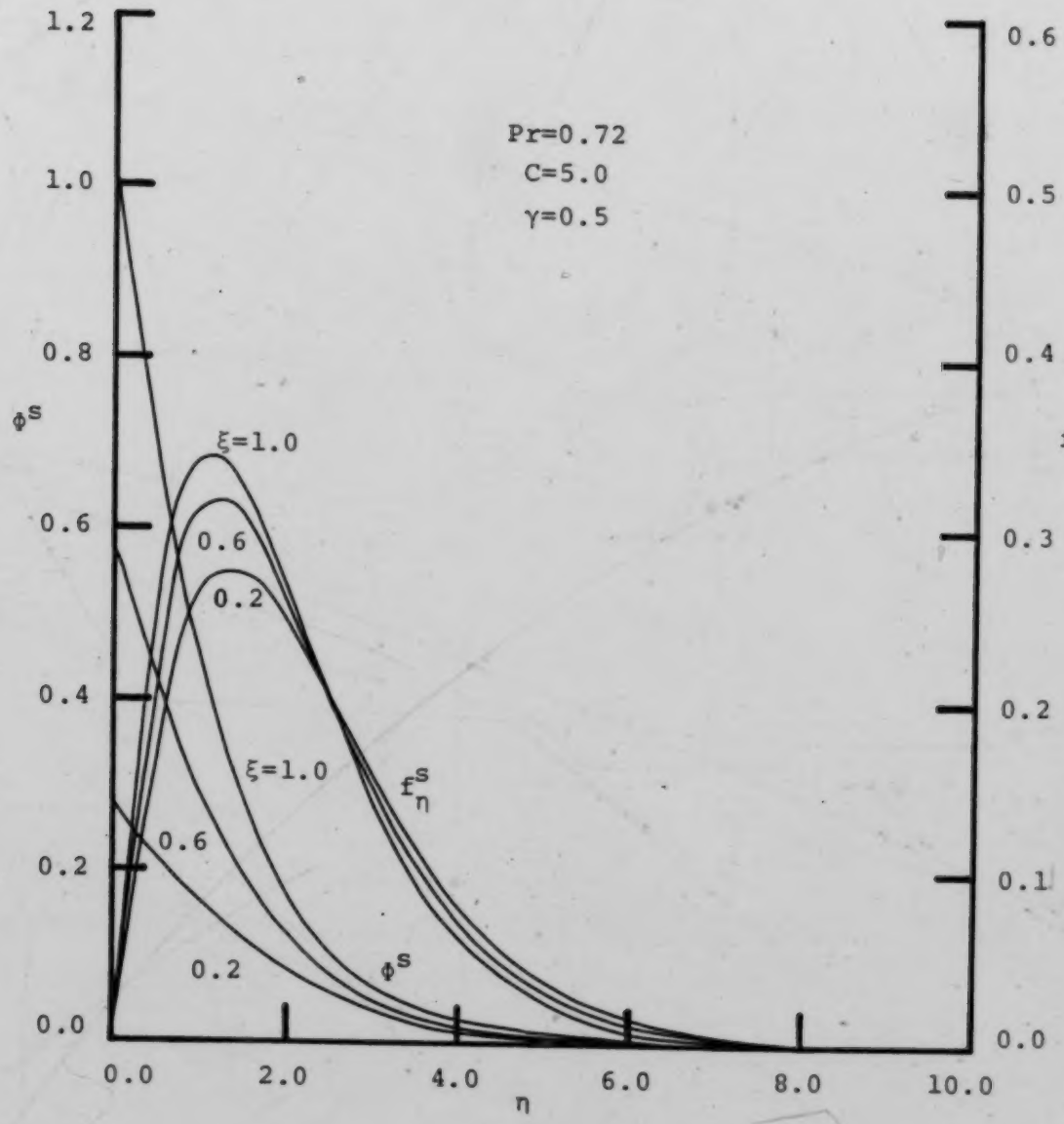

Figure 4.1 Departure of Quasi-Steady Boundary Layer Solutions From Similarity

apparently, departure from similarity is quite significant in both profiles of this boundary layer problem. However, the fact that both thermal and momentum boundary layer thicknesses remain almost unchanged along the fin direction in the ξ-η domain, substantiates the coordinate stretching feature of the Blasius-Howarth type transformation (3.5).

4.1.1-2 EFFECT OF PARAMETER γ

To study this effect, velocity and temperature profiles at the root of the rotating fin with parameter C=1.0 are plotted in figure (4.2) for three values of γ (0.1, 0.3 and 0.5). The velocity varies considerably with γ, but the temperature changes only slightly. Moreover, the thicknesses of the thermal and momentum boundary layers are nearly unaffected by γ.

4.1.1-3 EFFECT OF PARAMETER C

Since the magnitude of parameter C represents the degree of coupling between convection and conduction, investigation of this parameter effect covers four order-of-magnitudes of C (0.01, 0.1, 1.0 and 10.0) for γ=0.1, as shown in figure (4.3). Apparently, parameter C does produce a significant effect on both velocity and temperature profiles at the root of the fin. In addition, the effect on the former profiles is by far more noticeable than on the latter. In contrast to these, neither the thermal nor the momentum boundary layer thickness at this fin root varies noticeably with the parameter C.

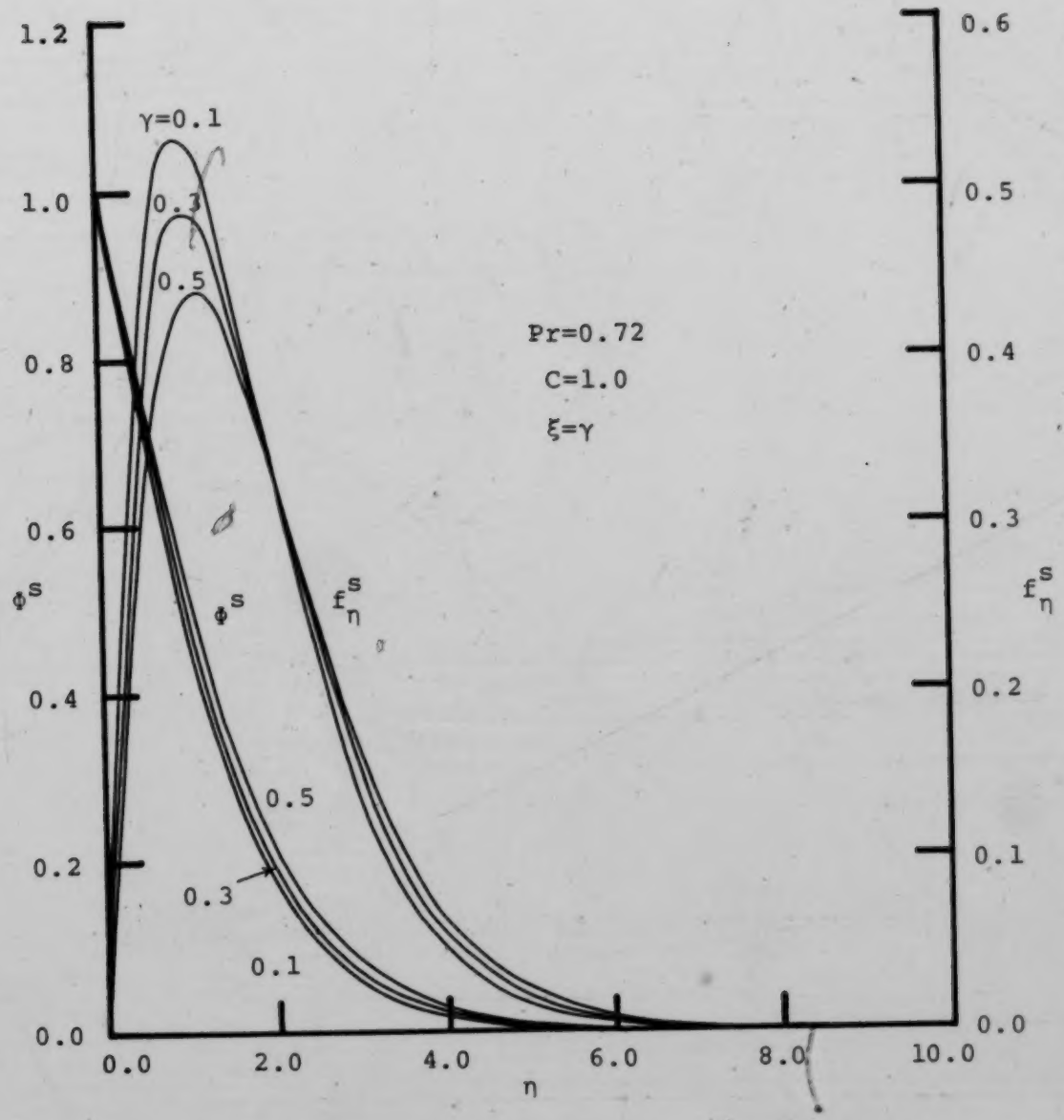

Figure 4.2 Effect of γ on Quasi-Steady Boundary Layer Solutions

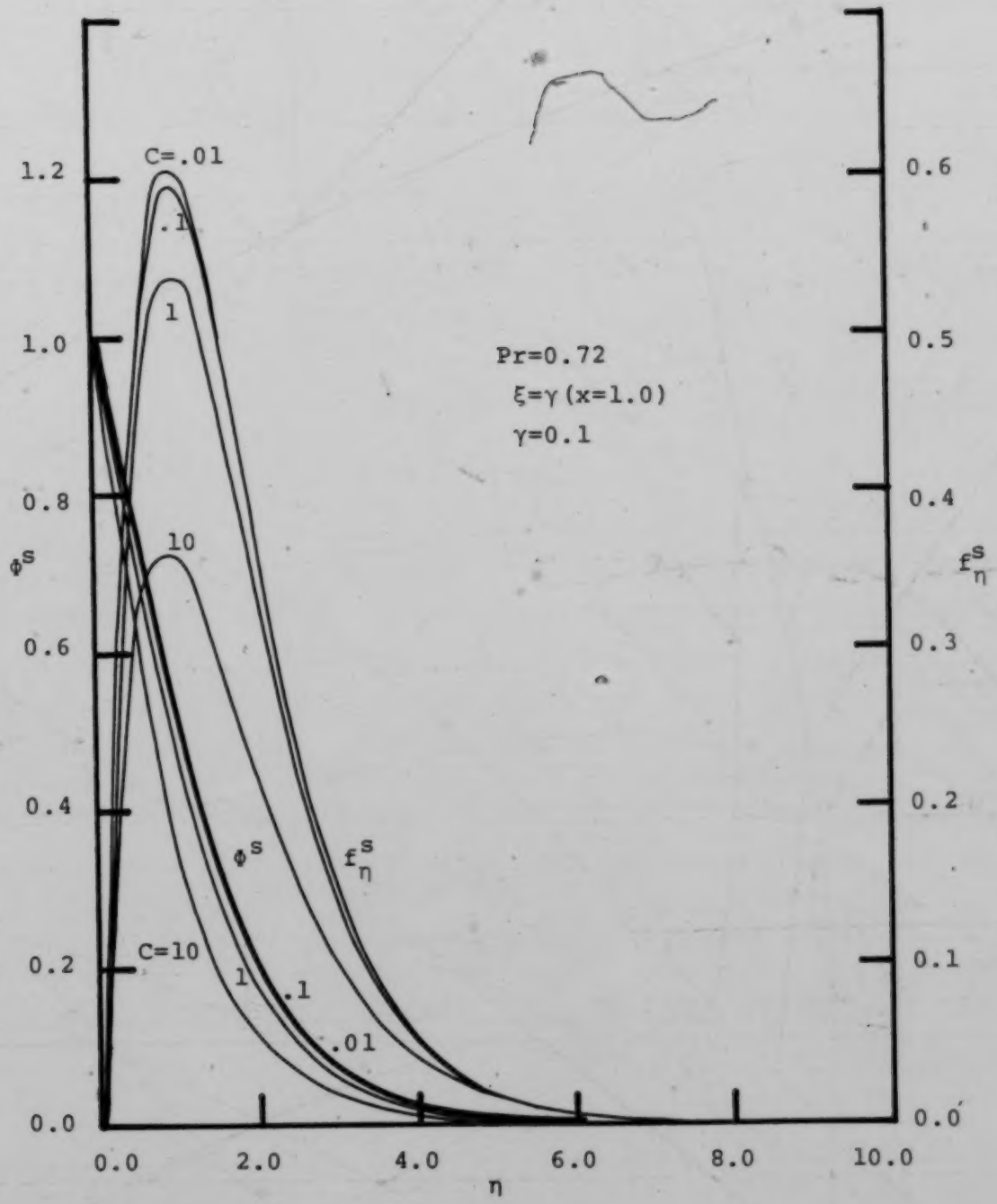

Figure 4.3 Effect of C on Quasi-Steady Boundary Layer Solutions

4.1.2 SOLUTIONS OF CONDUCTION PROBLEM

The main interest of this investigation is on the temperature distribution along the fin. In most studies of the free convection problems [39-43], heat conduction in the solid is ignored, and either a power law or an exponential temperature distribution is assumed along the solid-fluid interface. It is logical to inspect the validity of these assumptions for such a coupled conduction-convection problem.

4.1.2-1 EFFECT OF PARAMETER γ

Figure (4.4) shows the interfacial temperature along the fin for four values of C (0.01, 0.1, 1.0 and 10.0) and two values of γ (0.1 and 0.5). The actual investigation includes five values of γ (0.1, 0.2, 0.3, 0.4 and 0.5) for each value of C. All temperature profiles of γ=0.2, 0.3 and 0.4 fall between that of γ=0.1 and 0.5. For the sake of clearness, only profiles of γ=0.1 and 0.5 are presented on this plot.

The insensitivity of normalized fin temperature to the effect of γ provides a favourable feature from the economic point of view; that is, once a matched interfacial temperature for a problem with specific values of C and γ is obtained, it can be used as an extremely good initial guess of the interfacial temperature for all other problems

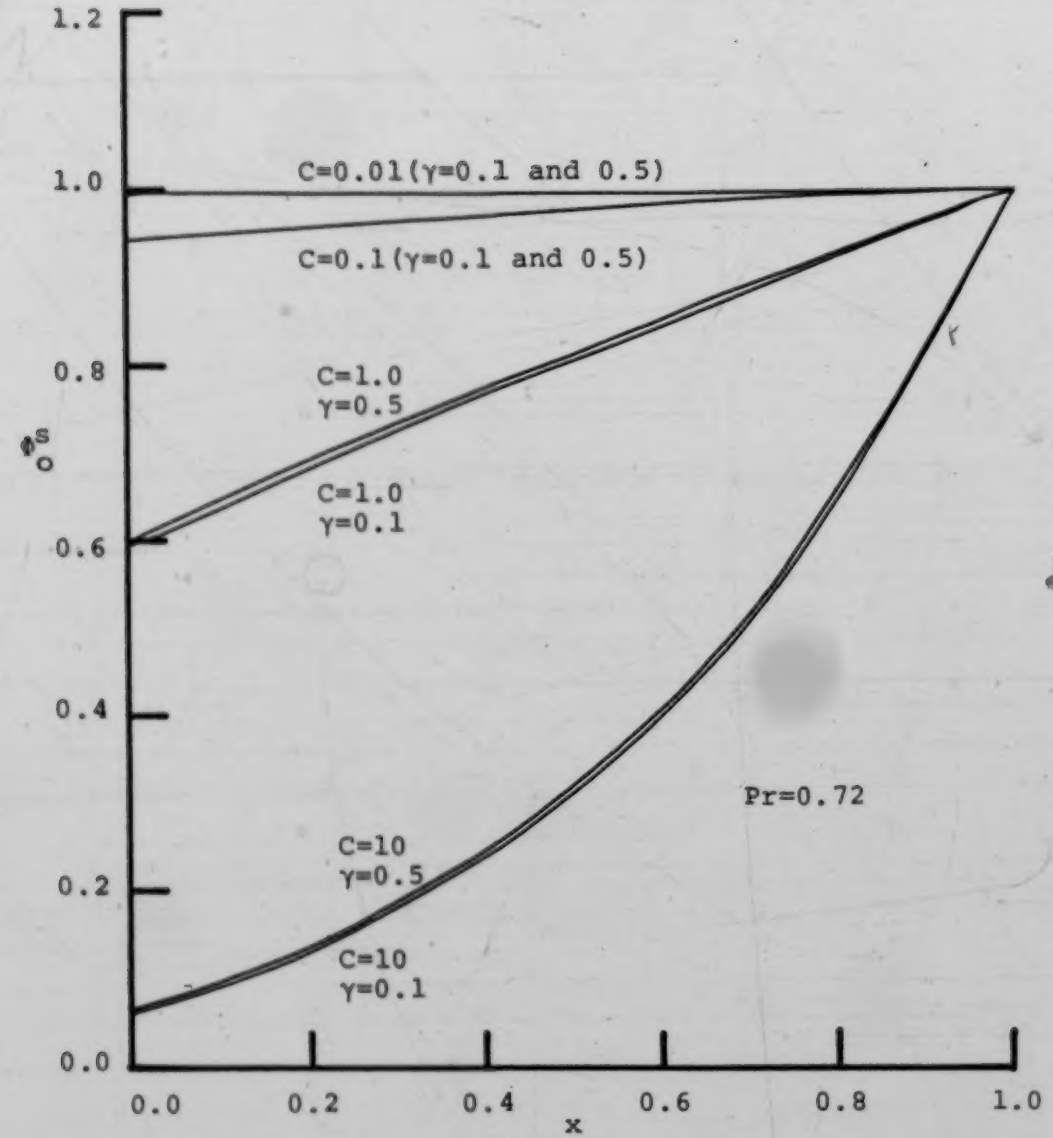

Figure 4.4 Effect of C and γ on Quasi-Steady Interfacial Temperature

of the same C value but with different parameter γ. Large amounts of computation are hence saved due to the fast convergence of the interfacial temperature.

4.1.2-2 EFFECT OF PARAMETER C

Figure (4.4) also shows the significant effect of C on the solid fin temperature. It is clear that an isothermal surface temperature is a good assumption to the boundary condition of a free convection problem only if the parameter C is very small. As the value of C increases, the assumption of constant fin temperature becomes increasingly invalid; but for C=O[1], a linear profile with a non-zero temperature at the tip of the fin is still the character of the fin temperature. The assumption of zero tip temperature for the fin is only a valid approximation when the magnitude of C is much greater than order one.

4.1.2-3 COMPARISON WITH POWER LAW ASSUMPTION

If the matched interfacial temperature ϕ_o^s follows the conventional power law assumption $\phi_o^s=ax^n$ of free convection problem, it should have the following features:

(i) $\phi_o^s=0$ at x=0, except for the isothermal case where n=0. According to figure (4.4), this is only possible when C>>O[1].

(ii) The plot of ϕ_o^s vs. x on a log-log scale should reveal a straight line.

To check the validity of this power law assumption to the interfacial temperature of this quasi-steady conduction-convection heat transfer problem, the matched temperature along a fin of =0.3 is plotted in figure (4.5) on a log-log scale for six values of C (0.01, 0.1, 1.0, 3.0, 5.0 and 10.0). It is obvious that linearity only occurs when the value of C is very small. In other words, a power law temperature distribution is a good assumption in the present problem only if the value of n is extremely small, that is, when it is close to an isothermal fin problem. In general, the power law interfacial temperature does not exist for C equal to or greater than one.

4.1.2-4 COMPARISON WITH EXPONENTIAL ASSUMPTION

Lock [44] has shown that in two-dimensional free convection problems, the exponential surface temperature, $\phi=e^{mx}$, for similarity, is merely an asymptote of the conventional power law distribution $\phi=x^n$ when n approaches infinity. In order to check the possibility of the matched interfacial temperature following such an exponential form, logarithmic values of ϕ_o^s are plotted against x in figure (4.6).

Again, the linear relationship is achievable only when the value of C is much less than one. In addition, the profile for C=10 is almost a straight line near the root of the fin (x=1); this indicates that when the magnitude of C is much greater than one, an exponential

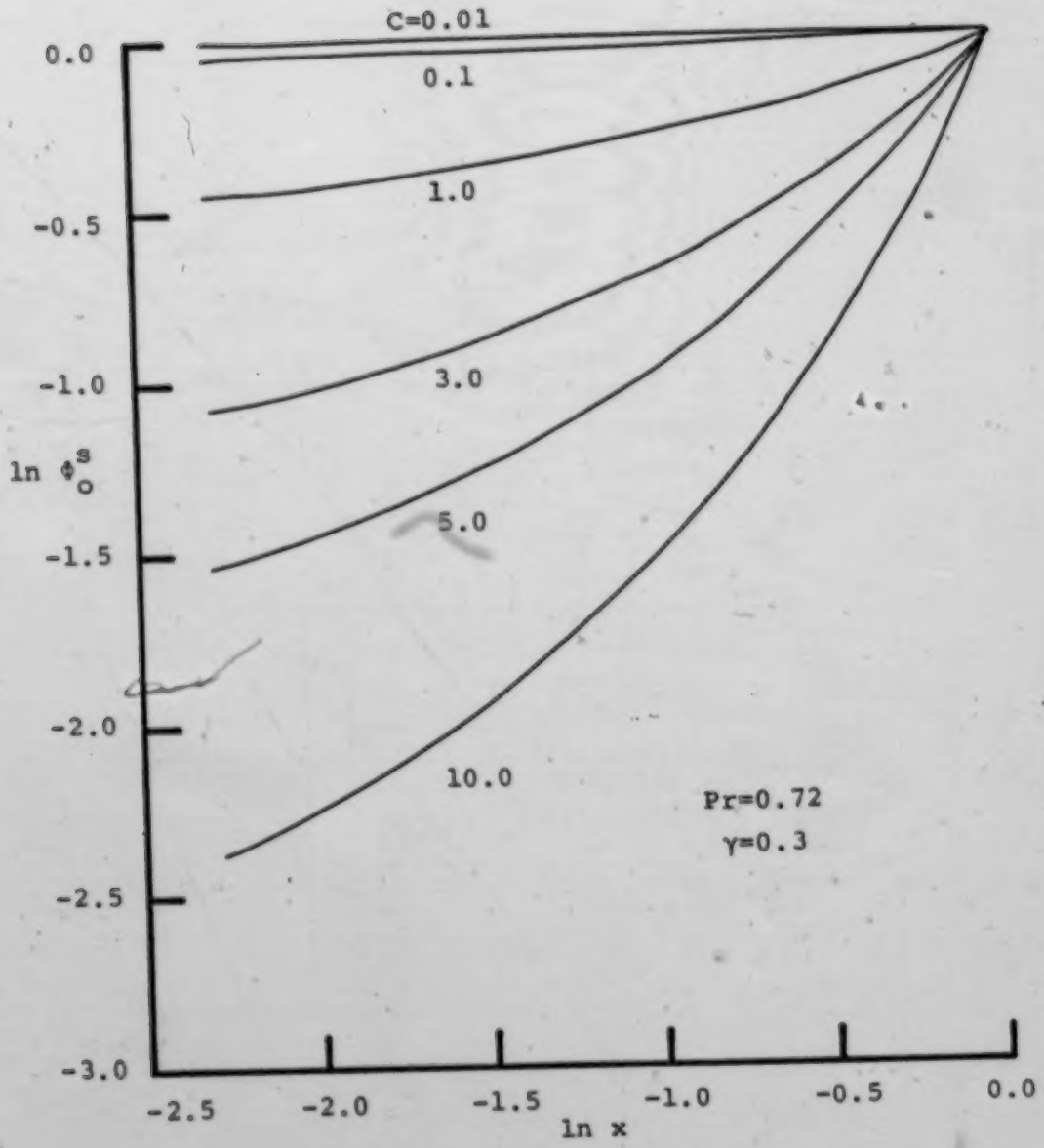

Figure 4.5 Quasi-Steady Interfacial Temperature Profiles for Checking the Possibility of Power Law Assumption

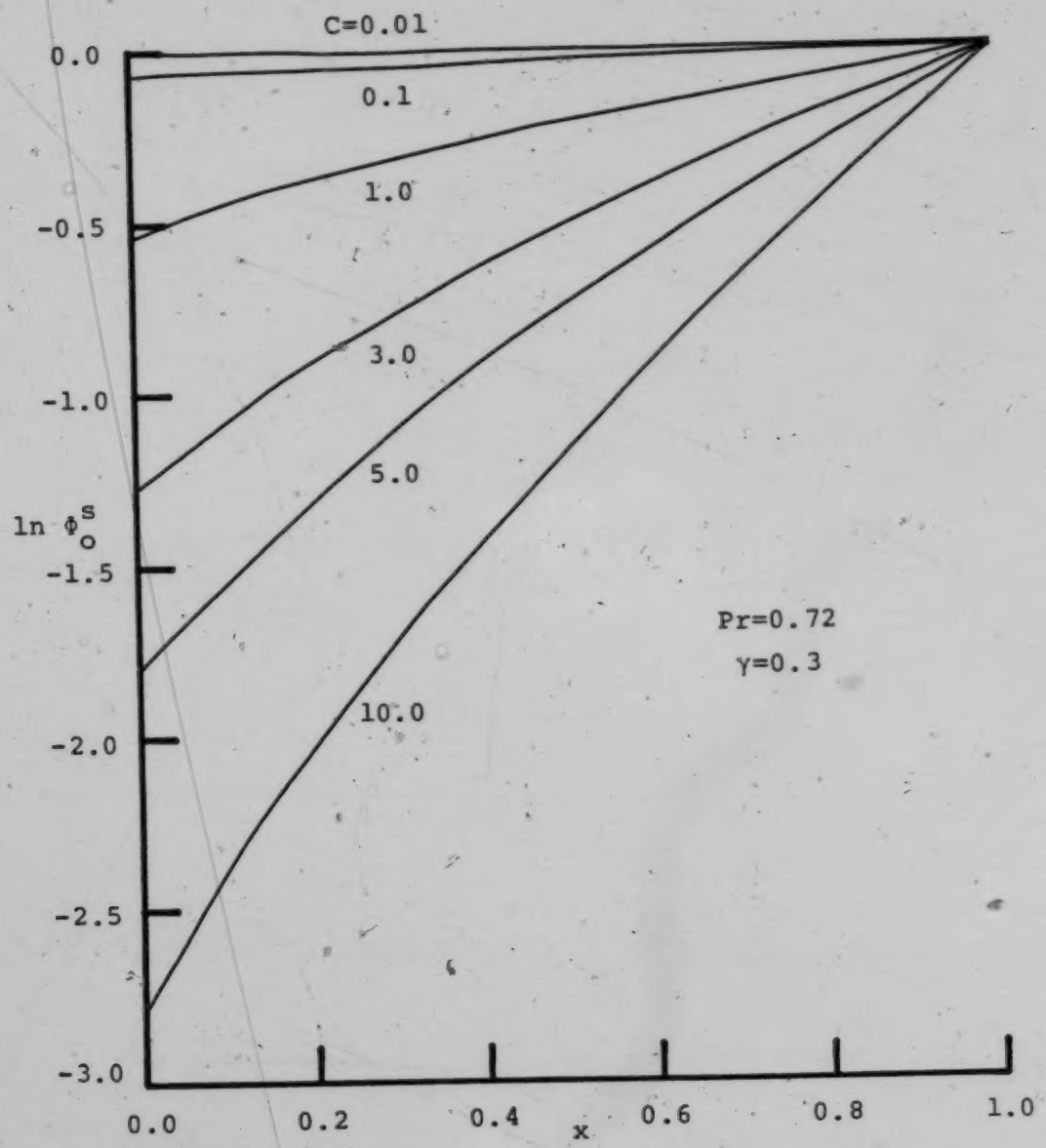

Figure 4.6 Quasi-Steady Interfacial Temperature Profiles for Checking the Possibility of Exponential Assumption

assumption may be a good approximation to the temperature distribution near the root.

4.1.3 SOLUTIONS OF OVERALL PROBLEM

As far as the overall fin problem is concerned, interest centres on the total heat transfer rate, the Nusselt number, and the fin effectiveness.

4.1.3-1 TOTAL HEAT TRANSFER RATE

If the base area of fin is $2W\bar{D}$ (see figure 2.2), the total quasi-steady heat transfer rate, Q^s, through this fin is

$$Q^s = 2W\bar{D}K_s \frac{dT_o^s(L)}{dX} \tag{4.2}$$

and the heat transfer rate per unit area is

$$q^s = K_s \frac{dT_o^s(L)}{dX} \quad \text{or} \quad q^s = \frac{K_s \theta_r}{R} \frac{d\phi_o^s(\gamma)}{d\xi} \; ; \tag{4.3}$$

therefore when both the dimensions and the temperature are fixed at the fin base, the total heat transfer rate of this quasi-steady problem can be expressed by the temperature gradient $\frac{d\phi_o^s(\gamma)}{d\xi}$ at the fin root.

A plot of this heat transfer rate versus parameter C is presented in figure (4.7) for five values of γ(0.1, 0.2, 0.3, 0.4 and 0.5). As expected, the stronger the coupling of the convection and conduction problems, the higher the total heat transfer rate. A much more interesting result is shown in figure (4.8) where plotting total heat transfer rate against parameter γ on a log-log scale reveals that linearity between $\ln\frac{d\phi_o^s(\gamma)}{d\xi}$ and $\ln\gamma$ can be obtained for

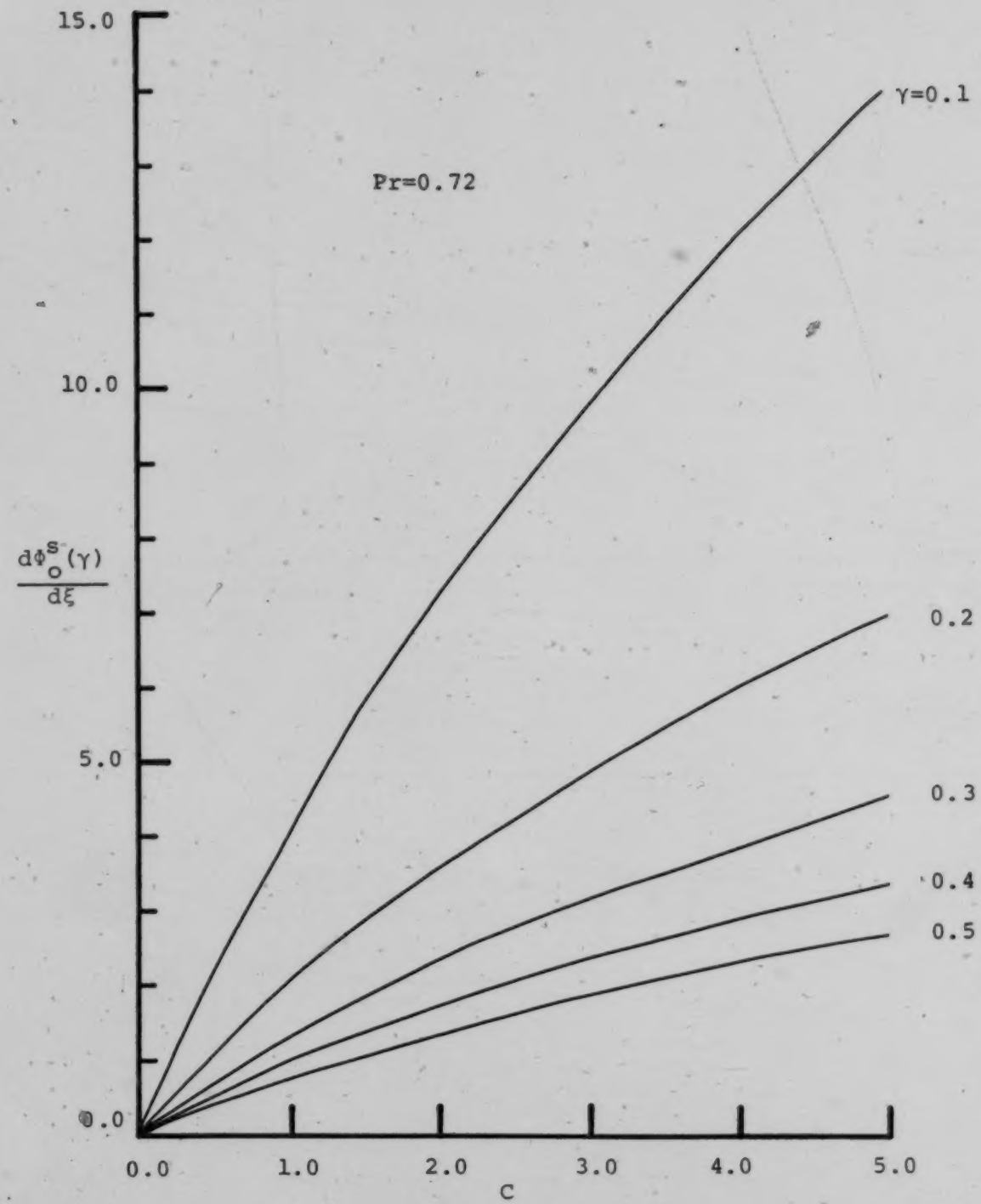

Figure 4.7 Effect of C on Quasi-Steady Heat Transfer Rate

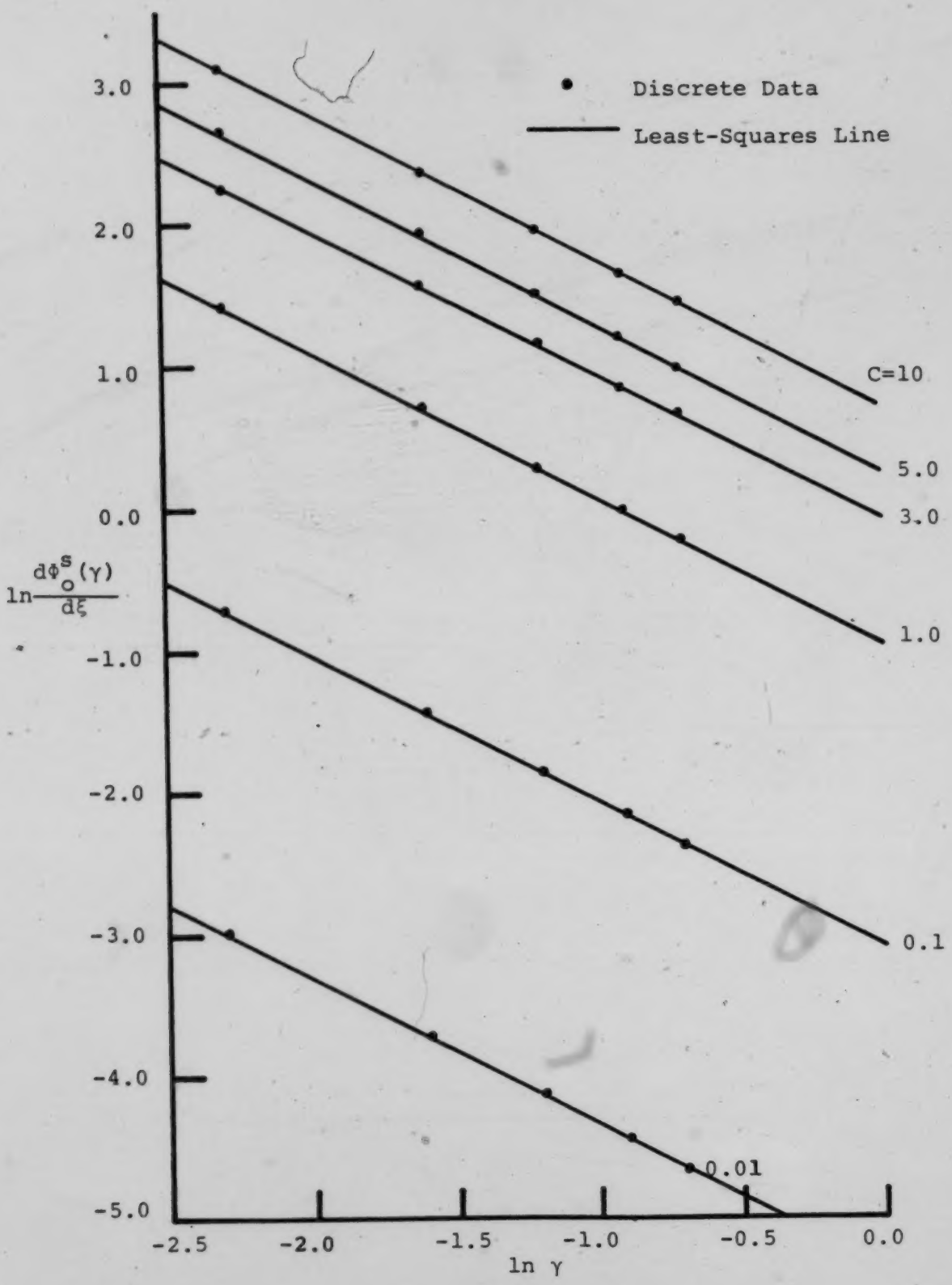

Figure 4.8 Effect of γ on Quasi-Steady Heat Transfer Rate

every C value. In other words, the total heat transfer rate can be expressed by

$$\frac{d\phi_o^s(\gamma)}{d\xi} = a\gamma^m \qquad (4.4)$$

where both "a" and "m" are functions of parameter C. For any straight line in figure (4.8), "m" is its slope and "a" is the exponent of heat transfer rate at the intersection of this line and the vertical line $\ln \gamma = 0$. Moreover, the parallel character of all the straight lines in figure (4.8) suggests that "m" can be a common slope for all these lines and is hence independent of parameter C.

In order to determine whether the slope m is a fixed constant for all values of parameter C within the range of this study, a least-squares method has been used to calculate the best fitted values of "a" and "m" for each straight line. Calculated results and associated fitting errors are listed in table below:

Table 4.1 Curve Fitting for Total Heat Transfer Rate Versus γ Plot with Different Slopes.

C	a(C)	m(C)	Sum of Least-Squares Errors
0.01	0.00461	-1.0324	1.3×10^{-4}
0.10	0.04518	-1.0324	1.3×10^{-4}
1.00	0.38132	-1.0332	1.4×10^{-4}
3.00	0.90409	-1.0349	1.6×10^{-4}
5.00	1.29554	-1.0364	1.8×10^{-4}
10.00	2.06882	-1.0315	0.5×10^{-4}

These results suggest a much simpler form of the empirical equation. The tabulated sums of least-squares errors are all in the order of 10^{-4}; this indicates the goodness of these linear curve fittings on the log-log scale. In addition, all these slopes agree with each other to the second decimal place; that is, with less than 0.4% deviation. Based on this overwhelming observation, a least-squares method was again used to calculate a common slope "m" and values of "a" for all the lines. The results are presented in Table (4.2):

Table 4.2 Curve Fitting For Total Heat Transfer Rate Versus Parameter γ Plot With Common Slope.

$m = -1.03386$

C	a(C)	Sum of Least-Squares Errors
0.01	0.00461	1.4×10^{-4}
0.10	0.04509	1.4×10^{-4}
1.00	0.38095	1.4×10^{-4}
3.00	0.90538	1.7×10^{-4}
5.00	1.30000	2.0×10^{-4}
10.00	2.06170	0.6×10^{-4}

Sums of least-squares errors remaining in the order of 10^{-4} substantiates that an empirical equation takes the form

$$\frac{d\phi_o^s(\gamma)}{d\xi} = a(C)\gamma^{-1.03386} \qquad (4.5)$$

A further attempt was to express "a" in terms of powers of parameter C. A multiple linear regression technique [47] was applied to fit a polynomial in the form

$$a(C) = b_0 + b_1C + b_2C^2 + b_3C^3 + b_4C^4 + b_5C^5$$

The best fitted polynomial was found to be

$$a(C) = 0.44066C - 0.067003C^2 + 0.007993C^3 - 0.00036377C^4$$

which yielded a total least-squares error of 0.015887 to the empirical equation (4.5).

An alternative attempt was to fit an empirical equation in a simpler form of

$$\frac{d\Phi_o^s(\gamma)}{d\xi} = a'(C)\gamma^{-1} \qquad (4.5a)$$

where function a'(C) was again expressed as a polynomial of parameter C. The result of the same multiple linear regression analysis program suggested a polynomial of

$$a'(C) = 0.46123C - 0.070065C^2 + 0.00834C^3 - 0.00037781C^4$$

Based on this polynomial, the total least-squares error in fitting equation (4.5a) was 0.589297 and the maximum percentage error was 10%.

4.1.3-2 NUSSELT NUMBER

For the classical laminar free convection problem adjacent to a vertical plate in a uniform gravitational

force field [39-43], conduction heat transfer in the solid wall or plate is not considered and the Nusselt number can be expressed by $Nu = Nu(Gr, Pr)$. Previous study [27,28] has shown that when the free convection in the fluid is coupled with the conduction heat transfer along the wall and the gravitational force field is replaced by a centrifugal force field, such as in the present quasi-steady problem, the Nusselt number is also a function of parameter γ and C. If $\bar{Nu}^s$ represents the local Nusselt number at the fin root, then for Pr=0.72, it is found that

$$\bar{Nu}^s = Ra^{1/4}(F_1 - F_2\gamma) \tag{4.6}$$

where Ra=GrPr, and F_1 and F_2 are functions of the parameter C.

For comparison, the local Nusselt number of present study is defined by

$$\bar{Nu}^s = \frac{h(L)L}{K_f} \quad \text{or} \quad \bar{Nu}^s = -\left[\frac{3RaPr}{4(1+Pr)}\right]^{1/4} \Phi^s_\eta(\gamma,0) \tag{4.7}$$

Figure (4.9) shows that when $-\Phi^s(\gamma,0)$ is plotted against parameter γ on a linear scale, data points for every value of parameter C can be fitted accurately into least-squares line. In other words,

$$\bar{Nu}^s\left[\frac{3RaPr}{4(1+Pr)}\right]^{-1/4} = -\Phi^s_\eta(\gamma,0) = G_1 - G_2\gamma \tag{4.8}$$

where G_1 and G_2 are functions of the parameter C. The calculated values of G_1 and G_2 are listed in Table (4.3).

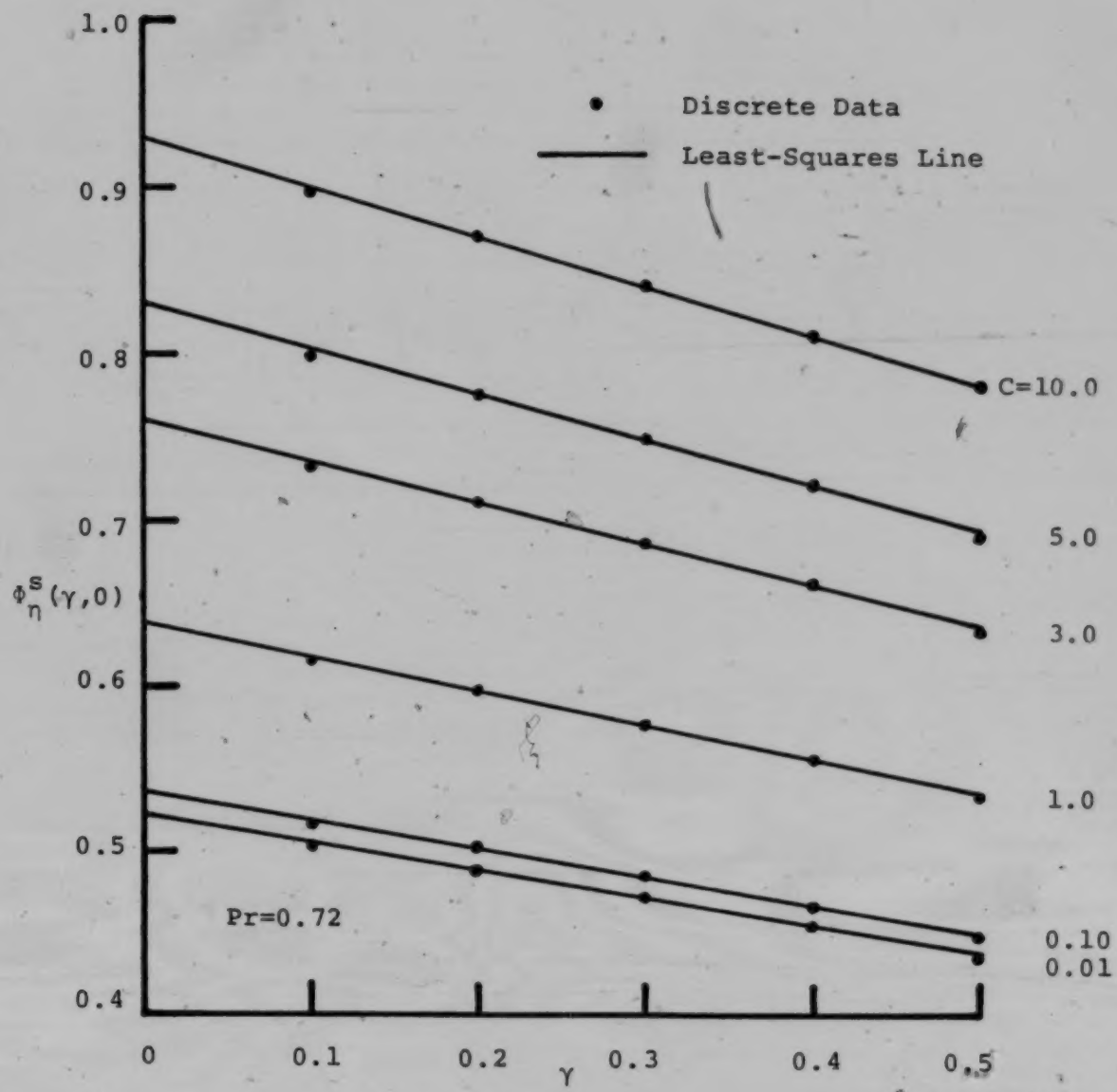

Figure 4.9 Nusselt Number of Quasi-Steady-State Solutions

Table 4.3 Curve Fitting For Nusselt Number Versus Parameter γ Plot.

C	G_1	G_2	Sum of Least-Squares Errors
0.01	0.522	0.167	0.8×10^{-5}
0.10	0.536	0.172	0.8×10^{-5}
1.00	0.638	0.206	1.2×10^{-5}
3.00	0.760	0.249	1.8×10^{-5}
5.00	0.830	0.275	2.2×10^{-5}
10.00	0.929	0.297	0.5×10^{-5}

In order to make comparisons between equation (4.6), obtained from previous study, and equation (4.8) of the present investigation, Pr=0.72 can be substituted into the latter to yield

$$\overline{Nu}^s = Ra^{1/4}(F_1' - F_2'\gamma) \qquad (4.9)$$

Here, F_2' is the slope of the least-squares fitted line of the $\overline{Nu}^s/Ra^{1/4}$ versus γ plot, and F_1' is nothing but the predicted value of $\overline{Nu}^s/Ra^{1/4}$ for $\gamma=0$; in fact, the static fin problem [35].

Calculated values of F_1' and F_2' are tabulated in Table (4.4) together with their comparative quantities F_1 and F_2 of previous work [27,28]. Apparently, there are some discrepancies between slopes F_2 and F_2' of the least-squares fitted lines. However, both F_1' of the present

study and F_1 of the previous work predict almost the same value of $\bar{Nu}/Ra^{1/4}$ for the static fin problem.

Table 4.4 Comparison of Least-Squares Fits

Parameter C	Previous Work F_1	Previous Work F_2	Present Study F_1'	Present Study F_2'
0.01	0.389	0.116	0.390	0.125
0.10	0.401	0.126	0.401	0.129
1.00	0.484	0.178	0.478	0.154
3.00	0.573	0.205	0.573	0.186
5.00	0.623	0.214	0.621	0.206
10.00	0.696	0.228	0.695	0.222

4.1.3-3 Fin Effectiveness ε

Lock and Gunn [35] have defined fin effectiveness for a variable heat transfer coefficient h along the fin surface to be

$$\varepsilon = \frac{\int_0^L h(X)\theta_o(X)dX}{h(L)\theta_o(L)L} \tag{4.10}$$

Since the numerator represents the total heat transfer rate across the thermal boundary layer at one side of the fin, it must be equal to one half of the total heat transfer rate across the fin base, that is

$$\int_0^L h(X)\theta_o(X)dX = -WK_s\frac{d\theta_o(L)}{dX} \tag{4.11}$$

where W is the half-width of the fin base. Moreover, the denominator in equation (4.10) represents the local

convective heat transfer rate at the fin root multiplied by the fin length; hence

$$h(L)\theta_o(L)L = -LK_f\theta_y(L,0) \qquad (4.12)$$

By combining equations (4.10)-(4.12) and also by using normalized variables (2.23) and transformations (3.5), the fin effectiveness becomes

$$\varepsilon = \frac{\gamma}{C}\left[\frac{4(1+Pr)}{3Pr}\right]^{1/4}\frac{d\phi_o^s(\gamma)}{d\xi}\Big/\phi_\eta^s(\gamma,0) \qquad (4.10a)$$

In order to compare this with the fin effectiveness obtained in the previous study [27,28], Pr=0.72 is again used in above equation. For the sake of clearness, only data for γ=0.1, 0.3 and 0.5 are compared in figure (4.10). The present data, represented by discrete points, are in excellent agreement with the curves of previous results.

4.2 PERTURBATION APPROXIMATION

When the Froude number is not extremely large, the governing equations (3.17)-(3.19) and boundary conditions (3.20)-(3.21) indicate that solutions of this periodic problem may be affected by parameters Fr, K_1, K_2, C, and γ. By means of the series expansion (3.22), Fr is removed from all the perturbation equations and their boundary conditions. Nevertheless, numerical work in solving equations (3.23)-(3.28) for the remaining four parameters at various levels is still expensive; only selected

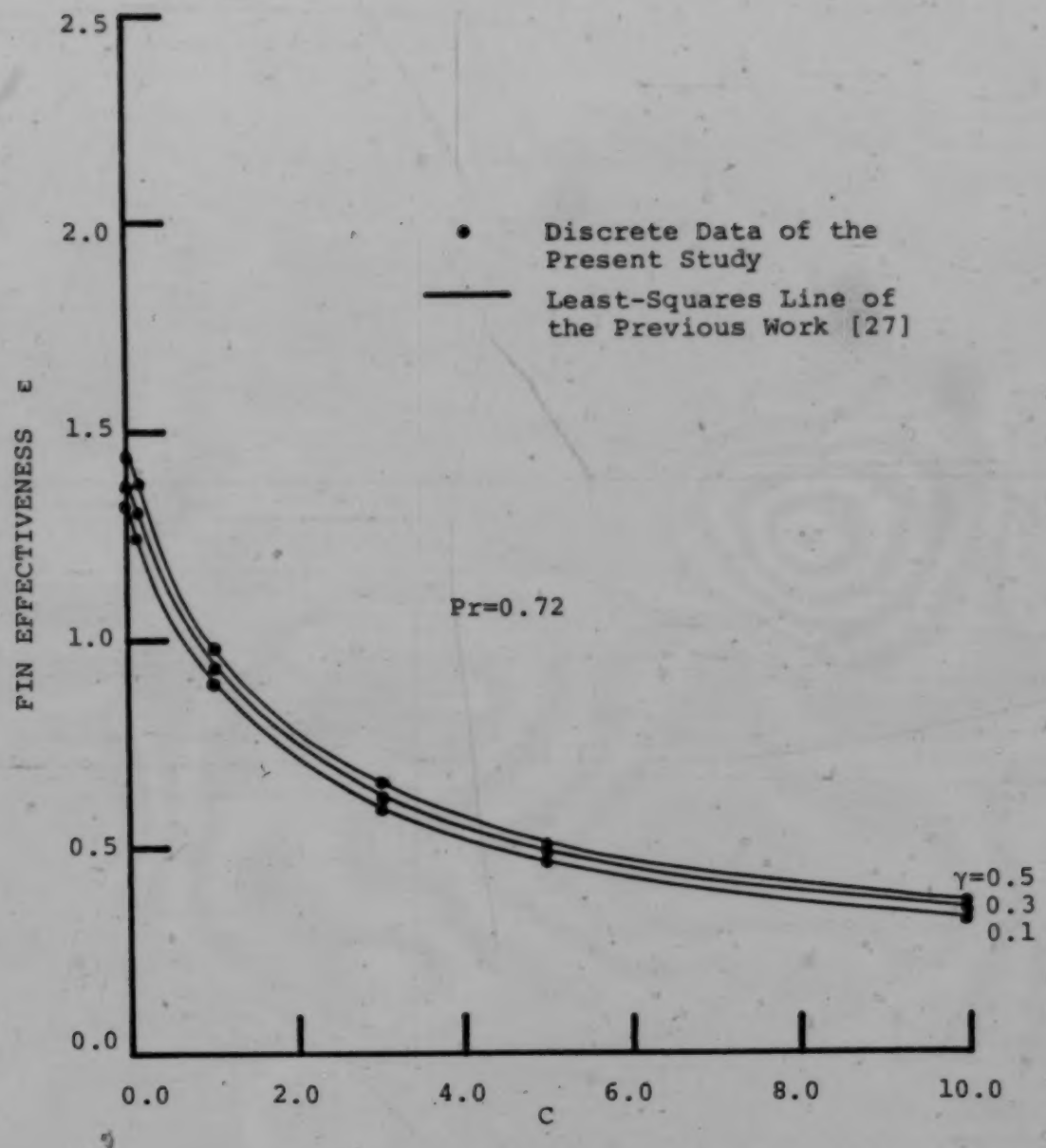

Figure 4.10 Fin Effectiveness of Quasi-Steady Solutions

parameter values are used here for economical reasons.

The rate of solution matching at the solid-fluid interface was investigated for one γ value. From the quasi-steady results, the effect of γ on the zeroth order perturbation solutions was found to be considerably smaller than that of C. Basically, one representative level of γ=0.1 was used throughout the investigation of this perturbation approximation, and only in some special cases, were solutions for γ=0.5 generated. Similar to the preceeding study, the effect of C was reviewed at six parameter levels (0.01, 0.1, 1.0, 3.0, 5.0 and 10.0) for K_1=1.0 and K_2=1.0; no difficulty was encountered during the integration of equations (3.23)-(3.28). Perturbed solutions of the conduction problem generally matched with that of the free convection problem along the solid-fluid interface within 8-10 iterations. An exception was the case of C=10 which took 25 iterative loops to procure the convergence in two interfacial temperature profiles $\hat{\Phi}_o$ and $\tilde{\Phi}_o$. On average, one iteration required approximately one minute computation on an IBM 360/67 computer.

By setting C=1.0 and K_2=1.0, the parameter effect of K_1 on the convergent rate of interfacial solutions was investigated at four levels (0.1, 1.0, 10, and 100). Except when K_1=100, solutions in general took 7-9 iterations, i.e. 7-9 minutes, to converge. An attempt for K_1=100 was

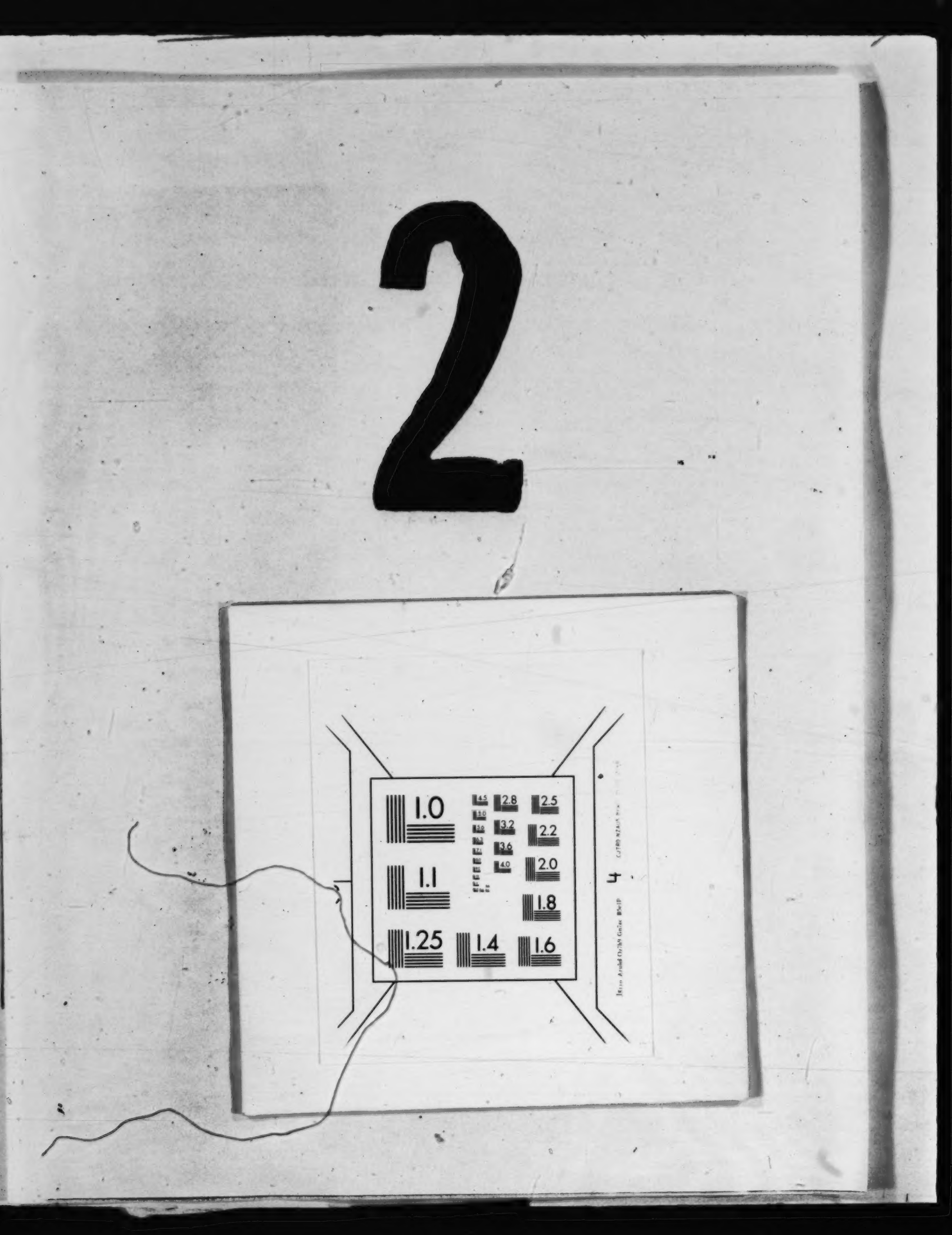
2
1.0
1.1
1.25
1.4
1.6
1.8
2.0
2.2
2.5
2.8
3.2
3.6
4.0
4.5
5.0
5.6
6.3
7.1
8.0
9.0
10
11
12
14
16
18
20
22
25
28
32
36
40
45
50
56
63
71
80
90
100
4

unsuccessful due to the divergence of the solutions. An alternative attempt using K_1=50 led to the converged solutions after 20 iterative loops. A further try using K_1=50 and resetting C=0.01, reduced the required number of iterations to 5. This observation again emphasized the anticipated fact that the stronger the coupling of conduction and free convection problems, the more difficult the convergence of their solutions.

The effect of parameter K_2 on the solution matching at the interface was also studied. When C=1.0 and K_1=1.0, solutions converged within 7 iterations for all four parameter levels of K_2 (0.1, 1.0, 10 and 100). In fact, a further attempt for K_2=1000 also produced converged result within 11 iterative loops. It was therefore concluded that when C=1.0 and K_1=1.0, the convergent rate of the perturbation solutions was rather insensitive to the parameter K_2.

4.2.1 SOLUTIONS OF BOUNDARY LAYER PROBLEM

Prior to investigating velocity and temperature profiles of the recombined (i.e. perturbed) results, it is logical to explore some characteristics of the perturbation solutions.

The amplitudes of the first-order perturbation solutions: $\tilde{f}_\eta$, $\tilde{\Phi}$, $\hat{f}_\eta$, and $\hat{\Phi}$, for a typical example of γ=0.1, C=0.01, K_1=1.0, and K_2=100 are presented in figure (4.11)

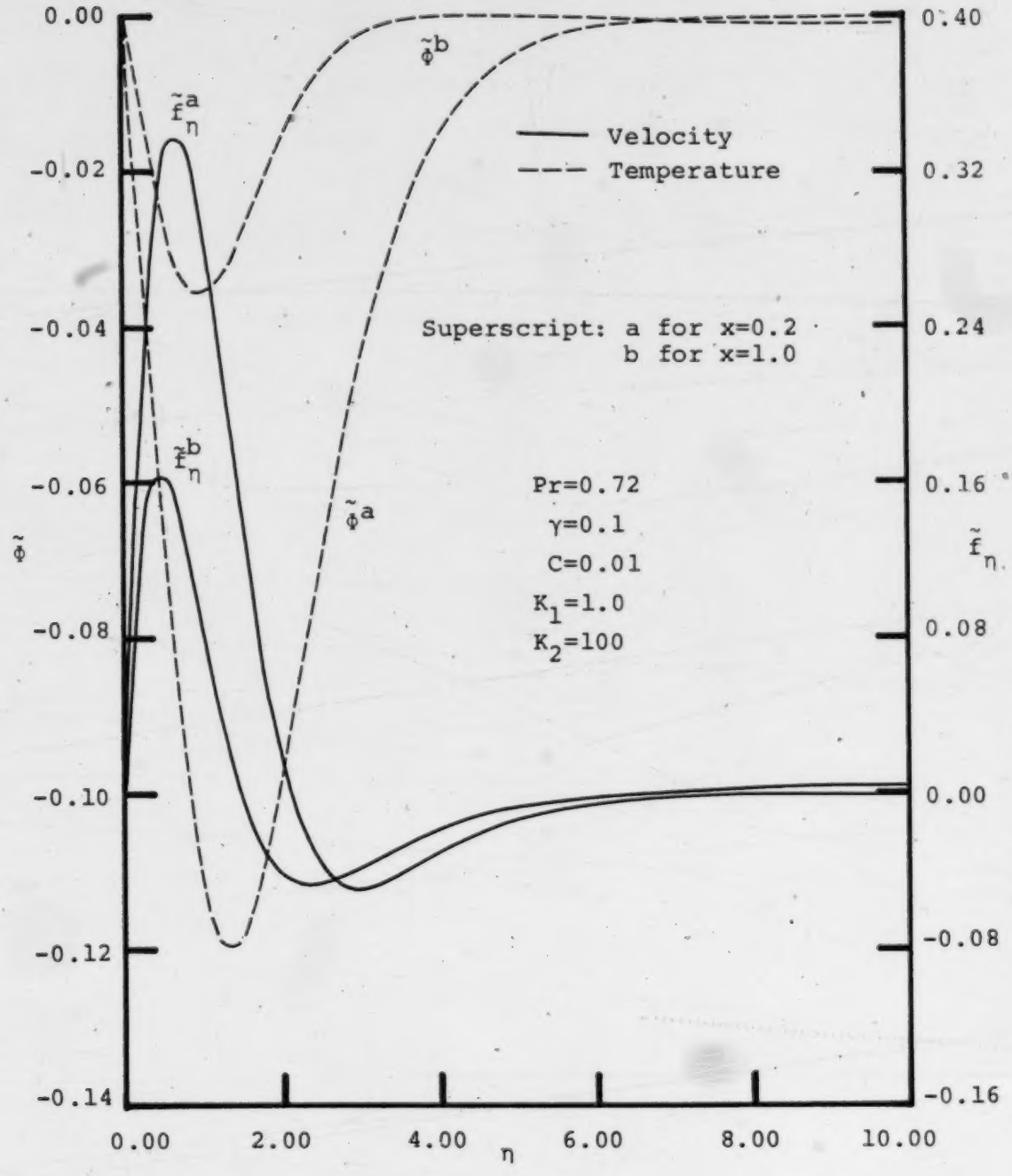

Figure 4.11 Even Part of the Perturbation Solutions for the Boundary Layer Problem

and (4.12). The odd parts of the perturbation to the steady solutions are approximately ten times smaller than the even parts. Examination of all the cases under this study shows that this observation is generally true except in the cases of $K_1>0$ [1], where both odd and even parts of the perturbation solutions are of the same order of magnitude. In spite of these relative magnitudes, it is more important to determine whether they can introduce significant periodic effects with a reasonable degree of accuracy.

In general, the truncation error of a first-order perturbation series expansion can be estimated by the magnitude of the second-order terms. Accordingly the accuracy of the present results relies on the product of Fr^{-2} and the second-order perturbation solutions. On account of the fact that both steady and periodic parts of the solutions have been properly normalized in Appendix B (during the derivation of governing equations), the magnitude of the second-order perturbation results is of order one and the accuracy of this first-order perturbation approximation is therefore in the order of Fr^{-2}. If a truncation error of $O[10^{-2}]$ is the acceptable limit, ten is then the smallest Fr value to be used in studying these perturbation solutions.

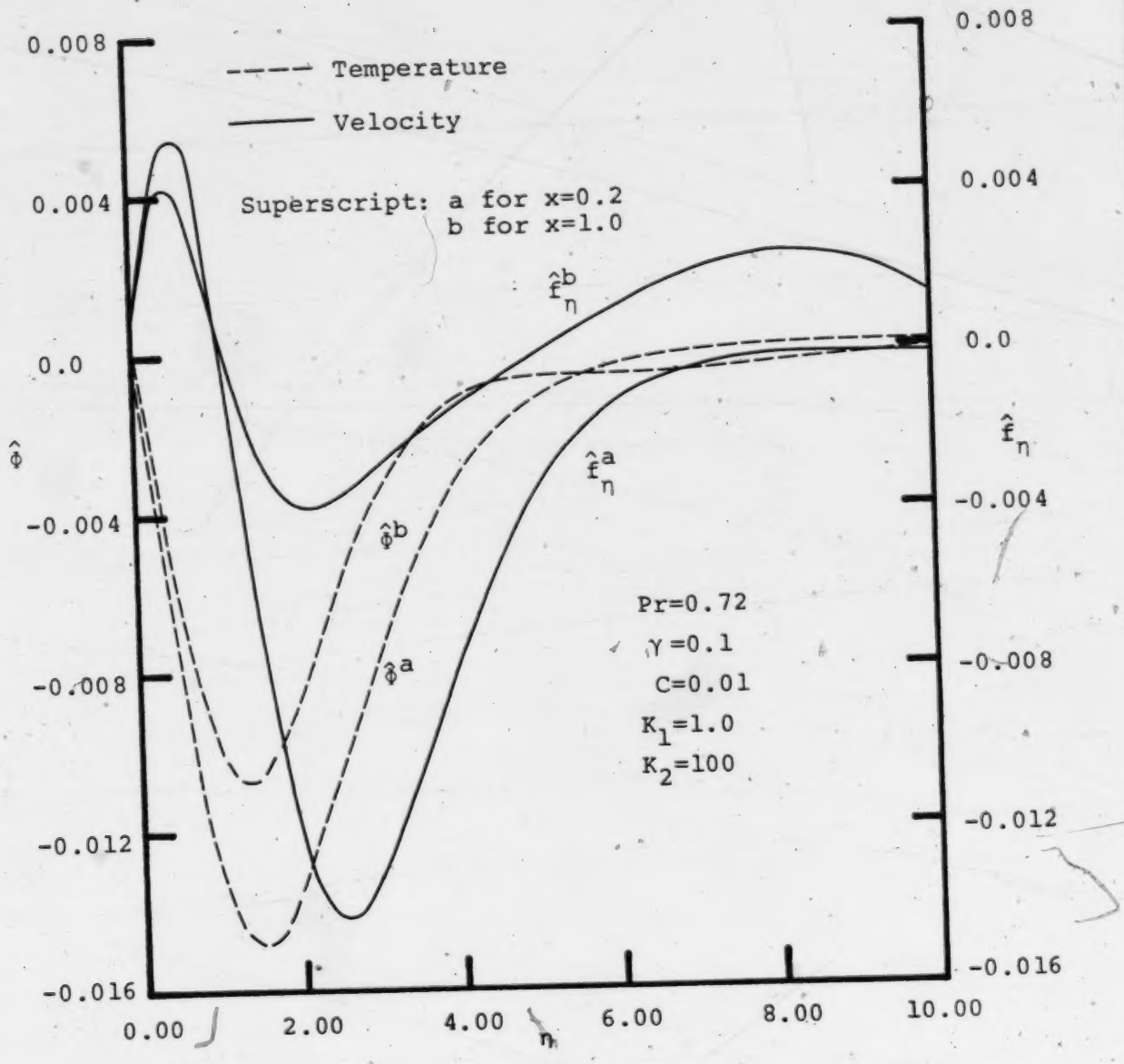

Figure 4.12 Odd Part of the Perturbation Solutions for the Boundary Layer Problem

Figures (4.13)-(4.18) show some examples depicting the periodic features of boundary layer solutions for different parameter values. None of them shows a noticeable periodicity in the fluid temperature when Fr is equal to or greater than 10; on the other hand, velocity profiles for Fr=10 all reveal some periodic feature in the vicinity of their maximum values. Figure (4.18) shows that this periodicity disappears in both temperature and velocity profiles when Fr=100; it would appear that the problem has reached its quasi-steady state when Fr approaches this order of magnitude.

4.2.1-1 EFFECT OF PARAMETER γ

Boundary layer solutions at the roots of two different fins (γ=0.1 and 0.5) are compared in figure (4.13) for C=0.01, K_1=1.0, K_2=1.0, and Fr=10. Both thermal and momentum boundary layers are seen to increase their thicknesses with parameter γ; but as far as the normalized quantities are of concern, the greater the parameter γ the smaller the magnitude of the maximum velocity. Although the non-periodic temperature across the boundary layer for γ=0.5 is generally higher than that for γ=0.1, the steeper temperature gradient for the latter indicates a higher local heat transfer rate at the fin root when the parameter γ is smaller.

Figure (4.13) also shows that solutions vary with the fin position. The inclination of the rotating fin is indicated by the angle starting from 0^o when the fin is

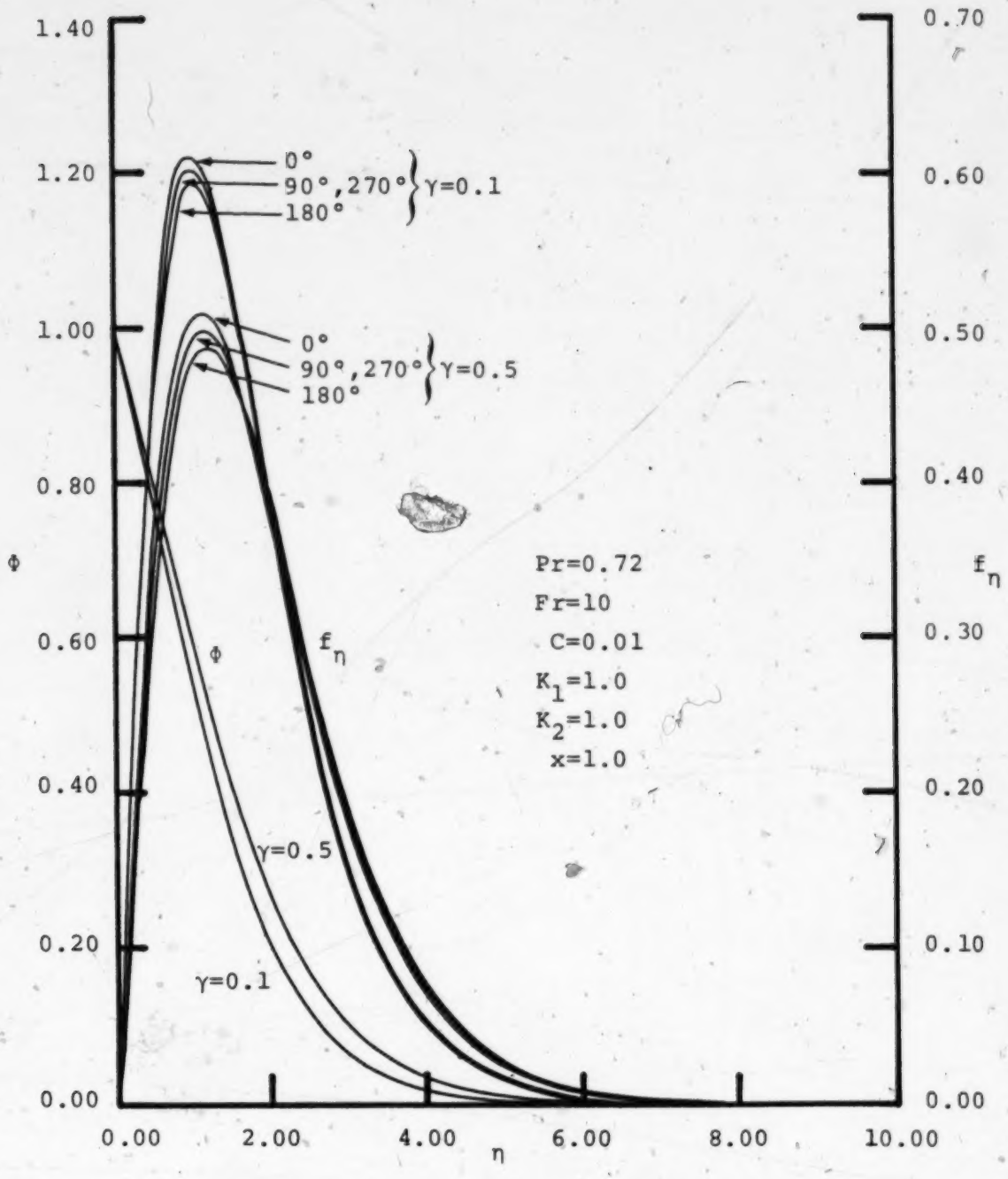

Figure 4.13 Effect of γ on the Perturbed Boundary Layer Solutions

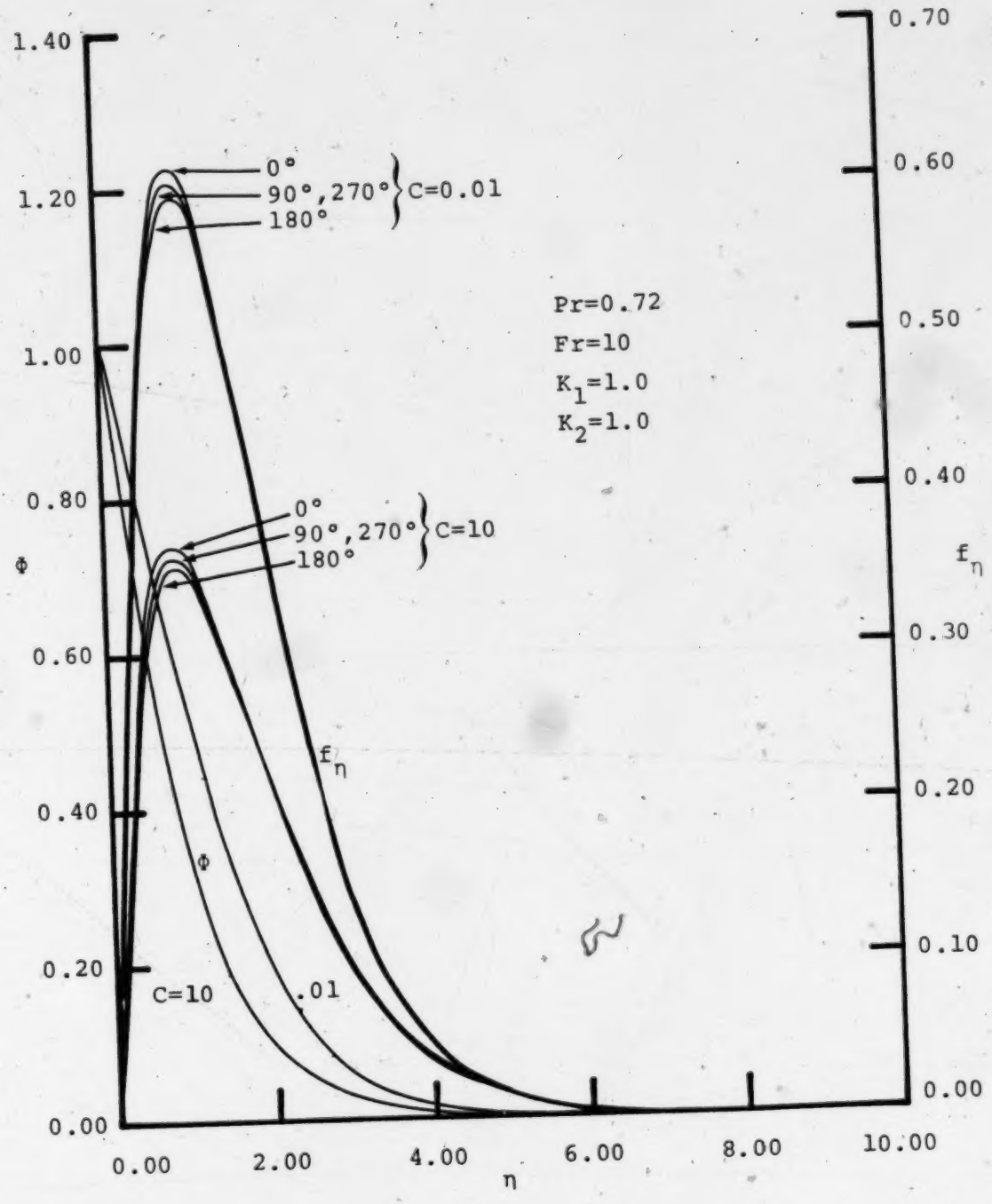

Figure 4.14 Effect of C on the Perturbed Boundary Layer Solutions

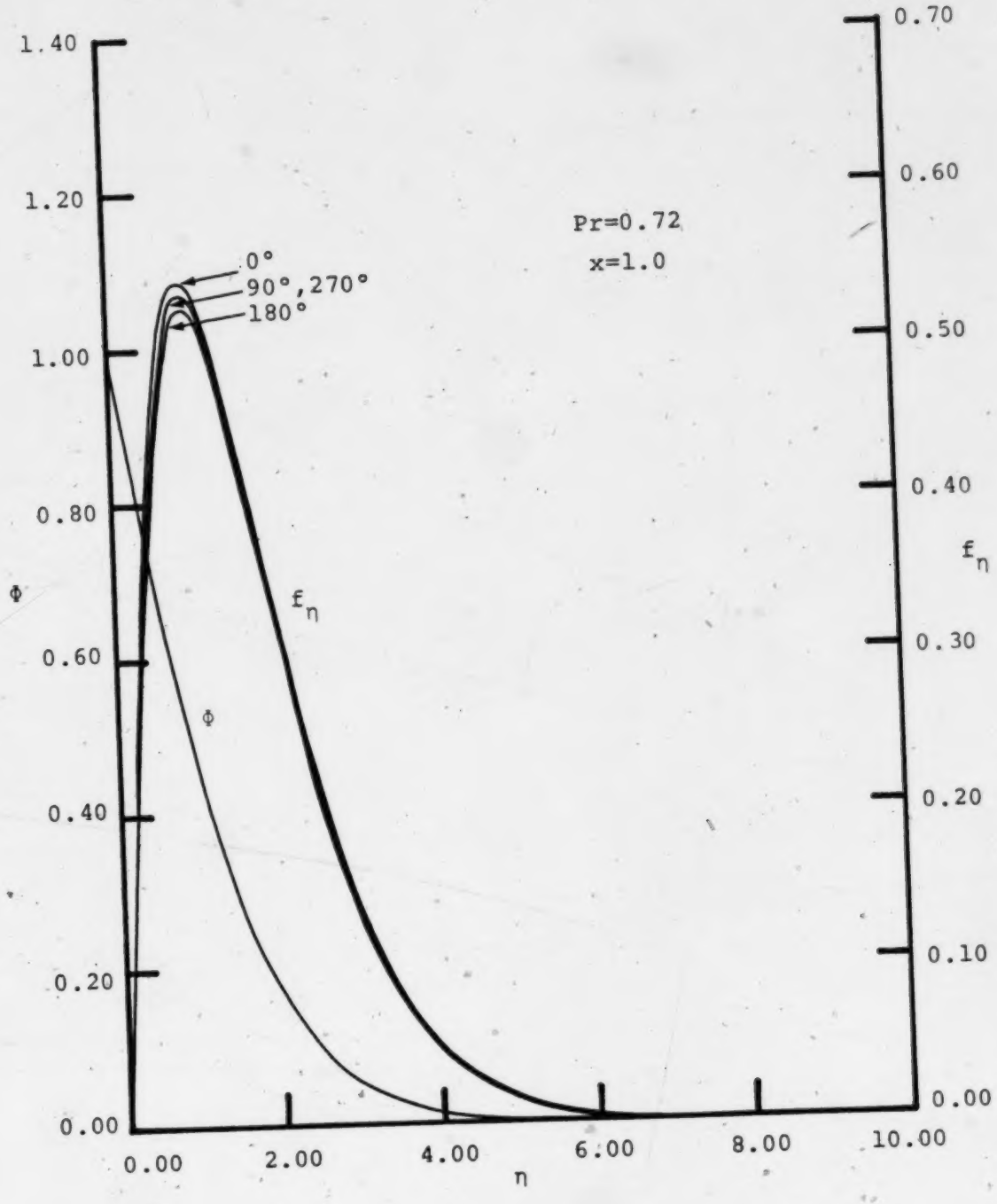

Figure 4.15 Perturbed Boundary Layer Solutions for Fr=10, C=1, K_1=1, K_2=1 and γ=0.1

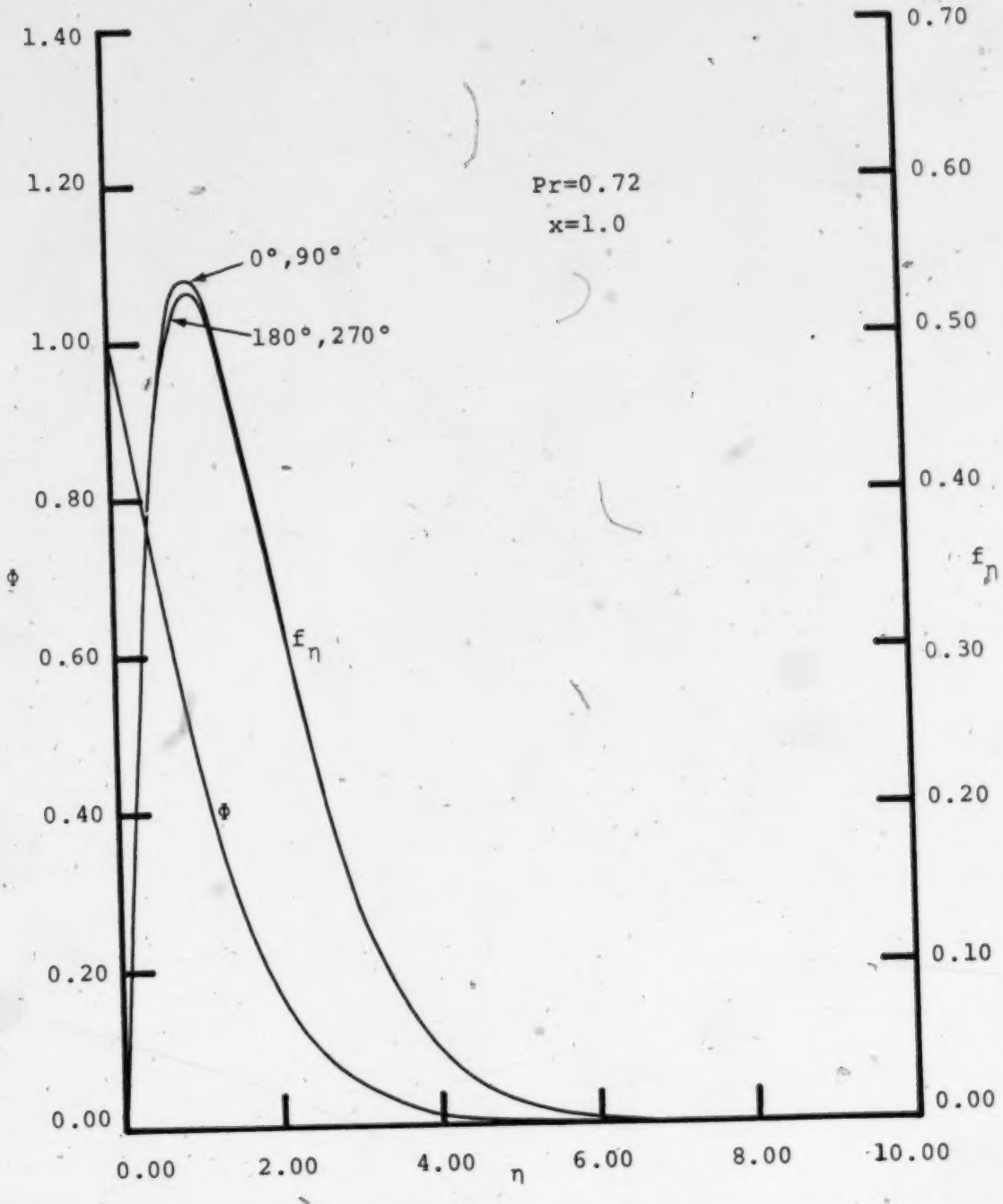

Figure 4.16 Perturbed Boundary Layer Solutions for Fr=10, C=1, K_1=50, K_2=1 and γ=0.1

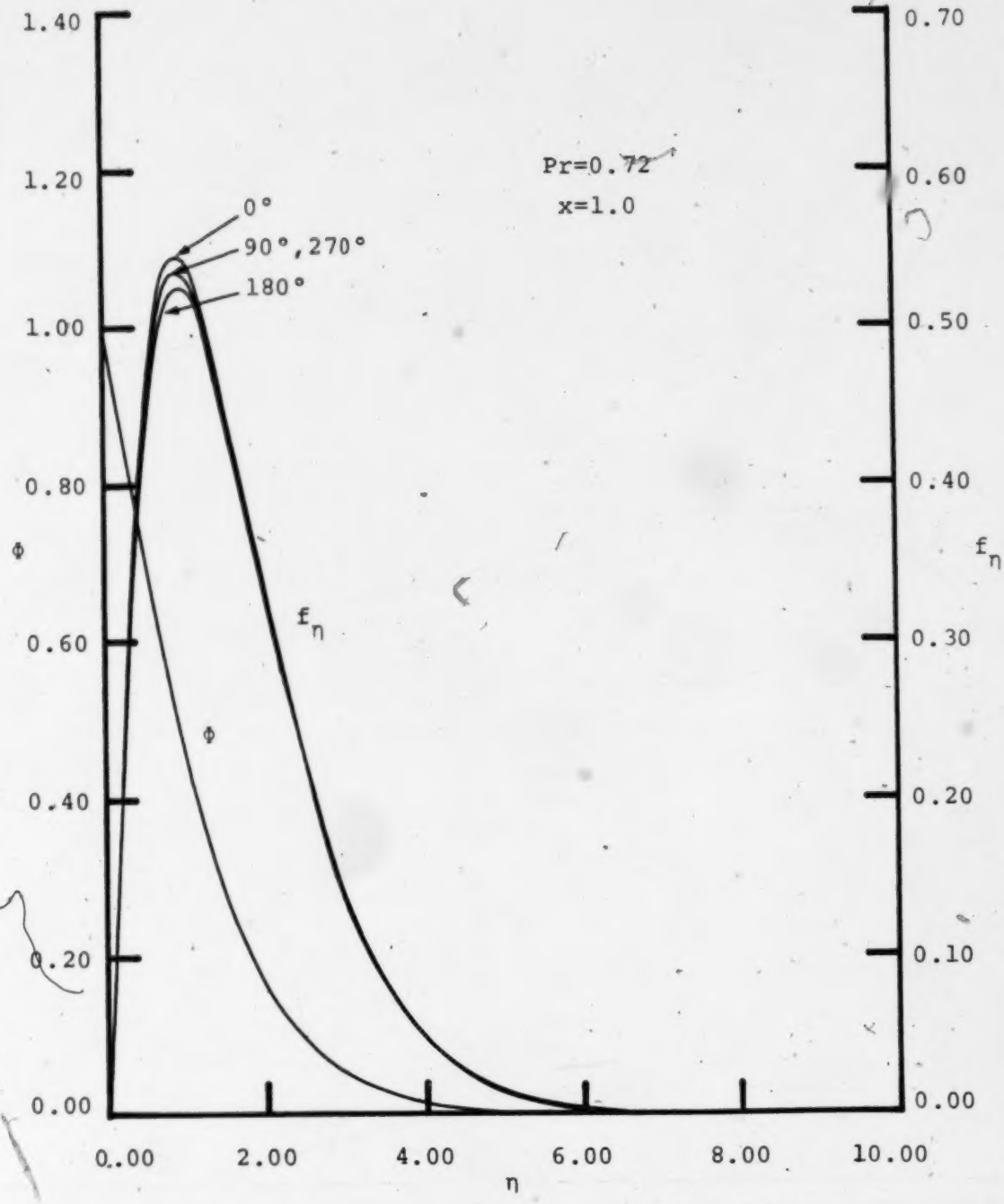

Figure 4.17 Perturbed Boundary Layer Solutions for Fr=10, C=1, K_1=1, K_2=100 and γ=0.1

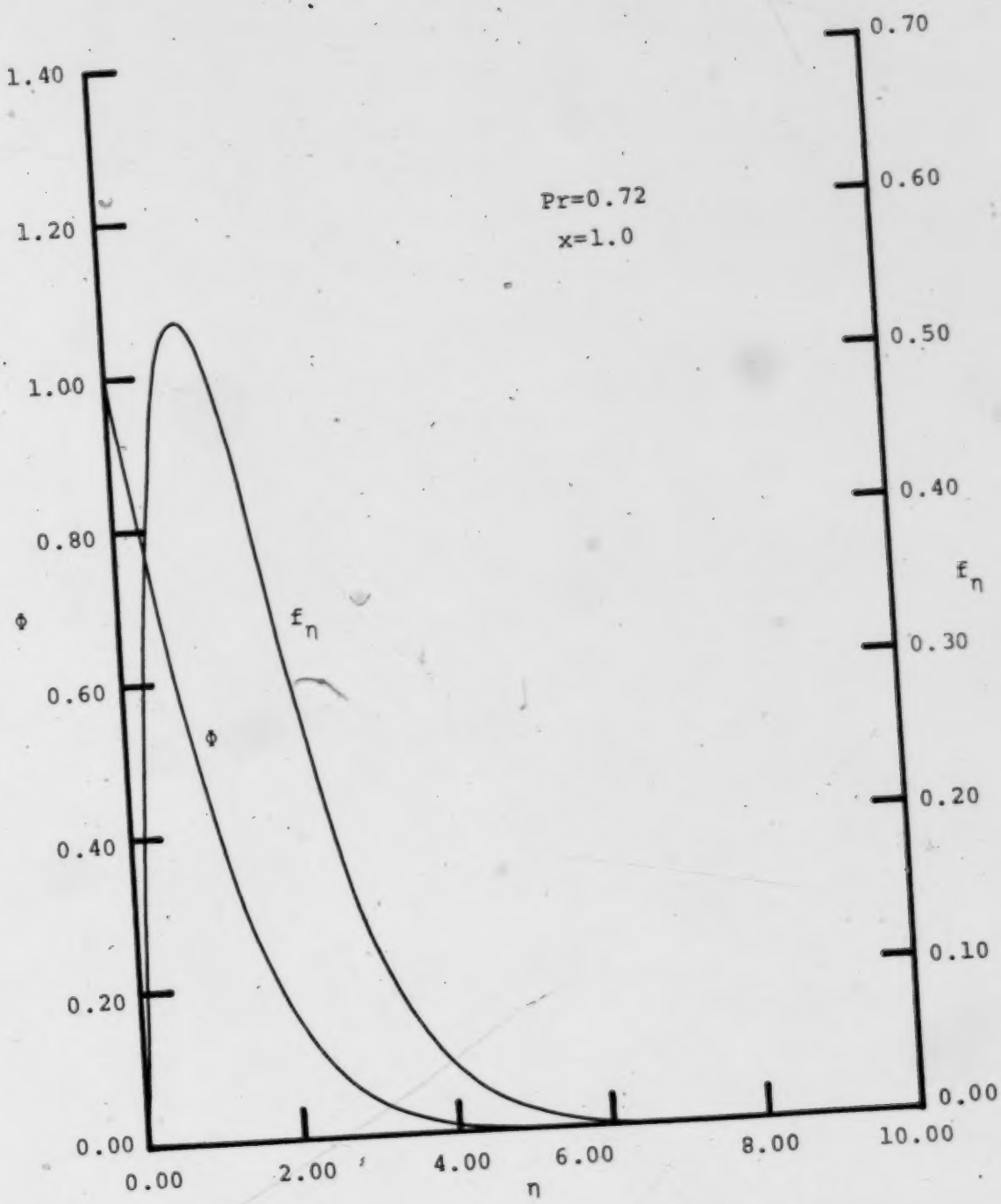

Figure 4.18 Perturbed Boundary Layer Solutions for Fr=100, C=1, K_1=1, K_2=1 and γ=0.1

pointing downward and rotating counter-clockwise. When the fin is making a 0^{o}-angle with the vertical line, the buoyancy effects of gravity and centrifugal force concur; the resultant velocity f_n is hence greater than that for the 180^{o} position, in which these two driving forces oppose each other and their total buoyancy effect decreases accordingly. No difference in the velocity profiles for the fin at the two horizontal positions has been noticed.

4.2.1-2 EFFECT OF PARAMETER C

Figure (4.14) discloses the effect of parameter C on the thermal and the momentum boundary layers. The thicknesses of these boundary layers are insensitive to parameter C, although both the temperature and the velocity are greater when C is smaller. Moreover, the temperature gradients at the solid-fluid interface (η=0) suggest a higher heat transfer rate from solid to fluid at the fin root when the parameter C increases. This is logical because the more conductive the fluid (i.e. the greater C) the higher the heat transfer rate. Again, fluid velocity for the fin 0^{o} is greater than that at 180^{o}, and no deviation is noticeable between the velocity profiles for the fin at 90^{o} and 270^{o} positions.

4.2.1-3 EFFECT OF PARAMETER K_1

By using the same parameters C, K_2, and Fr, the velocity and temperature profiles of the fluid at x=1.0

for K_1=1.0 and 50.0 are presented in figures (4.15) and (4.16) respectively. For K_1=1.0, no difference is noted in the velocity profile when the fin is at two horizontal positions (corresponding to 90° and 270° in the drawing). This agreement in velocity profile is mainly due to the extremely small value of $\hat{f}_\eta$ in the perturbation solutions when K_1=1.0. However when K_1=50, figure (4.16) shows that the velocity f_η for the fin at 90° deviates appreciably in its peak value from that at 270°. On the other hand, this velocity profile hardly varies as the fin rotates from 0° to 90° or from 180° to 270°. This temporary steadiness in fluid velocity is because the odd part $\hat{f}_\eta$ of the perturbation solutions has the same order of magnitude as the even part $\tilde{f}_\eta$, and generates noticeable effect on the solution f_η when the parameter K_1 increases.

The rate of solution convergence can be affected by parameter K_1. Mathematically, this K_1 value represents the intensity of coupling between the perturbed boundary layer equations while physically it indicates the significance of transient effects on the boundary layer solutions. As mentioned before, the difficulty in achieving the interfacial convergence of the perturbed solutions increases with parameter K_1, but decreases more rapidly with parameter C. In other words, the parameter C plays a much more important role than K_1 in the convergence of interfacial solutions; however, a large K_1-value does aggravate the

convergence problem when the parameter C is not much smaller than unity.

4.2.1-4 EFFECT OF PARAMETER K_2

Like figure (4.15) for K_2=1, figure (4.17) depicts the perturbed boundary layer solutions for K_2=100 while the other parameters remain unchanged. Almost identical solutions from the above two figures reveal that this parameter K_2 has no influence at all on the perturbed boundary layer solutions.

4.2.1-5 EFFECT OF FROUDE NUMBER (Fr)

The larger the Froude number the smaller its effect on the solutions. Figure (4.18) gives the boundary layer solutions at x=1.0 for Fr=100. Comparison of these solutions with those presented in figure (4.15) discloses that the periodic feature vanishes, as expected, when the Froude number becomes very large. In fact it is reasonable to predict that the solution in figure (4.18) is very close to the quasi-steady results for extremely large Froude number. This prediction is proved to be correct as solutions in figure (4.18) match completely with the quasi-steady solutions for γ=0.1 presented in figure (4.2).

4.2.2 SOLUTIONS OF CONDUCTION PROBLEM

Parameter C has a significant effect on the convergence of the perturbation temperatures along solid fin. The magnitudes of all the perturbation temperatures $\tilde{\Phi}_o$ and $\hat{\Phi}_o$ obtained in this study are so small that after being

divided by the minimal Froude number of 10, none of them can give rise to any noticeable change in the quasi-steady solution Φ_o along the fin. Therefore, none of these parameters noticeably affect the solution Φ_o in the conductive fin problem. Nevertheless, experience shows that it is more difficult to satisfy the convergent criterion of 10^{-5} for these perturbation temperatures $\tilde{\Phi}_o$ and $\hat{\Phi}_o$ when the parameter C becomes larger. This implies that at least one of the above perturbation temperature either increases its magnitude or change profile with C.

Convergent rate of the perturbation temperature along the fin decreases inversely with magnitude. Figure (4.19) depicts solutions $\tilde{\Phi}_o$ and $\hat{\Phi}_o$ for γ=0.1, K_1=1.0 at three levels of parameter C: 0.01, 1.0, and 10. When C=0.01, both $\tilde{\Phi}_o$ and $\hat{\Phi}_o$ are very small and their magnitudes decrease monotonically from fin tip (x=0) to fin root (x=1); these two favourable features contribute to the rapid convergence of the solutions at the solid-fluid interface. As the parameter C changes from 0.01 to 1.0, the magnitudes of $\tilde{\Phi}_o$ and $\hat{\Phi}_o$ increase approximately fifty times without losing the aforesaid monotonically decreasing feature; this increase in magnitude results in the requirement of more iterations for the interfacial convergence.

Shapes of the perturbation temperatures $\tilde{\Phi}_o$ and $\hat{\Phi}_o$ significantly affect the rate of solution convergence.

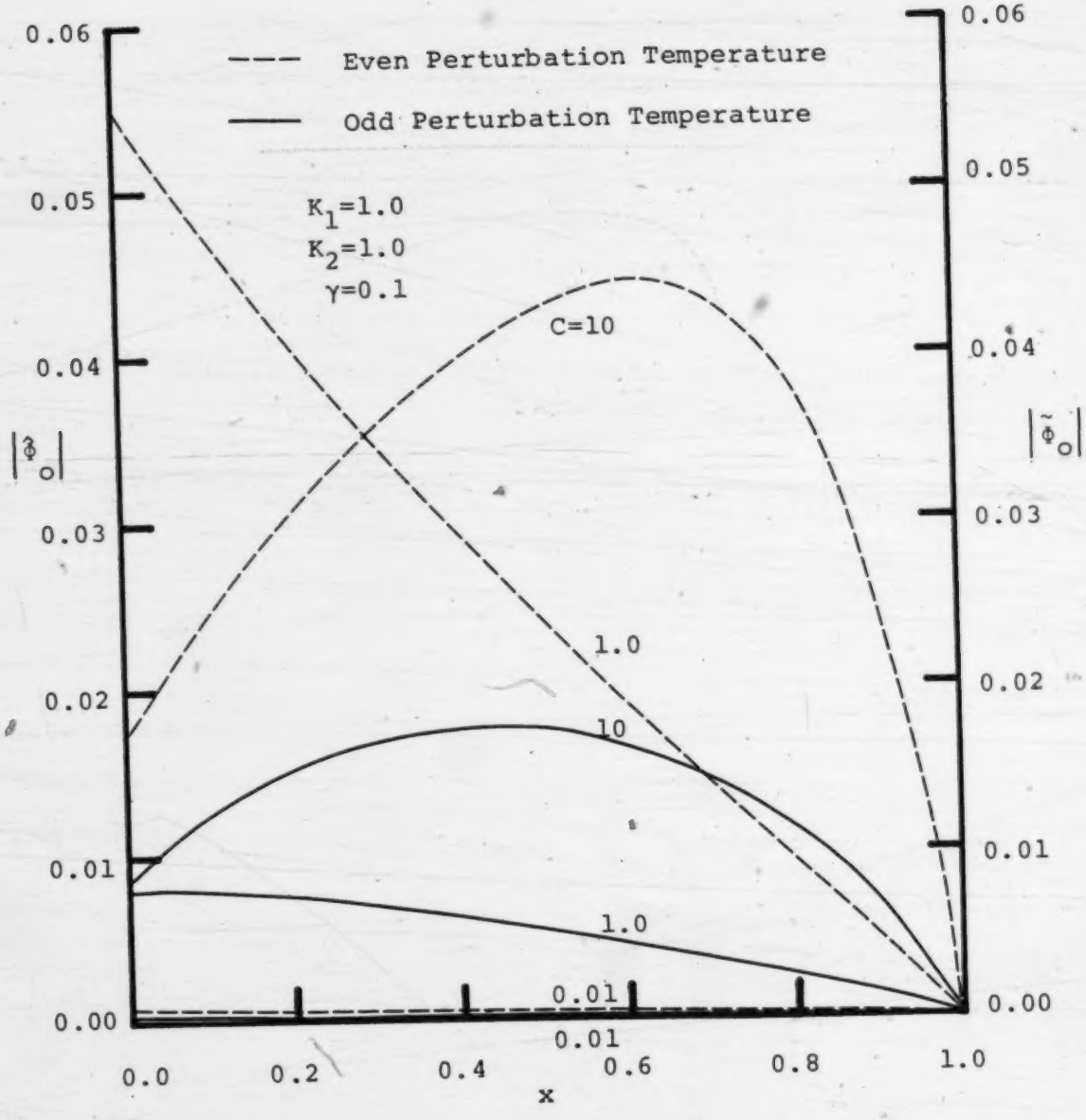

Figure 4.19 First-Order Perturbation Temperatures Along Solid Fin

an obvious change in the profiles of these perturbation temperatures appears when C=10. In spite of keeping the same order of magnitude as when C=1, both $\tilde{\Phi}_o$ and $\hat{\Phi}_o$ increase with distance x from the fin tip to their maximal magnitudes at certain (but different) x-values, and then decrease inversely with x to zero at the fin root. This loss of monotonically varying characteristic in the magnitudes of $\tilde{\Phi}_o$ and $\hat{\Phi}_o$ is possibly the major hindrance to the rapid convergence of these perturbation solutions at the solid-fluid interface when the parameter C is much greater than unity.

4.2.3 SOLUTIONS OF OVERALL PROBLEM

It has been found that when the Froude number is not less than ten, the temperature of neither fluid nor solid fin experiences any noticeable disturbance from the perturbation solutions. An alternative investigation may be undertaken on the possible disturbance in temperature gradient and heat flux which, as demonstrated in section 4.13, are closely related to the total heat transfer rate, the Nusselt number, and the fin effectiveness.

4.2.3-1 TOTAL HEAT TRANSFER RATE

By referring to equation (4.3), the heat transfer rate per unit base area of the fin is

$$q = \frac{K_s \Theta_r}{R_t} \frac{\partial \Phi_o(\gamma, \tau)}{\partial \xi} \qquad (4.13)$$

That is, the total heat transfer rate across the fin base at time τ is proportional to the temperature gradient $\frac{\partial \Phi_o(\gamma,\tau)}{\partial \xi}$, which can be further approximated by the perturbation result:

$$\frac{\partial \Phi_o(\gamma,\tau)}{\partial \xi} = \frac{d\Phi_o^s(\gamma)}{d\xi} + \frac{1}{Fr}\left[\frac{d\tilde{\Phi}_o(\gamma)}{d\xi}\cos(2\pi\tau) + \frac{d\hat{\Phi}_o(\gamma)}{d\xi}\sin(2\pi\tau)\right] \tag{4.14}$$

Figure (4.20) demonstrates the periodic variation of the root heat transfer rate as the fin changes its position angle α while rotating (the fin is projecting downward when τ=0 or 1). It is clear that if Fr increases to 100, the total heat transfer rate approaches that of the quasi-steady solution. When Fr decreases to 10, the fluctuating amplitude of this total heat transfer rate increases to approximately 2% of the quasi-steady solution. A dashed line for Fr=2 is also presented in figure (4.20) though the accuracy of this first-order perturbation approximation is considered to be extremely questionable when this Fr value is less than 10. The plot, however, still indicates that a fluctuation in the order of 10% is plausible for Fr=2.

All the curves in figure (4.20) have some common features which may be used to determine the proper initial time level for the direct integration approach. First, every curve is fairly linear when τ varies from 1/8 to 3/8

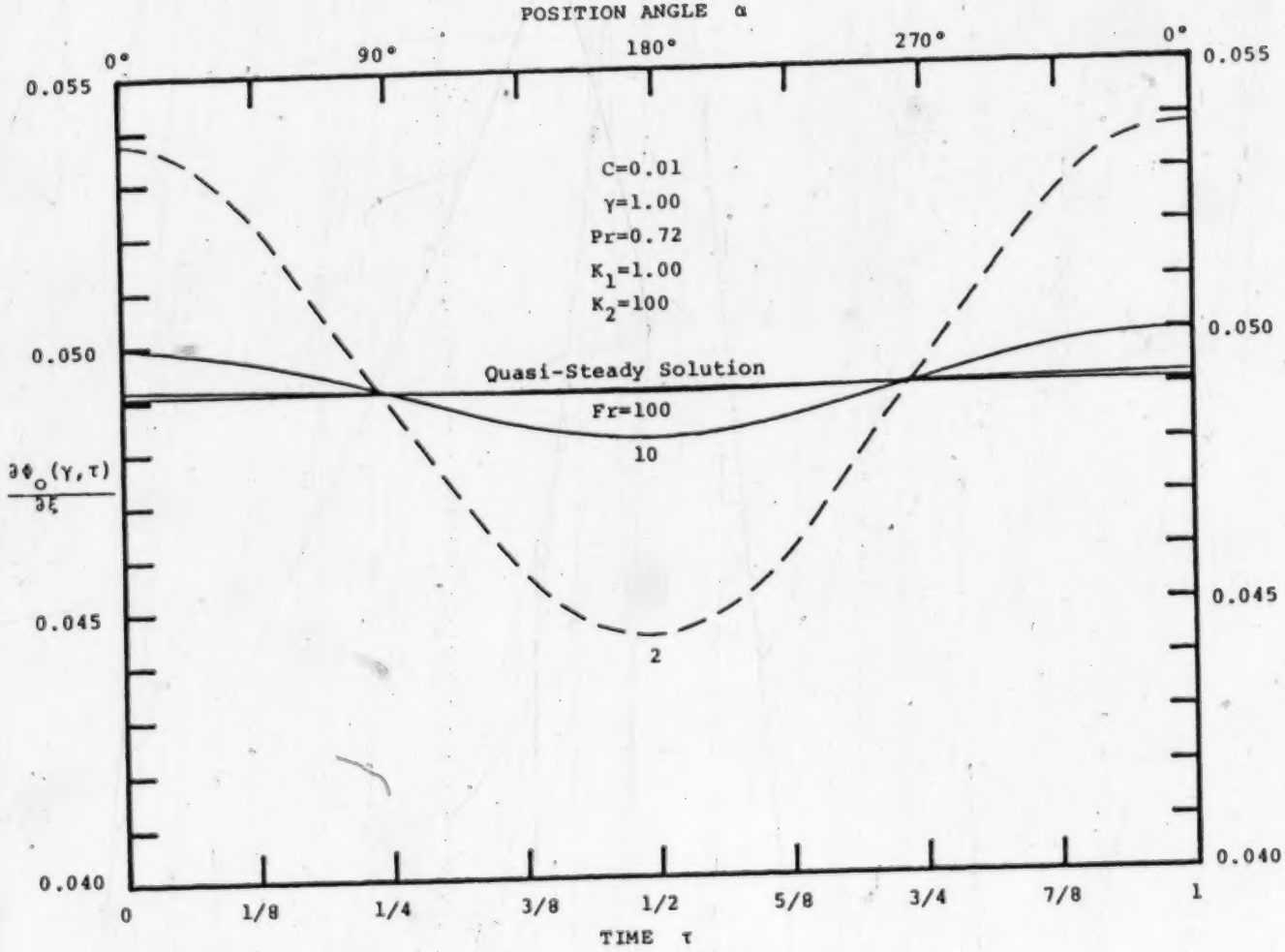

Figure 4.20 Periodic Variation in Perturbed Heat Transfer Rate

and from 5/8 to 7/8. In addition, the peak point and valley point of every curve are always situated at τ=0 and 1/2, respectively, and all the curves intersect the quasi-steady result in the vicinity of two points: τ=1/4 and 3/4. All this suggests that either τ=1/4 or 3/4 may be chosen as the initial time level for the direct integration of governing equations (3.17)-(3.19).

4.2.3-2 NUSSELT NUMBER

From equation (4.7), the Nusselt number at the root of a rotating fin for this periodic heat transfer problem can be deduced: that is

$$Nu = -\left[\frac{3RaPr}{4(1+Pr)}\right]^{1/4} \Phi_\eta(\gamma,0,\tau) \tag{4.15}$$

where Φ_η can be approximated by

$$\Phi_\eta(\gamma,0,\tau) = \Phi_\eta^s(\gamma,0) + \frac{1}{Fr}[\tilde{\Phi}_\eta(\gamma,0)\cos(2\pi\tau) + \hat{\Phi}_\eta(\gamma,0)\sin(2\pi\tau)] \tag{4.16}$$

A plot of this temperature gradient versus time τ (and position angle α) for several magnitudes of Froude number is presented in figure (4.21). By comparison with figure(4.20), this plot reveals that the Nusselt number at the fin root has a lower percentage fluctuation than the total heat transfer rate in the present case. Also, all the points of interest, i.e. the peak points, the valley points, and the points where curves intersect the horizontal line for the quasi-steady solution, seem to shift slightly rightward (10°) in figure (4.21). In spite

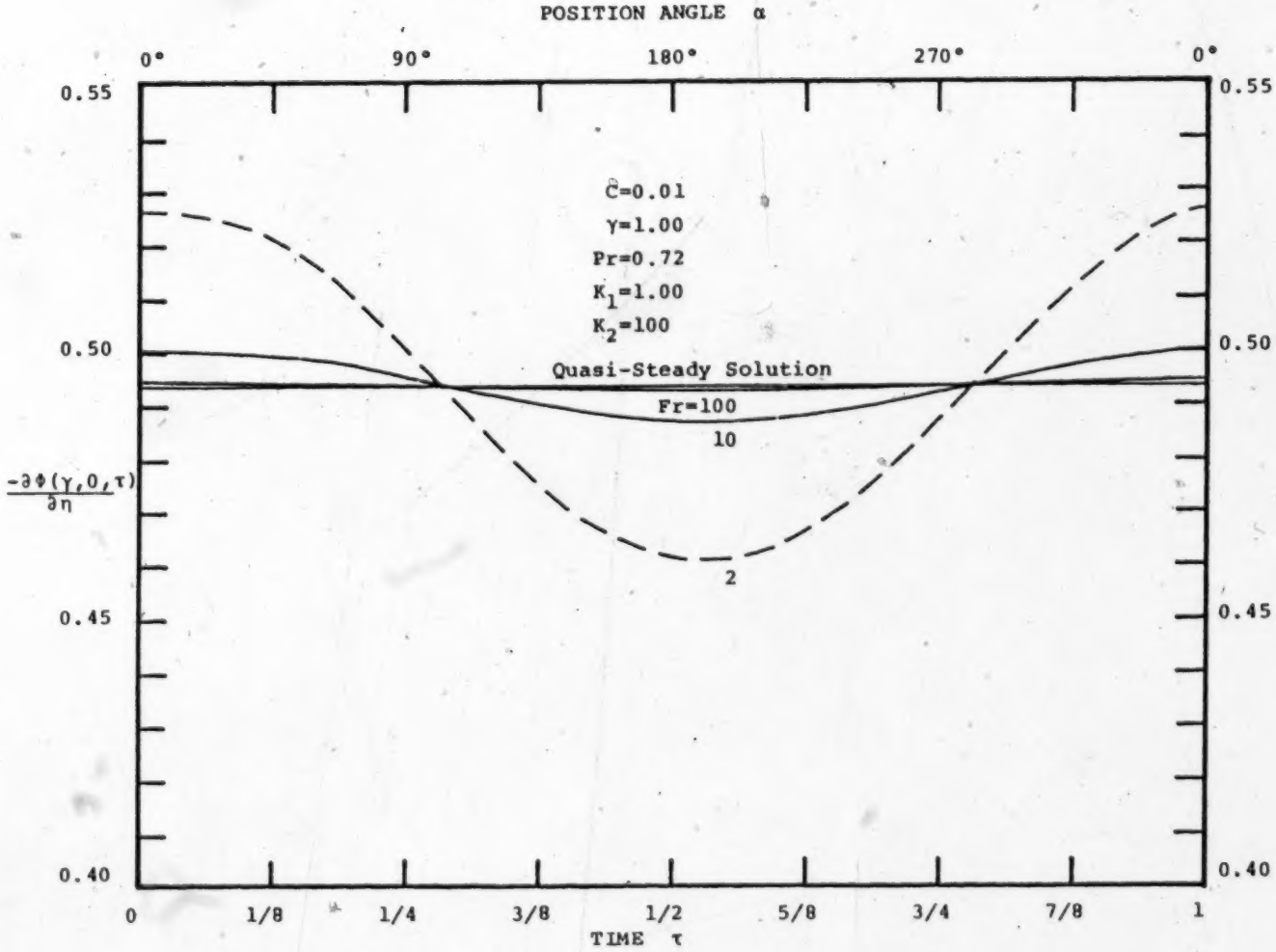

Figure 4.21 Periodic Variation in Nusselt Number of Perturbation Result

of this, the nearly linear feature of all the curves when the rotating fin changes its position from $\tau=1/4$ to $\tau=3/8$ and from $\tau=3/4$ to $\tau=7/8$, again suggests that both $\tau=1/4$ and $\tau=3/4$ may be the proper initial time levels for the direct integration approach.

In fact, even if this plot of $\Phi_\eta(\gamma,0,\tau)$ versus τ does not support that of $\frac{\partial\Phi_o(\gamma,\tau)}{\partial\eta}$ versus τ in determining the initial time level, the recommendation from the latter should be the proper one because $\frac{\partial\Phi_o(\gamma,\tau)}{\partial\xi}$ represents a physical measure of the overall problem while $\Phi_\eta(\gamma,0)$ only provides a local indication.

4.2.3-3 FIN EFFECTIVENESS

A significant amount of phase-shift appears in figure (4.22) where the fin effectiveness ε, defined by

$$\varepsilon = \frac{\gamma}{C}\left[\frac{4(1+Pr)}{3Pr}\right]^{1/4}\frac{\partial\Phi_o(\gamma,\tau)}{\partial\xi}\Big/\Phi_\eta(\gamma,0,\tau) \qquad (4.17)$$

is plotted versus time τ and position angle α of the rotating fin. Apparently, all the points of interest show the same excursion to the left of the graph. For example, the fin effectiveness predicted by this perturbation solution reaches its maximum value approximately 30° before the fin rotates to its vertically downward position ($\tau=0$ or 1) where the maximum total heat transfer rate takes place.

Unlike $\frac{\partial\Phi_o(\gamma,\tau)}{\partial\xi}$ and $\Phi_\eta(\gamma,0,\tau)$, which are real entities directly involved with the integration of the governing equations, fin effectiveness defined by equation

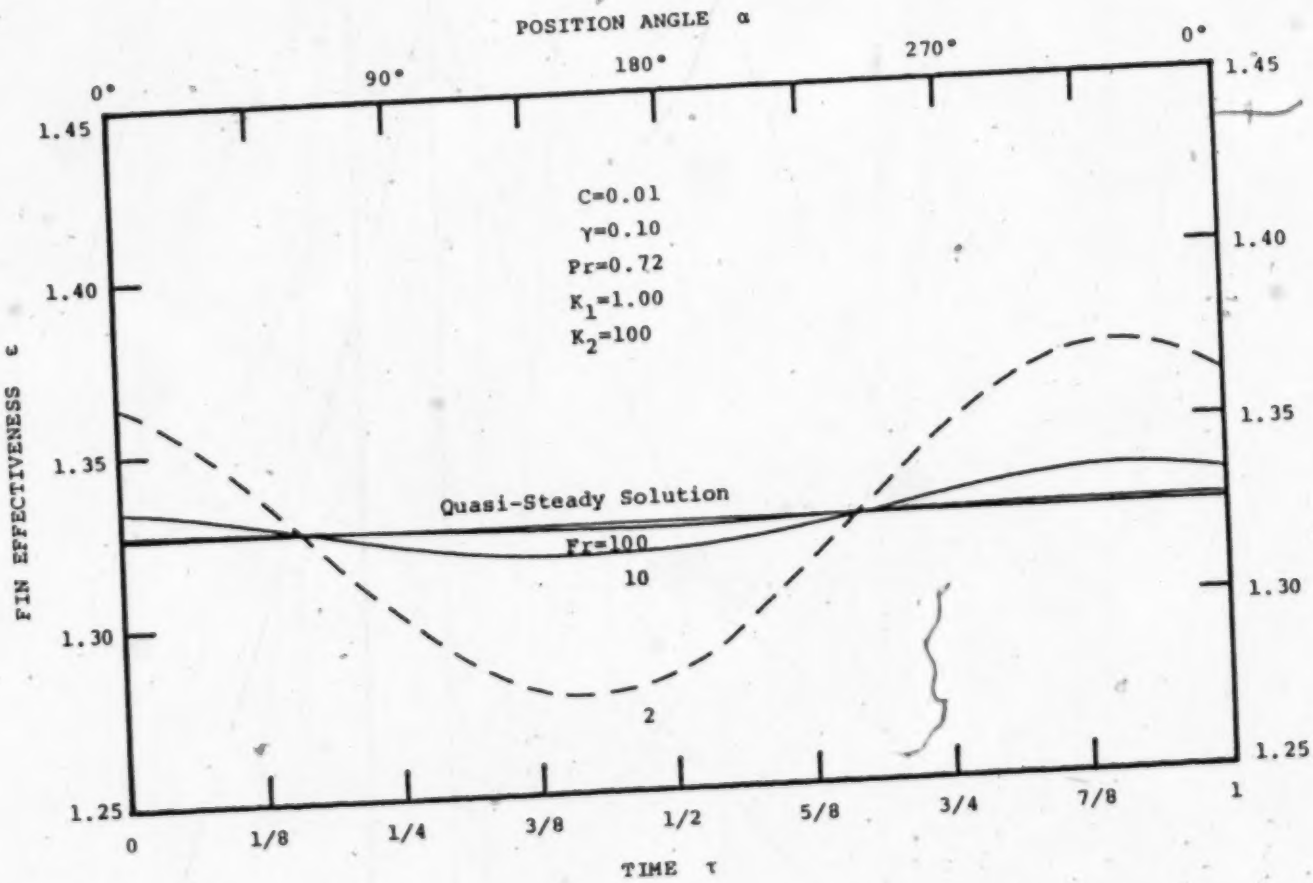

Figure 4.22 Periodic Variation in Fin Effectiveness of Perturbation Result

(4.17) is merely an intuitive appraisal of the problem; neither physically nor mathematically can it affect the direct integration to any extent. For this reason, use of figure (4.22) is not recommended in the determination of initial time level for the direct integration approach though both $\tau=1/4$ and $\tau=3/4$ are still indicated by this plot to be two time levels of satisfactorily small curvature.

Again, the fin effectiveness for Fr=100 fluctuates almost imperceptibly about the quasi-steady result in figure (4.22). This fluctuation increases to about 1% and 3.5% as the Fr value decreases to 10 and 2, respectively.

4.3 "EXACT" SOLUTIONS

An "exact" solution in this study refers to the numerical solution obtained from the direct integration of equations (3.17)-(3.19). General guidelines for this direct integration have been described in section 3.2.2 through some examples depicted by figures (3.1)-(3.6).

The suggested use of first-order perturbation to approximate the exact solutions at a proper initial time level in this work postulates that the variation of Froude number would not cause significant phase-shift in the solutions; that is, cases similar to either figure (3.1) or (3.3) are assumed. This assumption is later verified a posteriori.

Because of the expensive numerical work expected in this approach of direct integration, the study centred on the effect of Froude number, the most important parameter of this periodic problem. Exact solutions were obtained at four levels of Froude number (2, 10, 100 and 10^5) for a representative set of parameters: γ=0.1, Pr=0.72, C=0.01, K_1=1.0, and K_2=100.

In order to reduce the computing time, integrations were carried out by using the step sizes of $\Delta\eta$=0.1, $\Delta\xi$=0.01, and $\Delta\tau$=1/8. By virtue of the first two step sizes, quasi-steady and perturbation solutions could be secured within seven and three minutes of computation on an IBM 360/67 machine.

In the direct integration of the governing equations (3.17)-(3.19) for a large Froude number, the proper initial time level was determined from the perturbation result. In this study, the predominance of the even part of the perturbation solutions over the odd part hinted at the possible resemblance between the exact solutions and a cosine curve. Moreover, the assumption of no significant phase-shift among solutions for different Froude numbers suggested approximately linear solutions with respect to time in the vicinity of τ=1/4, which was therefore chosen as the initial time level for large Froude numbers.

For comparison, quasi-steady and perturbation results were separately used as the initial solution at $\tau=1/4$. By means of the quasi-steady result, timewise convergence was achieved for $Fr=10^5$ after 135 minutes of computation, but failed completely for Fr=100. When the perturbation approximation was used, however, solutions in both cases ($Fr=100$ and 10^5) were obtained with 25 minutes of computing time. Therefore, a search for the perturbation result prior to the exact solution is both necessary and economical even if the Fr value is not small.

The initial time level for all the small Froude number cases (Fr=2 and 10) was also set at $\tau=1/2$. In the present study, the exact solutions for large Froude numbers all deviated from their perturbation approximations in the manner demonstrated by figure (3.1); namely, no appreciable phase difference was revealed. It was assumed that same phase behaviors held between the exact and perturbed solutions for a small Froude number.

Numerical experiments were conducted to choose a proper initial solutions for the small Froude number. With the exact solutions for Fr=100 as the initial solutions, the periodic solutions were matched to better than the third decimal place within 40 minutes of timewise iteration. The overall computing time for a small Froude number was in the order of 75 minutes. Both quasi-steady and perturbation

results were also used separately as the trial initial solutions in this direct integration approach for small Froude numbers. The former often led to solution divergence or numerical overflow while the latter produced convergence after 200 minutes of extremely long calculation. Undoubtedly, direct integration of the governing equations for a large Froude number before solving the case for small Froude number, would shorten a prodigious amount of computing time.

The demonstrated approach for the direct integration of equations (3.17)-(3.19) assures fast timewise convergence of the periodic solutions. Notwithstanding all endeavors and successes in saving computing time, the minimum requirement of 75 minutes for solving a small Froude number case may still make the whole scheme seem economically unattractive. Closer examination reveals that this long computation solely reflects the complexity of the coupled heat transfer model at each time step. In fact, periodicity of the solutions can be obtained after three timewise iterations.

4.3.1 SOLUTIONS OF BOUNDARY LAYER PROBLEM

To compare the exact solutions of the boundary layer problem with their perturbation approximations, two sample solutions for Fr=10 are presented in figure (4.23) and (4.24). Apparently, there is very little difference

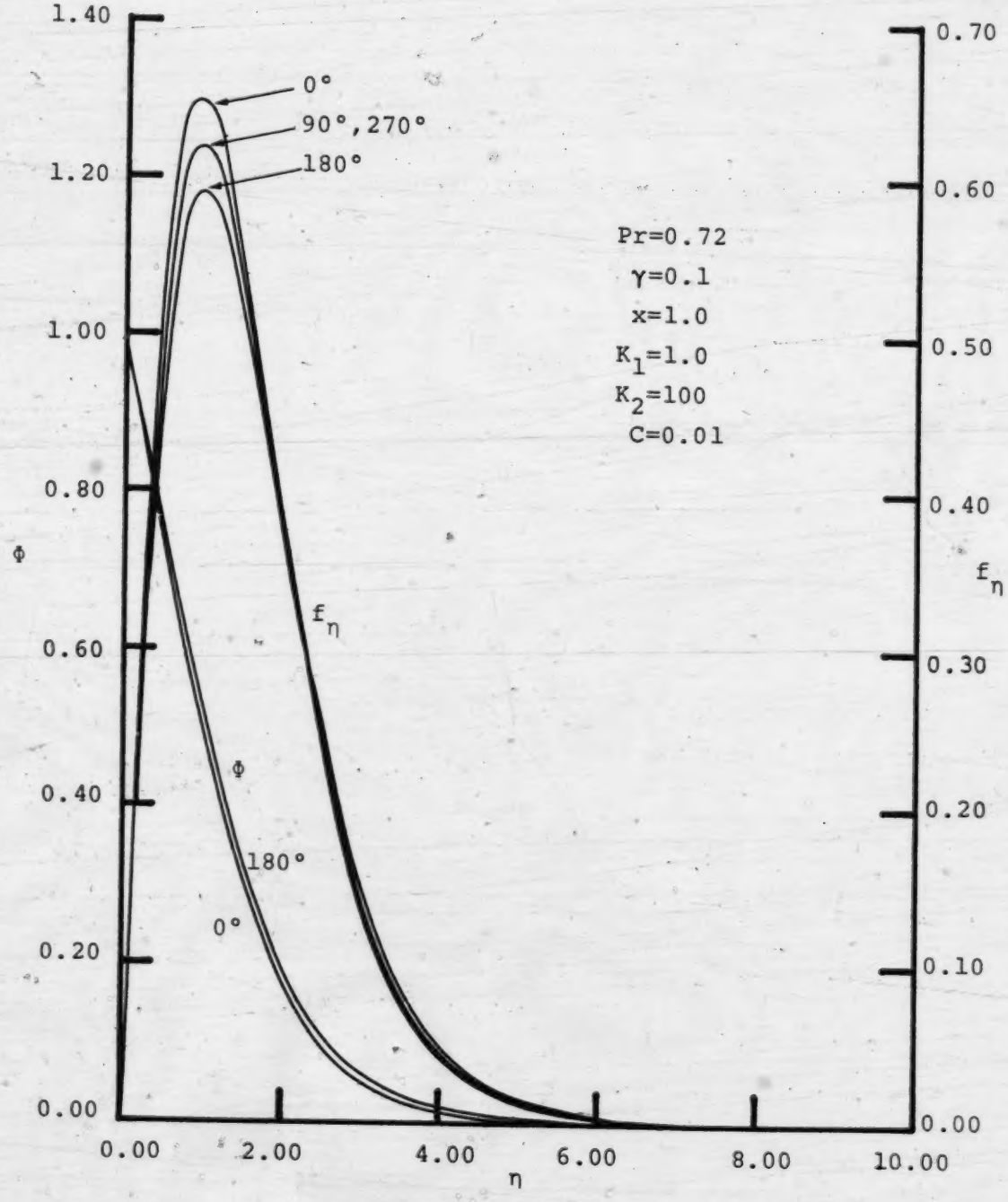

Figure 4.23 Periodic Boundary Layer Solutions Obtained from Perturbation Approximation for Fr=10

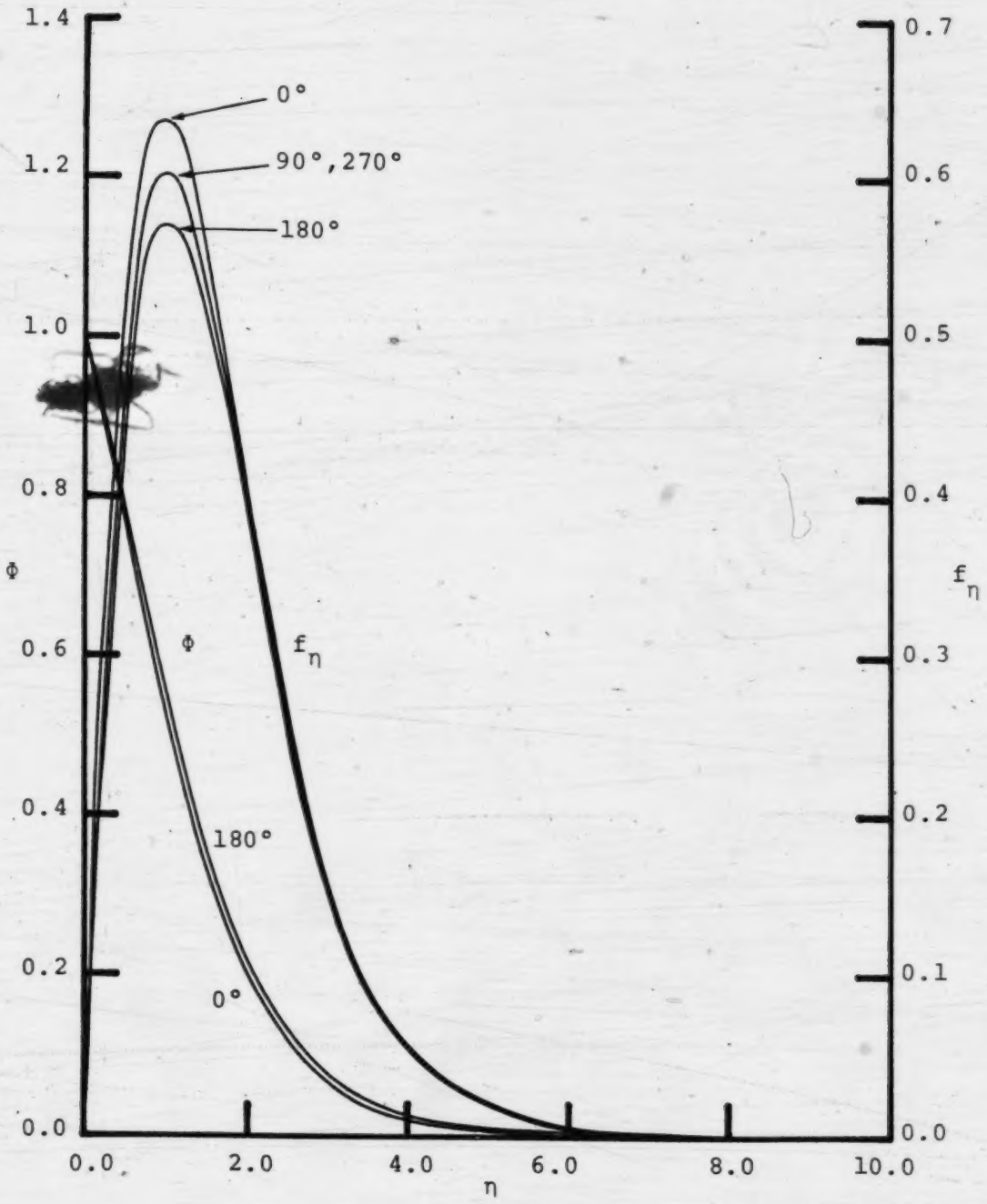

Figure 4.24 Periodic Boundary Layer Solutions Obtained by the Direct Integration Method for Fr=10

in the temperature profiles Φ between these two graphs. In contrast to this, the velocity approximated by the perturbation results in figure (4.23) is generally higher than its exact value in figure (4.24) despite the fact that they both fluctuate in nearly the same magnitude and reveal the same boundary layer thickness. As far as the accuracy of the perturbation approximation is concerned, however, the greatest velocity difference of three per cent between these two sample solutions is still within the truncation error, $O[10^{-2}]$, of the perturbation results.

Figure (4.24) depicts physically sound velocity profiles. As the fin is projecting downward, i.e. 0°, concurrence of the gravitational and the centrifugal forces induces a fluid velocity higher than that of 180°, where opposition of forces reduces the net buoyancy effect on the fluid. No appreciable difference exists between the velocity solutions at the two horizontal positions (90° and 270°).

The fluctuation in fluid temperature profile is very small. For this reason, only the limiting temperature profiles at two vertical fin positions of 0° and 180° are plotted in figure (4.24); temperature profiles at other fin positions are virtually enclosed by these two limits.

The boundary layer solutions obtained by the direct integration method for Fr=2 is shown in figure (4.25).

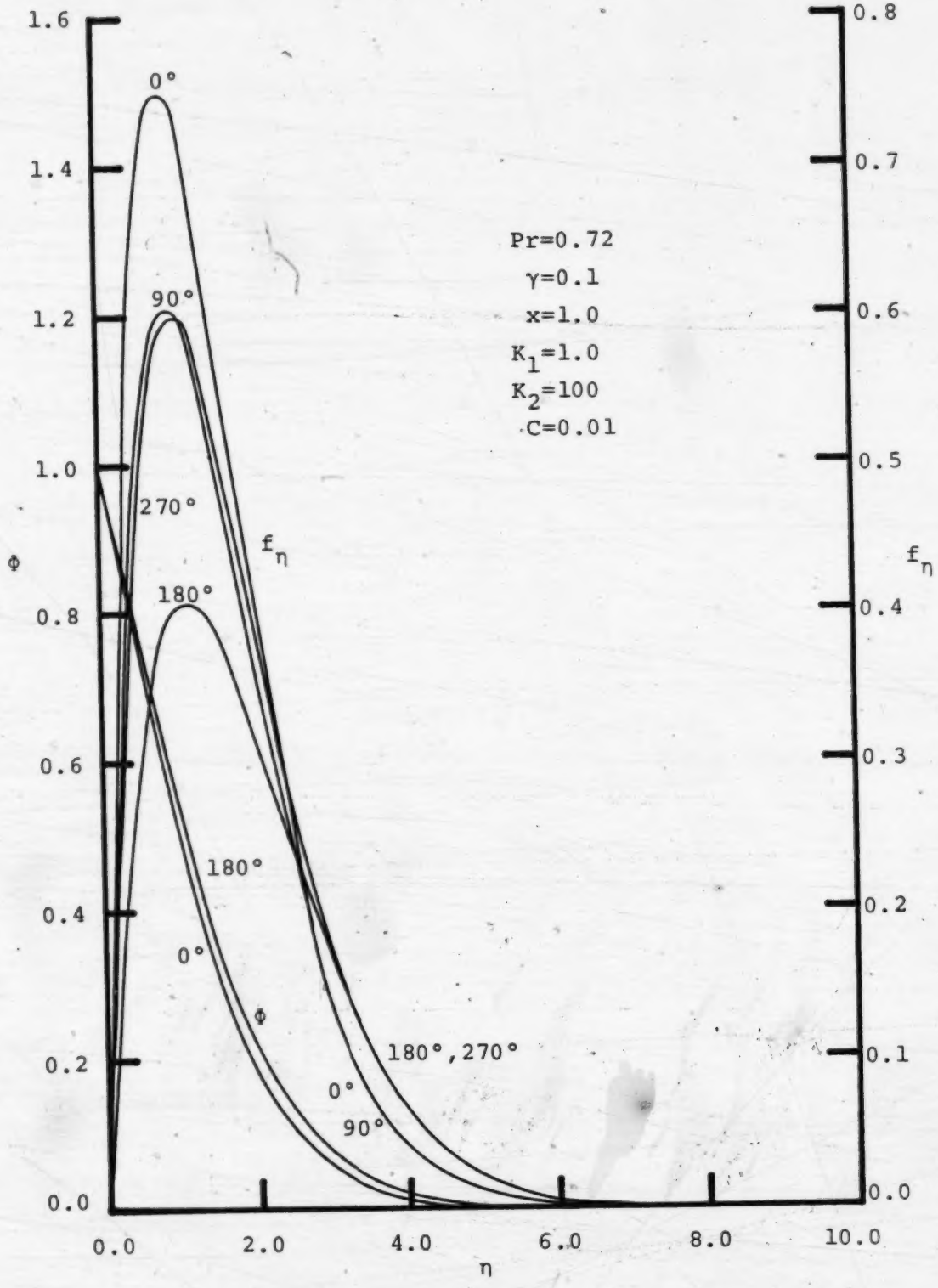

Figure 4.25 Periodic Boundary Layer Solutions Obtained by the Direct Integration Method for Fr=2

The temperature profiles vary slightly with the position of the rotating fin but the velocity profiles fluctuate so intensively that they even present noticeable differences at the two horizontal fin positions. In particular, the momentum boundary layer at the position angle of 270° is thicker than that of 90°. The solutions also indicate that although the maximum velocity varies significantly when the fin rotates from 0° to 90° (or from 180° to 270°), the thickness of this momentum boundary layer stays nearly unchanged.

4.3.2 SOLUTIONS OF CONDUCTION PROBLEM

Figure (4.26) shows the periodic fluctuation in the solid fin temperature obtained by direct integration of equations (3.17)-(3.19) for Fr=2. When the heated rotating fin is projecting downward (0^{o}), concurrence of centrifugal and gravitational forces enhances the cooling effect of the ambient fluid and, as shown, results in a lower fin temperature profile. On the other hand when the rotating fin is projecting upward (180^{o}), opposition of the two body forces reduces the cooling effect and accordingly leads to a higher fin temperature distribution. Similar graphs have been constructed for other Fr values and, as expected, the difference between these temperatures at two vertical fin positions varies inversely with Fr and eventually disappears when Fr is greater than 100. It is also shown in figure (4.26) that when the fin is in the two horizontal positions (90^{o} and 270^{o}), the difference in the corresponding fin temperature is negligibly small.

4.3.3 SOLUTIONS OF OVERALL PROBLEM

Periodic variations in the total heat transfer rate, the Nusselt number, and the fin effectiveness for exact solutions are presented in figure (4.27), (4.28), and (4.29) at four levels of the Froude number (2, 10, 100 and 10^{5}) when C=0.01, γ=0.1, Pr=0.72, K_1=1.0, and K_2=100.

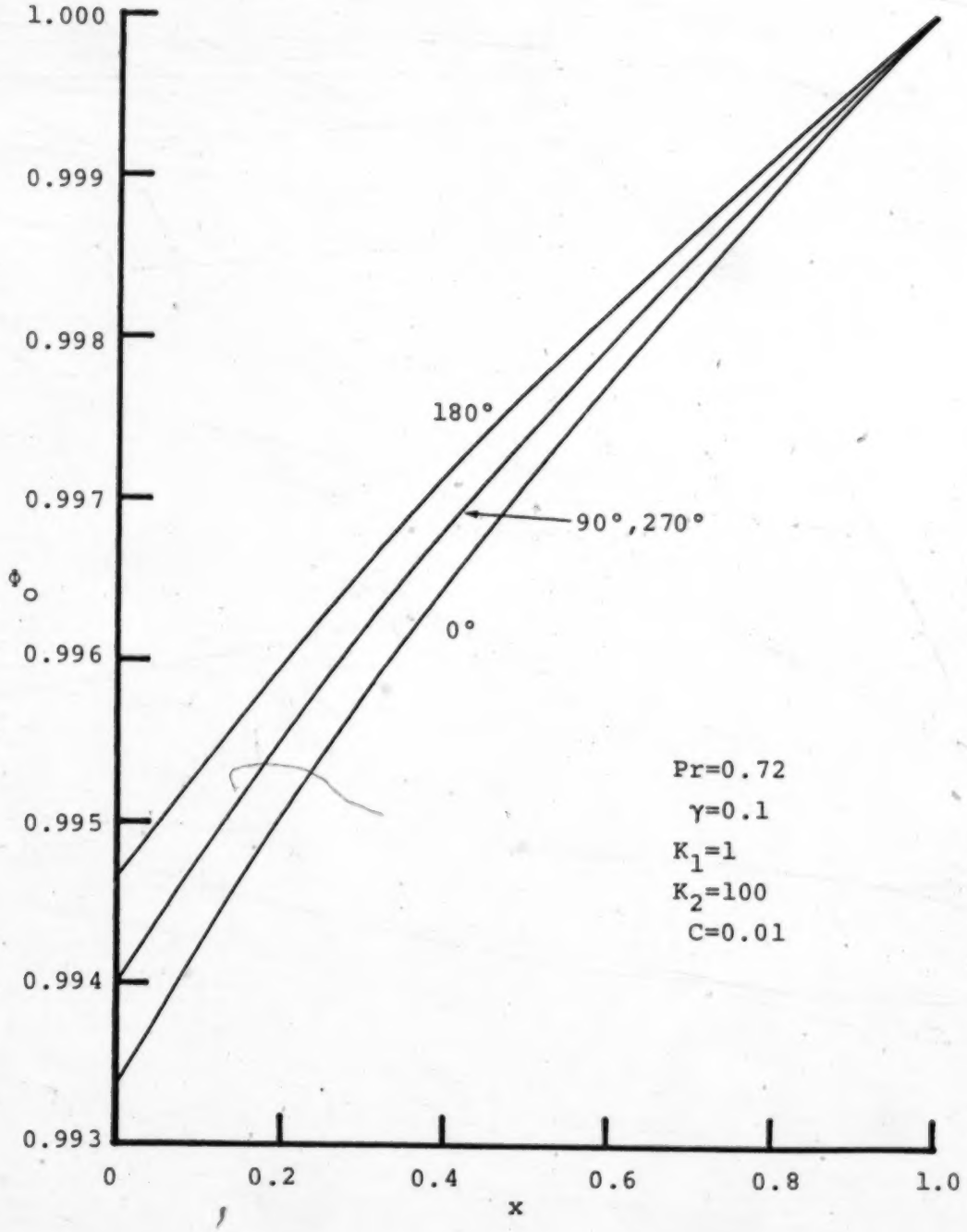

Figure 4.26 Periodic Fin Temperature Obtained by the Direct Integration Method for Fr=2

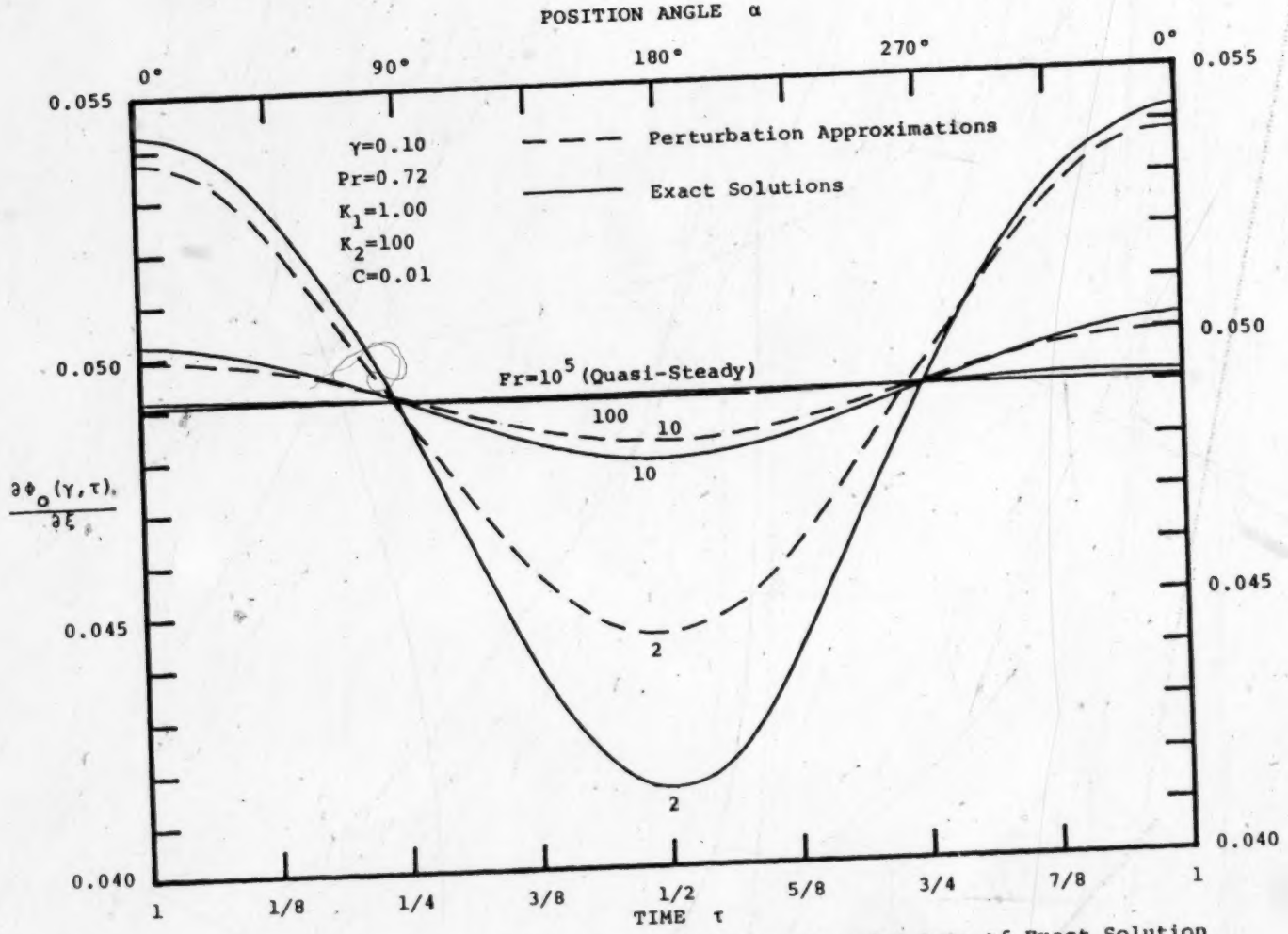

Figure 4.27 Periodic Variation in the Total Heat Transfer Rate of Exact Solution

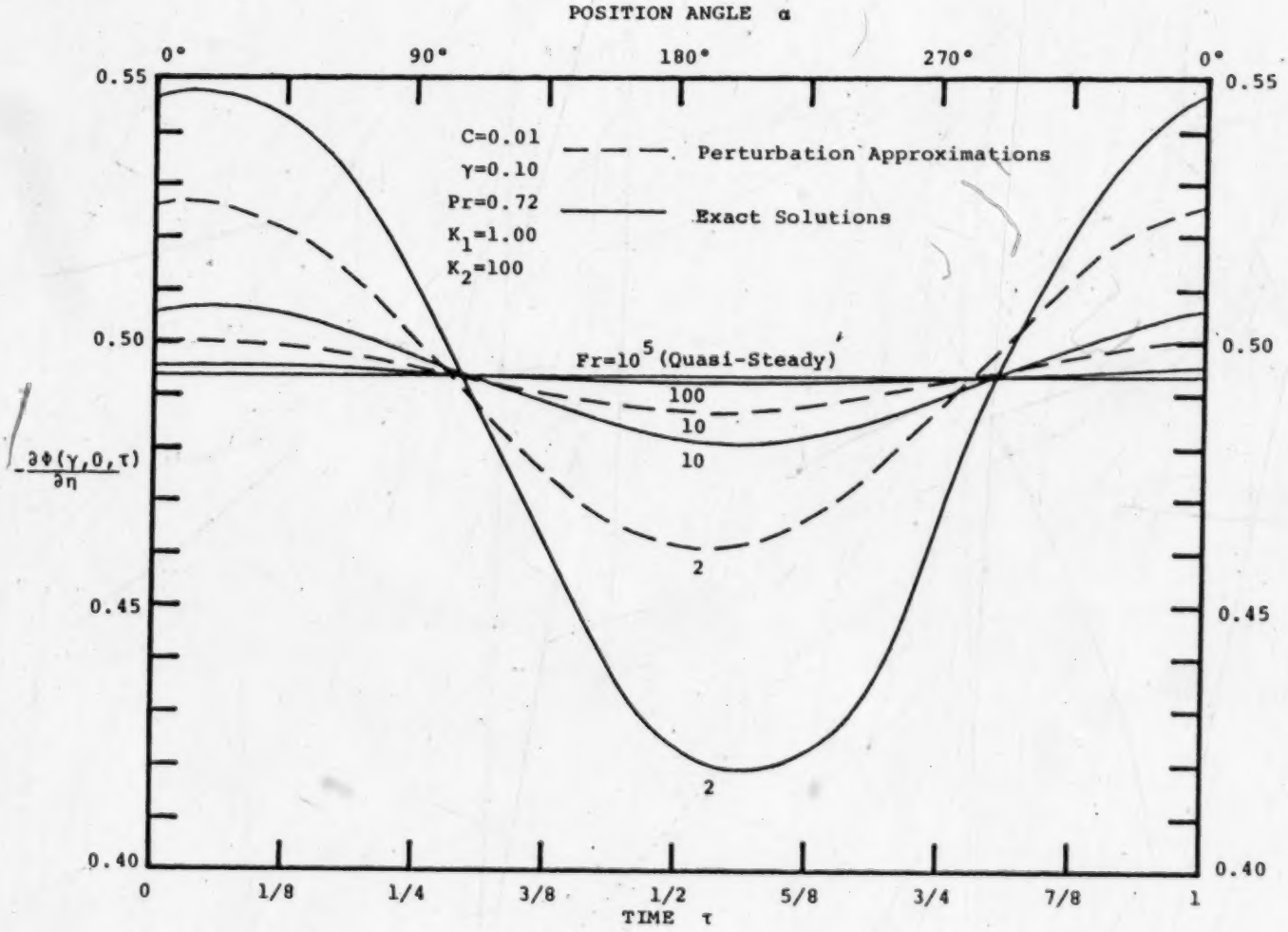

Figure 4.28 Periodic Variation in the Nusselt Number of Exact Solution

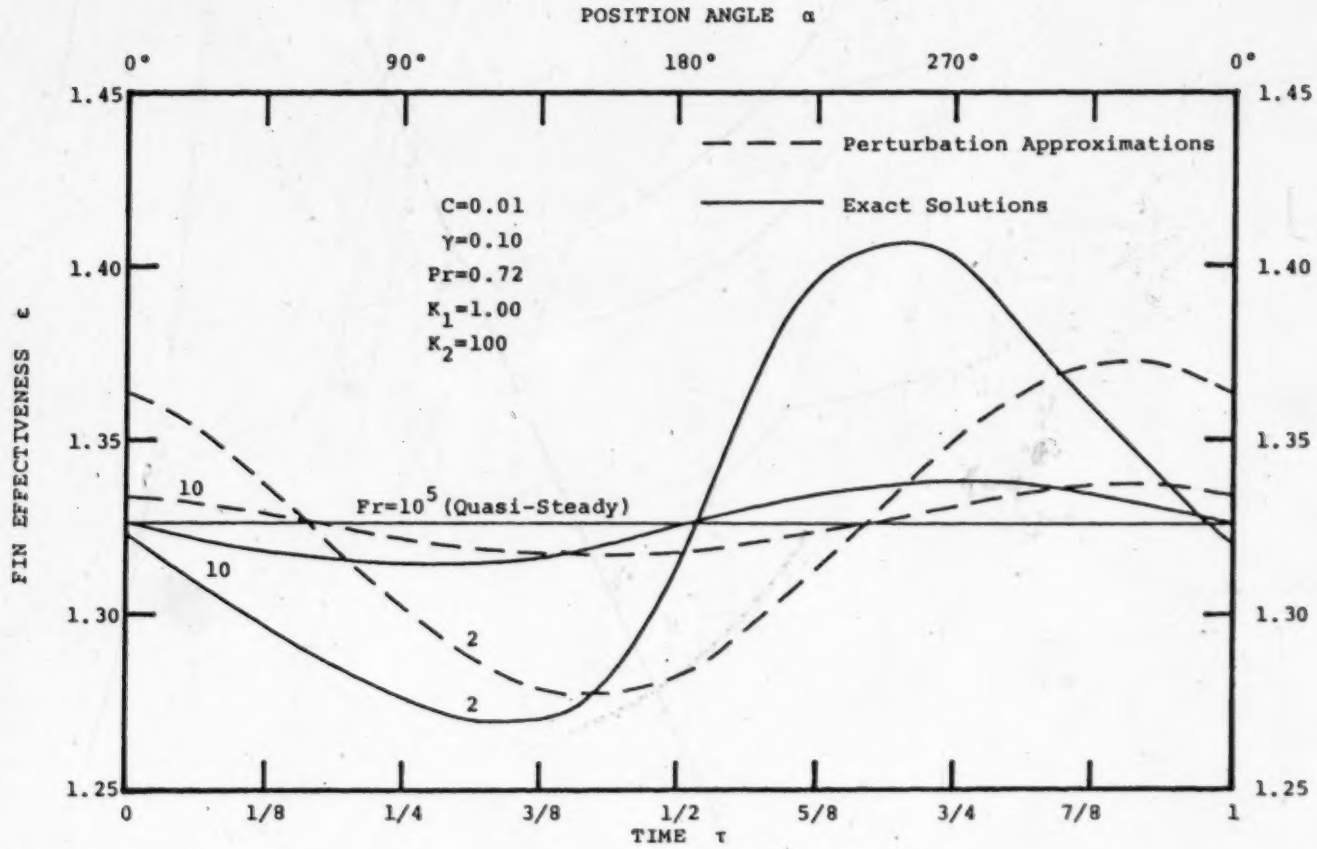

Figure 4.29 Periodic Variation in Fin Effectiveness of Exact Solution

For comparison, the perturbation results are also plotted as dashed lines for both Fr=2 and 10.

4.3.3-1 TOTAL HEAT TRANSFER RATE

From equations (4.2) and (4.3), the total heat transfer rate Q for this periodic problem can be derived as

$$Q(\tau) = \left[2WD\frac{K_s\Theta_r}{R_t}\right]\frac{\partial\Phi_o(\gamma,\tau)}{\partial\xi} \qquad (4.18)$$

As all the bracketed quantities in the above equation are set constant for a given problem, this total heat transfer rate can be expressed by the temperature gradient $\frac{\partial\Phi_o(\gamma,\tau)}{\partial\xi}$ at the root of the solid fin.

Several characteristics of the total heat transfer rate for a sample problem are disclosed in figure (4.27) where the temperature gradient is plotted against time τ and position angle α of the rotating fin. In agreement with the perturbation approximations, maximum heat transfer rates (peak points) of exact solutions for Fr=100, 10 and 2 all occur at $\alpha=0^\circ$ ($\tau=0$ or 1) while their minimum heat transfer rates always take place at $\alpha=180^\circ$ ($\tau=1/2$). Moreover, all the curves intersect the quasi-steady result in the vicinity of $\alpha=90^\circ$ ($\tau=1/4$) and $\alpha=270^\circ$ ($\tau=3/4$). The nearly linear sections between $\tau=1/4$ and 3/8 of all the curves shown in figure (4.27) verify that the use of $\tau=1/4$ as an initial time level in obtaining exact solutions for these cases is perfectly acceptable.

It is also worth noting that magnitude of the Froude number can affect the total mean heat transfer rate of the problem. When the Froude number is much greater than one, the total heat transfer rates indicated by the exact solutions in figure (4.27) fluctuate almost symmetrically about the quasi-steady result; namely, their total mean heat transfer rate equals the quasi-steady solution to a close degree. However when the Froude number is of order one, this mean value becomes significantly less than the quasi-steady result.

Discripancy in the total heat transfer rate between the exact and the perturbed solutions increases inversely with the Froude number. In general, a decrease of the Froude number undulates both the perturbation result and the exact solution, but to a greater extent in the latter case. Figure (4.27) reveals that the maximum discrepancies between the exact solutions and their first-order perturbation approximations are respectively 0.5% and 7% for Fr=10 and 2. In comparison with the estimated corresponding truncation error, i.e. $O[Fr^{-2}]$, of this first-order perturbation series expansion, these low discrepancies suggest that the total magnitude of all the high-order perturbation terms is relatively small in this study and the use of the first-order perturbation approximation alone is acceptably accurate in most cases provided the Froude number is not too small.

4.3.3-2 NUSSELT NUMBER

Equation (4.15) indicates that for a given problem, the Rayleigh number (Ra) and the Prandtl number (Pr) are fixed and the Nusselt number at the root of a rotating fin can be expressed by the temperature gradient $\Phi_\eta(\gamma,0,\tau)$ of the fluid at the solid-fluid interface. This temperature gradient is plotted against time τ and position angle α in figure (4.28).

Several characteristics of the time-dependent Nusselt number are observed. In comparison with figure (4.27), all the curves in figure (4.28) take an excursion to the right. Nevertheless, linearity still appears between τ=1/4 and 3/8 for every curve; this trend again substantiates the wisdom of choosing τ=1/4 as the initial time level in the direct integration approach. Similar to the total heat transfer rate, the Nusselt number undulates its fluctuation but decreases in its mean value as the Froude number becomes smaller.

It is found that the perturbation approximation is less reliable when Fr=O[1]. As far as the magnitude of fluctuation is concerned, the perturbation results of both figure (4.27) and (4.28) estimate a lower percentage change in the Nusselt number than in the total heat transfer rate for Fr=2; exact solutions, however, manifest an equal percentage variation in both entities and hence disprove the

observation deduced from perturbation results. In figure (4.28), the perturbation results for Fr=10 and 2 can deviate up to 1.5% and 11% respectively from their approximated exact solutions. These deviations still concur with the estimated truncation error, $O[Fr^{-2}]$, of the perturbation approximation. Apparently, the use of the first-order perturbation series expansion to approximate the exact solutions at the chosen initial time level $\tau=1/4$ in this study is sound if the Froude number is much greater than one.

4.3.3-3 FIN EFFECTIVENESS

Equation (4.17) of section 4.3.2-3 is used in determining the fin effectiveness ε of every directly integrated exact solution. The calculated results and their approximated values for both Fr=2 and 10 are plotted versus dimensionless time τ and fin position angle α in figure (4.29).

Several distinct features are present in figure (4.29). First, none of the periodic fin effectivenesses resembles a cosine curve; all the peak and valley points deviate from 0° ($\tau=0$ and 1) and 180° ($\tau=1/2$) to an appreciable degree. For Fr=10, the exact solution indicates a fin effectiveness fluctuating about the quasi-steady result ($Fr=10^{-5}$) similar to a negative sine curve, i.e. with the valley at 90° and peak at 270°. In other words, the phase angles between a peak and a following valley, or vice versa, is always half a period (180°); this also holds for the perturbation results for both

Fr=2 and 10. The exact solutions for Fr=2, however, present completely different features for fin effectiveness, which takes about one third of a period to rise from its valley to its peak but needs the remaining two thirds of the period to subside to the valley point of the next cycle. In addition, this fin effectiveness of the exact solutions for Fr=2 reveals a mean value higher than the quasi-steady result although its perturbation approximation predicts a lower mean value than the latter.

Despite all the differences in phase angle, shape, fluctuating magnitude, as well as in the mean value, maximum descrepancies in fin effectiveness between perturbation result and their corresponding exact solution are 0.8% for Fr=10 and 6% for Fr=2.

4.4 LIMITS OF APPLICABILITY

Applicability of the present result is subject to some basic constraints of this problem. Assumptions utilized in appendices A and B to derive the laminar boundary layer equations (B.34)-(B.37) impose the following limits on the solutions:

(1) Limit for laminar free convection phenomena.

In order to avoid the development of turbulent flow in conventional free convection problems, i.e. gravity is the only body force for the entire system, the Rayleigh number should be less than 10^8. By assuming that this limit on the Rayleigh number also holds for a laminar free convection

problem in a centrifugal force field, the Rayleigh number defined by

$$Ra = \frac{\beta R \omega^2 \theta_r L^3}{\nu \kappa_f} ,$$

should satisfy the following:

$$Ra < 10^8 . \qquad (4.19)$$

(2) Limit for boundary layer flow.

A boundary layer flow will take place when

$$Ra > 10^4 . \qquad (4.20)$$

(3) Limit for insignificant Coriolis force.

The Coriolis force effect in the momentum equation (B.11) can be ignored if

$$Ek^{-1} Ra^{-3/4} << O[1]$$

where the Ekman number is defined as

$$Ek = \frac{\nu}{\omega L^2} .$$

For convenience, the above condition is replaced by

$$Ek^{-1} Ra^{-3/4} < 0.1 . \qquad (4.21)$$

(4) Limit for negligible viscous dissipation.

All the viscous dissipation effects, represented by the last three terms on the right-hand-side of the energy equation (B.13), become vanishingly small if the ostrach number defined by

$$Os = \frac{\beta R \omega^2 L}{c_p}$$

is much less than one, i.e.

$$Os < 0.1 \qquad (4.22)$$

(5) Limit for no reversal flow.

When the centrifugal acceleration at the fin root is greater than the gravitational acceleration, i.e.

$$(R-L)\omega^2 > g \ , \tag{4.23}$$

the fluid in the boundary layer will always flows radially inward; no reversal flow will take place.

(6) Limit for Oberbeck-Boussinesq approximation.

Applicability of the Oberbeck-Boussinesq approximation:

$$\rho = \rho_\infty(1-\beta\theta) \ , \tag{A.5}$$

relies on the assumption

$$\beta\theta << 1 \ , \tag{A.6}$$

or more specifically,

$$\beta\theta_r < 0.1 \tag{4.24}$$

Actual constraints on the applicability of the solutions given here can be clearly illustrated by delineating these limits on a properly chosen coordinate system. If air at a temperature of 68^oF is the ambient fluid of a 6-inch rotating fin, and $\theta_r=10^oF$, the estimated value of

$$\beta\theta_r = \frac{10}{460+68} = 0.019$$

automatically satisfies the inequality (4.24). Furthermore, substitution of the physical quantities [48] of air:

$$\kappa_f = 236 \times 10^{-6} \ ft^2/sec \ ,$$

$$\nu = 160 \times 10^{-6} \ ft^2/sec \ ,$$

and

$$c_p = 6000 \ ft^2/sec^2\text{-}^oR$$

into the remaining inequalities (4.19)-(4.23) yields the following more rigorous constraints:

$$R\omega^2 < 1595 \quad , \tag{4.19a}$$

$$R\omega^2 > 0.16 \quad , \tag{4.20a}$$

$$R\omega^{2/3} > 6.232 \quad , \tag{4.21a}$$

$$R\omega^2 < 633600 \tag{4.22a}$$

and

$$(R-0.5)\omega^2 > 32.2 \tag{4.23a}$$

These inequality constraints are shown in figure (4.30) where lnR is plotted versus lnω. The shaded side of each constraint contour indicates the region where the solutions illustrated can not be applied. Applicability of these solutions is limited to the dotted region in figure (4.30). The actual constraints are, therefore, determined by limits (1), (3) and (5), i.e. inequalities (4.19), (4.21) and (4.23).

In figure (4.30), different portions of the dotted region corresponds to different possible applications of the presented results. Solutions for the upper portion of the dotted region can be used in a re-entry environment because of large radius R and low angular velocity ω. On the other hand, solutions for the lower portion, which is characterized by small radius and medium angular velocity, may only be applied to a centrifugal machine rotating at relatively low rpm. It is shown in figure (4.30) that the highest angular

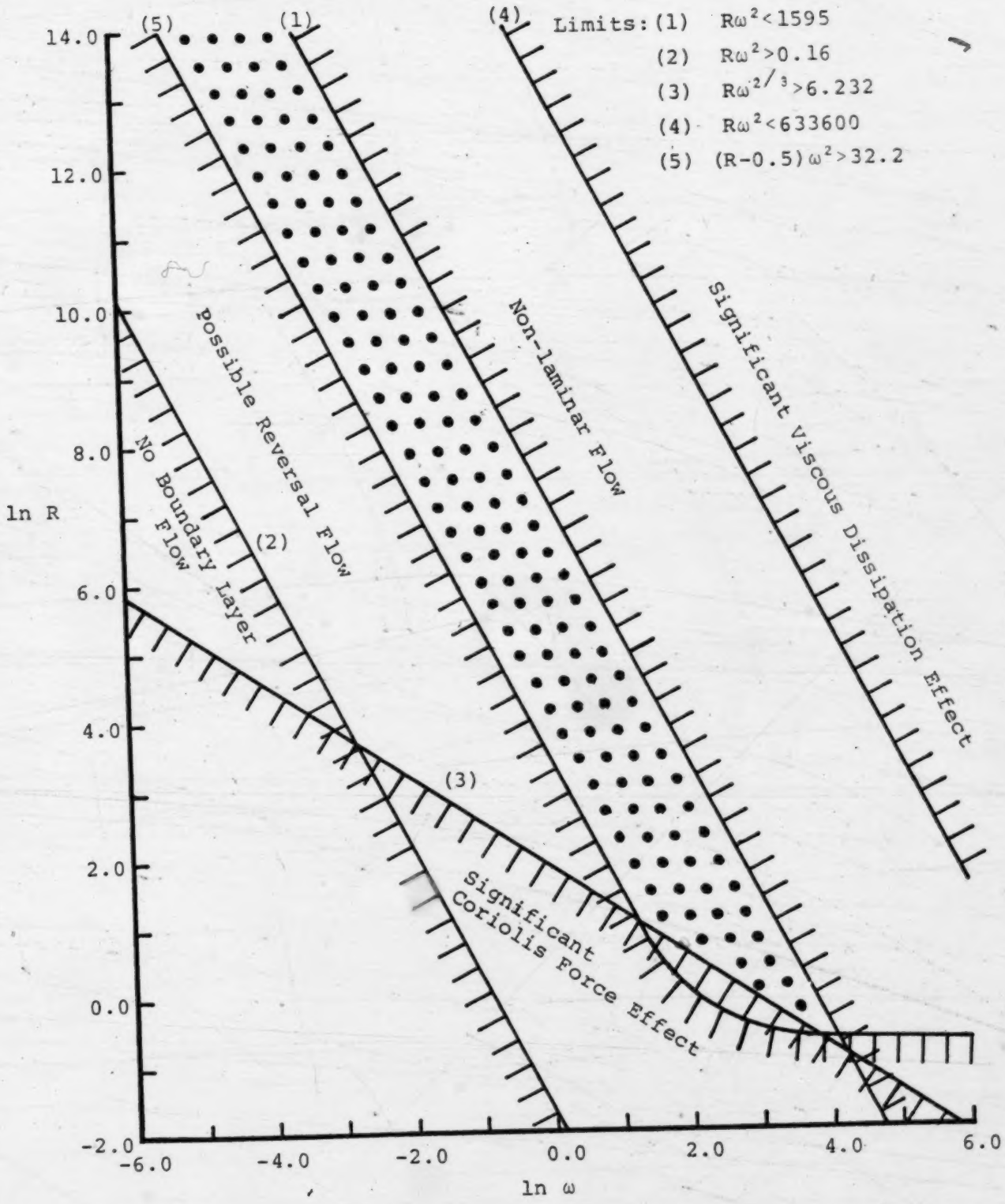

Figure 4.30. Limits of Solution Applicability: an illustration

velocity for the dotted region should be less than the angular velocity associated with the intersection of limits (1) and (5). By solving the simultaneous equations:

$$R\omega^2 = 1595$$

and

$$(R-0.5)\omega^2 = 32.2 \quad ,$$

which are deduced from these two limits, the angular velocity for the intersection is found to be

$$\omega = 56 \text{ rad/sec} = 535 \text{ rpm};$$

such a low limit on the angular velocity indicates that solutions illustrated have no application to high speed turbines. In addition, based on the inequality (4.19a), the solutions can not be applied to a rotating system with the centrifugal acceleration greater than 50g.

CHAPTER V

CONCLUSIONS AND RECOMMENDATIONS

5.1 CONCLUSIONS

The two chief objectives of this work have been successfully achieved. First, a periodic heat transfer problem of coupled conduction and free convection for a heated triangular fin rotating together with surrounding air has been thoroughly studied. Second, by using this periodic heat transfer problem as a vehicle, a rational approach has been developed for solving this type of periodic problems characterized by finite fluctuating amplitudes in the solutions.

As a result of rotation, three body forces are involved in this periodic heat transfer problem. The centrifugal force provides a persistent drive to the fluid flow while the gravitational force brings the periodicity into the problem. The Coriolis force does not have any significant effect on either the temperature or velocity solutions; it can however contribute to the pressure gradient in the lateral direction of the boundary layer. The ratio of the centrifugal force to the gravitational force is the Froude number (Fr) for this rotating system.

This Froude number was found to be the most important parameter in the present study. Formulation of this periodic

heat transfer problem revealed an unsteady-state, two-dimensional, mathematic model of six control parameters: γ, C, K_1, K_2, Fr, and Pr. By means of a Lefevre-type transformation, the effect of Pr on the solutions was virtually eliminated. Among the remaining five parameters, the Froude number (Fr) would determine the fluctuating amplitude of the periodic solutions; the larger the Froude number the smaller the fluctuation. For an extremely large Froude number, a quasi-steady-state system containing only parameters γ and C was obtained.

The quasi-steady-state solutions of the simplified time-independent equations (3.7), (3.8), and (3.13) were studied for different values of parameters γ and C. The results agreed well with those of previous work [27, 28]. In general, the parameter C had a significant effect on all the solutions while the parameter γ could hardly influence the temperature field.

Two empirical equations in the forms of

$$Q^s = a(C)\gamma^{-1.03386} \tag{4.5}$$

and

$$N\bar{u}^s = \left[F_1'(C) - F_2'(C)\gamma\right]Ra^{1/4} \tag{4.9}$$

were obtained for the total heat transfer rate (Q^s) and the Nusselt number ($N\bar{u}^s$) at the fin root under this quasi-steady-state condition. Values of the functions a(C), $F_1'(C)$ and

$F_2'(C)$ were tabulated for various levels of parameter C. A least-squares fit of Q^s in a simpler form of

$$Q^s = a'(C)\gamma^{-1}$$

was also conducted and the function a'(C) was approximated by a fourth-order polynomial of the parameter C; the maximum percentage error of 10% due to this curve fit was considered acceptable from a practical engineer's viewpoint. The tabulated values of F_1' were also of practical use to a design engineer in estimating the periodic heat transfer rate from a heated rotating fin system (appendix E).

Perturbation solutions were used to study the periodic problem for small fluctuations, and the investigation was conducted for different values of parameters γ, C, K_1, K_2, and Fr. The parameter C had a significant effect on both the velocity and the temperature solutions; whereas, the parameter γ presented a greater effect on the velocity than on the temperature. The perturbation results also revealed that in general, the periodic heat transfer problem of a rotating fin was nearly symmetric about the two vertical fin solutions (straight down and straight up). Namely, solutions at the two horizontal fin positions were normally identical. Only when $K_1 >> 10$ and $C >> 1$, did these two solutions have appreciable difference in their velocity profiles. The fourth parameter K_2, however, had no bearing whatsoever on the boundary layer solutions of all the cases studied in this work. As far as

the periodic phenomena were concerned, periodicity appeared clearly in the velocity solutions when Fr=10 and became vanishingly small when Fr=100; no significant fluctuation was ever present in the temperature solutions.

The perturbation results for a representative situation of C=0.01, γ=0.1, K_1=1.0, and K_2=100, were compared with the quasi-steady-state solutions for the same values of γ and C. The total heat transfer rate of the perturbation solutions for Fr=10^5 matched closely with both the quasi-steady-state result and the mean value of the periodic total heat transfer rate corresponding to a smaller Froude number. The perturbation solutions also showed that the fluctuating amplitude of the total heat transfer rate stayed small when Fr=100 and increased to approximately one per cent of the quasi-steady-state result when Fr=10. Inspection of both the Nusselt number and the fin effectiveness revealed that their fluctuations were smaller than that of the total heat transfer rate. The average Nusselt number for any Fr value coincided with the quasi-steady-state result, but the average fin effectiveness seemed to decrease with Fr.

A far more prominent difference between the periodic total heat transfer rate, the Nusselt number, and the fin effectiveness was in the phase angle. For the aforementioned sample problem, the maximum and the minimum total heat transfer rates occured at the 0° and 180° position angles of the

rotating fin respectively; whereas, the maximum and the minimum Nusselt numbers at the fin root appeared to have a time lag equivalent to 10° angle behind these two extreme total heat transfer rates. On the other hand, the maximum and the minimum fin effectivenesses took place approximately 30° before the rotating fin reached these two vertical positions (i.e. 0° and 180° respectively).

The numerical solutions acquired from the direct integration of the time-dependent, governing equations (3.17)-(3.19) were used to study the periodic heat transfer problem for a small Froude number. Owing to the long and expensive numerical calculation of the coupled conduction-convection heat transfer problem at each time level, the study was mostly centred on the correlation between the Froude number and the periodicity. For the representative example of $C=0.01$, $\gamma=0.1$, $K_1=1.0$, and $K_2=100$, it was found that although the decrease in this most significant parameter (Fr) did introduce some degree of periodic fluctuation to the temperature solutions, the oscillation was in general small. In contrast to this, the variation of the Froude number appeared to have much influence on both the velocity profile and the heat transfer rate. When $Fr=10$, the directly integrated velocity solutions oscillated with respect to time (or position angle of the fin) in the same manner as the perturbation result except that the latter indicated a 3%

higher maximum velocity. Basically, this periodic variation in velocity profile remained symmetrical about the two vertical position angles (0° and 180°) of the fin until the Froude number decreased to order of one; in that case, the whole velocity field not only fluctuated more intensively but also became unsymmetrical about the two vertical fin positions. For example, the velocity profile for 90° was different from that for 270°.

The total heat transfer rate, the Nusselt number, and the fin effectiveness of this periodic heat transfer problem for a small Froude number were also studied. As predicted by the perturbation result, the maximum and the minimum total heat transfer rates obtained from the direct integration of the governing equations did occur at the 0° and 180° position angles respectively, while the corresponding extreme values of Nusselt number at the fin root showed a certain delay in occurrence. In both solutions, there was a 180° phase angle between two consecutive extreme values. Moreover, both the total heat transfer rate and the Nusselt number increased their fluctuating amplitudes but reduced their mean values when the Froude number decreased. The fin effectiveness calculated from the directly integrated solution, however, revealed a periodic phenomenon with entirely different phase shifts. As the Froude number was reduced to order of one, the occurrence of the minimum fin effectiveness

was delayed but that of the maximum value was advanced, i.e. a shorter build-up and a longer fall-off times in each periodic cycle. Notwithstanding all these periodic features, none of the fin effectiveness, total heat transfer rate, and Nusselt number ever yielded a mean value deviating by more than 3% from the quasi-steady-state solutions.

Applicability of the above solutions is basically limited by the necessary condition imposed on the Rayleigh number for a stable laminar free convection flow. If the limit of $Ra<10^8$ for the laminar free convection flow in a constant body force field is also used for this periodic heat transfer problem and air is assumed to be the fluid, the obtained solutions can only be applied to the rotating system where centrifugal acceleration is not greater than 50g, such as in a re-entry environment or a low speed centrifugal machine. These results may be applicable to a high speed turbine if the actual upper limit on the Rayleigh number for a stable laminar free convection flow in the periodically modulated body force field is greater than 10^8. This critical Rayleigh number can be determined by the stability study, for which the results obtained in this study provide the basic solutions.

Based on the assumption of $Ra<10^8$, a rotating fin presents better cooling effect than a stationary fin does. According to equation (E.10), the mean heat transfer rate

for a rotating fin is higher than that of the stationary fin by a factor of $Fr^{1/4}$, or $(R\omega^2/g)^{1/4}$. This means that in practical application, the cooling effect of a thermal fin can be improved to approximately 2.66 times that of a conventional stationary fin if it is economically and technically allowed to rotate the entire system to an acceleration of 50g.

Evidence has verified the reliability of the techniques and numerical programs utilized in this work. The close agreement between the present quasi-steady-state solutions and the results of previous work [27, 28] indicates that both the Blasius-Howarth type transformation and the numerical program developed for this quasi-steady-state problem are reliable. Further agreement between the quasi-steady-state solutions and the results obtained by directly integrating the time-dependent equations (3.17)-(3.19) for $Fr=10^5$, confirms that the simplification of these time-dependent, periodic equations into the quasi-steady-state equations (3.7), (3.8) and (3.13) for an extremely large Froude number is proper. That is, the normalization procedure adopted during the derivation of the governing equations is sound; in fact, that all the calculated functions and their derivatives are of order one is another evidence of the propriety of this normalization procedure. The agreement between the quasi-steady-state solutions and the time-dependent

results for an extremely large Froude number also assures the dependability of the numerical scheme in solving the periodic problem. This assurance is furthermore substantiated by the fact that these directly integrated solutions match closely with their corresponding perturbation approximations when the Froude number is much greater than one.

Two iterative processes were used in the numerical scheme of this study. All the quasi-steady-state solutions, the perturbation results, and the time-dependent solutions at each time step were obtained in a similar manner by alternatively solving the conduction and free convection problems. This iterative process converged when the temperature solutions of the conduction and free convection problems matched at the solid-fluid interface. On the other hand, the periodic solutions were sought through the timewise iterations, which continued until all the velocity, temperature, and their derivatives at each point throughout the two-dimensional (X-Y) domain converged.

The parameter C had a significant effect on the solution convergence rate of the iterative process between the conduction and free convection problems. The smaller the parameter C the faster the convergence.

The solution convergence rate of the timewise iterative process depended strongly on the judicious selection of initial conditions and time level. The periodic solutions

for a problem under very small fluctuation was expected to differ only slightly from the quasi-steady-state solutions; however, when these quasi-steady-state solutions were used as the starting solutions at $\tau=1/4$ for $Fr=100$ and the periodic equations (3.17)-(3.19) were integrated directly, solution divergence was found after numerous timewise iterations. In fact, neither could the rapid convergence be produced by using the perturbation results as the starting solutions for the periodic problem under moderate fluctuation. It was then imperative to develop a method of assuring accurate approximations to the missing initial conditions at a proper time level.

A rational approach, developed in the present study to produce rapid timewise convergence by providing good starting solutions at the proper initial time level of the period, is described below:

Step (1) The quasi-steady-state equations (3.7), (3.8) and (3.13) are solved.

Step (2) The obtained quasi-steady-state solutions are used as the zeroth-order perturbation approximations; the perturbation results P1 and P2, say, for the small and moderate fluctuations are generated successively.

Step (3) Based on the perturbation result P1, a proper initial time level is selected; the direct integraiton of the

time-dependent equations (3.17)-(3.19) is then initiated after all the time-derivatives have been approximated by P1.

Step (4) Integrations in the succeeding time levels can be carried out accordingly by replacing the time-derivatives in the equations with finite-difference approximations; the periodic solutions S1 for this small fluctuation problem are obtained through timewise iterations.

Step (5) Once the solutions P1, P2, and S1 are obtained, the proper initial time level and the associated initial conditions for the moderate fluctuation problem of interest can be determined by the rules given in section 3.2.2 through the illustration of some typical examples. Experience has shown that if the initial conditions and time level are selected in this manner, convergence of the solutions is generally achieved within three timewise iterations.

The above approach was proved effective and reliable in handling this diffusion-type, periodic problems under moderate fluctuations. The total computing time required by using this approach to solve the periodic heat transfer problem for Fr=2 was approximately 75 minutes on an IBM 360/67 computer. For comparison, a numerical experiment was conducted by approximating the initial conditions with either

the quasi-steady-state solutions of Step (1) or the perturbation result of Step (2), and integrating the time-dependent equations (3.17)-(3.19) for Fr=2. The former approximation led to solution divergence while the latter produced timewise solution convergence after 200 minutes of calculation. It was obvious that the approach developed in this study could save a great amount of computing time.

It should be noted that the long computation of 75 minutes by using the developed approach is mainly due to the complexity of the coupled conduction and free convection heat transfer model at each time step; the solution convergence rate of three timewise iterations is in fact very fast.

As far as the application is concerned, this approach can provide a general guideline for solving other periodic problems which occur in the physical world but remain analytically untouched because of their complex nonlinear phenomena aggravated by the finite fluctuation in the solutions. A typical example is the huff-and-puff steam flood process widely used by oil industry to recover very viscous oil from an underground oil reservoir. A certain amount of steam is injected into the reservoir to increase the formation temperature near the wellbore and lower the oil viscosity; the well is then shut in for a critical period of time to let the reservoir fluid flow into the wellbore; steam injection is re-started after this reservoir fluid has been produced from

the same well. The efficiency of this technique is very sensitive to the amount of steam injected and the critical shut-in time. The physical models developed in the laboratory have limited application value because of the radical changes in reservoir characteristics from well to well; the numerical models can easily accommodate any reservoir description but suffer a major setback due to the great difficulty in solving the diffusion-type, nonlinear, periodic equations for this intermittent steam injection and oil production scheme. One major oil company has spent multi-million dollars on conducting an 80-well pilot project in the Cold Lake area to determine the optimum steam injection rate and the critical well shut-in time. Apparently, a great amount of money and human efforts will be saved if the periodic solutions for this huff-and-puff process can be obtained by using the approach developed in this study.

5.2 RECOMMENDATIONS FOR FUTURE WORK

The stability study of this periodic heat transfer problem is recommended. As shown in section 4.4, the applicability of the obtained solutions depends mainly on the critical Rayleigh numer for having a stable laminar free convection flow. If the critical Rayleigh number determined by the stability study of this periodic heat transfer problem is in the order of 10^9, the obtained solutions may be applicable to the high speed turbines. In recent years,

Russian scientists have carried out extensive stability studies [16-24] on periodic free convection problems in a closed space. The periodicity enters the problems of their studies either by assuming a periodic temperature solutions or by vibrating the entire system in a gravitational force field. In most studies, high frequency modulation has been found to have a stabilizing effect on the solutions. Should the same conclusion be deduced from the stability study of the present periodic heat transfer problem, the applicability of the solutions presented in this work would be extended due to a greater critical Rayleigh number.

Experimental work to verify the theoretical result of this study is also recommended. The convection heat transfer phenomenon may be observed by means of a Mach Zehnder interferometer, and the temperature of the solid fin can be measured by thermocouples. In order to obtain representable interferograms, the relative distance and alignment between the fin and the optical plates of the interferometer must be exact to within 0.001 inch. Therefore in designing the rotating system, the possible mechanical vibration should be taken into account. Moreover, the FM transmitter can be used to transmit the electrical signals between the rotating system and the stationary instruments in the laboratory.

It is also worthwhile to examine the possibility of the flow reversal when $1-\gamma<\frac{1}{Fr}$. Boundary layer equation (3.3)

indicates that if the coefficient $(1-\gamma x)+\frac{1}{Fr}\cos(2\pi\tau)$ of the buoyancy force term is positive all the time or, more specifically, if $1-\gamma>\frac{1}{Fr}$ at the fin root, the fluid always flows in the radial inward direction from the tip to the root of the heated rotating fin. For $1-\gamma<\frac{1}{Fr}$, the flow is still in the radial inward direction when the rotating fin is projecting vertically downward ($\tau=0$ and $\cos(2\pi\tau)=1$). However, the situation may change when the fin rotates to the vertical upward position ($\tau=1/2$ and $\cos(2\pi\tau)=-1$); the buoyancy force tends to drive the fluid in the radial outward direction wherever $1-\gamma x<\frac{1}{Fr}$. Due to the inertia of the fluid, the flow may not reverse itself when $1-\gamma x$ is slightly less than $\frac{1}{Fr}$. On the other hand if the reversal of the flow does take place, it would most likely start from the fin root because of the minimum value of $1-\gamma x$ (i.e. $1-\gamma$); that is, a new leading edge of a boundary layer, where the fluid flows radially outward, may form at the fin root whenever the rotating fin approaches the vertical upward position. For a given geometric ratio γ, there will be a critical value of Fr for the excitation of this reverse-flow phenomenon. This critical Froude number is certainly worth exploring.

A further investigation is to determine whether the reverse flow can really develop so that the flow will oscillate along the fin with each revolution, or to the contrary,

the reversal of the flow will immediately break away the boundary layer.

In closing, it is strongly recommended to apply the developed approach to other periodic problems having non-synchronous solutions of finite fluctuating amplitudes. The immediate, feasible applications are to solve those periodic problems presented in references [1-9] for moderate and large fluctuations.

REFERENCES

1. LIGHTHILL, M.J., "The Response of Laminar Skin Friction and Heat Transfer to Fluctuations in the Stream Velocity," Proc. Roy. Soc. A, V.224, 1954, PP. 1-23.

2. STUART, J.T., "A Solution of the Navier-Stokes and Energy Equations Illustrating the Response of Skin Friction and Temperature of an Infinite Plate Thermometer to Fluctuations in the Stream Velocity," Proc. Roy. Soc. A, V.231, 1955, PP. 116-130.

3. ROTT, N. and ROSENZWEIG, M.L., "On the Response of the Laminar Boundary Layer to Small Fluctuations of the Free-Stream Velocity," J. Aerospace Sci. Vol. 27, 1960, PP. 741-747.

4. SCHOENHALS, R.J. and CLARK, J.A., "Laminar Free Convection Boundary-Layer Perturbations Due to Transverse Wall Vibration," Trans. ASME, Series C, Journal of Heat Transfer, Vol. 84, 1962, PP. 225-234.

5. NANDA, R.S. and SHARMA, V.P., "Free Convection Laminar Boundary Layers in Oscillatory Flow," Journal of Fluid Mechanics, Vol. 15, Part 3, 1963, PP. 419-428.

6. BLANKENSHIP, V.D. and CLARK, J.A., " Experimental Effects of Transverse Oscillations on Free Convection of a Vertical, Finite Plate," Trans. ASME, Series C, Journal of Heat Transfer, Vol. 86, 1964, PP. 159-165.

7. ESHGHY, S., ARPACI, V.S., and CLARK, J.A., "The Effect of Longitudinal Oscillations on Free Convection From Vertical Surfaces, "Journal of Applied Mechanics, Trans. ASME, Series E, Vol. 87, 1965, PP. 183-191.

8. MUHURI, P.K. and MAITI, M.K., "Free Convection Oscillatory Flow from a Horizontal Plate," Int. J. Heat Mass Transfer, Vol. 10, 1967, PP. 717-732.

9. KELLEHER, M.D. and YANG, K.T., "Heat Transfer Response of Laminar Free-Convection Boundary Layers Along a Vertical Heated Plate to Surface-Temperature Oscillations," Zeitschrift Fur Angewandte Mathematik und Physik, Vol. 19, 1968, PP. 31-44.

10. BURDE, G.I., "Numerical Investigation of Convection Arising with Fluctuations of the Temperature at Horizontal Boundaries," Fluid Dynamics, Vol. 6, No. 1, 1971, PP. 125-131.

11. ISHIGAKI, H., "Skin Friction and Surface Temperature of an Insulated Flat Plate Fixed in a Fluctuating Stream," J. Fluid Mech., Vol. 46, Part 1, 1971, PP. 165-175.

12. ISHIGAKI, H., "The Effect of Oscillation on Flat Plate Heat Transfer," J. Fluid Mech., Vol. 47, Part 3, 1971, PP. 537-546.

13. ISHIGAKI, H., "An Exact Periodic Solution of the Energy Equation," J. Fluid Mech., Vol. 50, Part 4, 1971, PP. 657-668.

14. SINGH, P. and SINHA, P.C., "Effect of Plate Temperature Fluctuations on Flow and Heat Transfer from a Horizontal Plate," Zeitschrift Fur Angewandte Mathematik und Mechanik Ingenieurwissenschaftliche Forschungsarbeiten, Band 51, Heft 3, 1971, PP. 167-176.

15. ISHIGAKI, H., "Heat Transfer in a Periodic Boundary Layer Near a Two-dimensional Stagnation Point," J. Fluid Mech., Vol. 56, Part 4, 1972, PP. 619-627.

16. GERSHUNI, G.Z. and ZHUKHOVITSKII, E.M., "On Parametric Excitation of Convective Instability," J. of Applied Math. and Mechanics (PMM), Vol. 27, No. 3, 1963, PP. 1197-1204.

17. ZENKOVSKAYA, S.M. and SIMONENKO, I.B., " Effect of High Frequency Vibration on Convection Initiation," Fluid Dynamics, Vol. 1, No. 5, 1966, PP. 35-37.

18. BURDE, G.I., "Numerical Study of the Onset of Convection in a Modulated External Forced Field," Fluid Dynamics, Vol. 5, No. 2, 1970, PP. 344-349.

19. GERSHUNI, G.Z., ZHUKHOVITSKII, E.M., and IURKOV, Iu.S., "On Convective Stability in the Presence of Periodically Varying Parameter," J. of Applied Math. and Mechanics (PMM), Vol. 34, No. 3, 1970, PP. 442-452.

20. MARKMAN, G.S. and YUDOVICH, V.I., "A Numerical Study of the Occurrence of Convection in a Liquid Layer Under the Influence of Periodic External Forces," Fluid Dynamics, Vol. 7, No. 3, 1972, PP. 434-438.

21. BURDE, G.I., "Finite Amplitude Convection Produced in a Modulated Gravitational Field," Fluid Dynamics, Vol. 7, No. 6, 1972, PP. 975-983.

22. MARKMAN, G.S., "The Development of Time Periodic Secondary Convective Flows," Fluid Dynamics, Vol. 8, No. 3, 1973, PP. 391-395.

23. MARKMAN, G.S., "Stability of the Equilibrium of a Liquid Layer Under the Influence of a Temperature Gradient That is Periodic in Time," Fluid Dynamics, Vol. 8, No. 5, 1973, PP. 805-808.

24. MARKMAN, G.S. and URINTSEV, A.L., "Effect of High-Frequency Vibration on the Development of Secondary Convective Conditions," Fluid Dynamics, Vol. 11, No. 2, 1975, PP. 245-250.

25. KO, R.S. and LOCK, G.S.H., "Laminar Free Convection in Periodic and Non-uniform Body Force Fields," 5th International Heat Transfer Converence, Sept. 3-7, 1974, Tokyo.

26. LIN, C.C., "Motion in the Boundary Layer with a Rapidly Oscillating External Flow," Proc. 9th Intern. Cong. Appl. Mech., Brussels 4, 1956, PP. 155-167.

27. KO, R.S., "Laminar Free Convection From a Radial Rotating Fin," M.Sc. Thesis, Univ. of Alberta, 1971.

28. LOCK, G.S.H. and KO, R.S., "Laminar Free Convection From a Rotating Radial Plate," J. of Heat Transfer, Trans. ASME, Series C, Vol. 94, No. 4, 1972, PP. 419-424.

29. LOCK, G.S.H. and KO, R.S., "Coupling Through a Wall Between Two Free Convective Systems," Int. J. Heat Mass Transfer, Vol. 16, 1973, PP. 2087-2096.

30. HAYDAY, A.A., BOWLUS, D.A., and MCGRAW, R.A., " Free Convection From a Vertical Flat Plate With Step Discontinuities in Surface Temperature," J. of Heat Transfer, Trans. ASME, Series C, Vol. 89, 1967, PP. 244-250.

31. LEFEVRE, E.J., "Laminar Free Convection From a Vertical Plane Surface," 9th International Congress of Applied Mechanics (Brussels), Vol. 4, 1957, PP. 168-174.

32. BLASIUS, H., "Grenzschichten in Flussigkeiten mit Kleiner Reibung," Z. Math. u. Phys. V. 56, 1908, PP. 1-37.

33. HOWARTH, L., "On the Solution of the Laminar Boundary Layer Equation," Proc. Roy, Soc. London A, Vol. 164, 1938, PP. 547-579.

34. HOWARTH, L., "Concerning the Effect of Compressibility on Laminar Boundary Layers and Their Separation," Proc. Roy. Soc. London A, Vol. 194, 1948, PP. 16-42.

35. LOCK, G.S.H. and GUNN, J.C., "Laminar Free Convection From a Downward-Projecting Fin," Trans. ASME, Series C, J. of Heat Transfer, Vol. 90, No. 1, 1968, PP. 63-70.

36. ROBERTS, S.M. and SHIPMAN, J.S., " Two-Point Boundary Value Problems: Shooting Methods." American Elsevier Publishing Company, Inc. 1972.

37. NACHTSHEIM, P.R. and SWIGERT, P., "Satisfaction of Asymptotic Boundary Conditions in Numerical Solution of Systems of Nonlinear Equations of Boundary-Layer Type," NASA-TN-D-3004, 1965.

38. POWER, M.J.D., "An Efficient Method of Finding the Minimum of a Function of Several Variables Without Calculating Derivatives," The Computer Journal, Vol. 7, 1964, PP. 155-162.

39. OSTRACH, S., "An Analysis of Laminar Free-Convection Flow and Heat Transfer About a Flat Plate Parallel to the Direction of the Generating Body Force," NACA TR 1111, 1953.

40. SPARROW, E.M. and GREGG, J.L., "Laminar Free Convection From a Vertical Plate with Uniform Surface Heat Flux," Trans. ASME, Series C, Vol. 78, 1956, PP. 435-440.

41. SPARROW, E.M. and GREGG, J.L., " Similar Solutions for Free Convection From a Nonisothermal Vertical Plate," Trans. ASME, Series C, Vol 80, 1958, PP. 379-386.

42. YANG, K.T., "Possible Similarity Solutions for Laminar Free Convection on Vertical Plates and Cylinders," Journal of Applied Mechanics, Vol. 27, Trans. ASME, Series E, Vol. 82, No. 2, 1960, PP. 230-236.

43. TAKHAR, H.S., "Free Convection From a Flat Plate," Journal of Fluid Mechanics, Vol. 34, Part 1, 1968, PP. 81-89.

44. Lock, G.S.H., "Steady Laminar Free Convection From Inclined, Arbitrarily Shape Plane Surfaces", Trans. ASME, Series C, Vol 84, 1964, PP. 669-673.

45. Ames, W.F., Nonlinear Ordinary Differential Equations in Transport Processes, Academic Press, 1968, P. 175.

46. Conte, S.D., Elementary Numerical Analysis, McGraw Hill, 1965, P. 236.

47. Daniel, C. and Wood, F.S., Fitting Equations to Data, Wiley-Interscience, 1971.

48. Schlichting, H., Boundary-Layer Theory, McGraw-Hill, 1968.

APPENDIX A

DERIVATION OF EQUATIONS

Under the assumptions given in section 2.1, the governing equations of this rotating fin problem are:

$$\rho_t + U\rho_X + V\rho_Y + \rho(U_X+V_Y) = 0, \tag{A.1}$$

$$\rho(U_t + UU_X + VU_Y) = -P_X + \mu(U_{XX} + U_{YY}) - \rho[(R-X)\omega^2 + 2\lambda\omega V + g\cos(\omega t)], \tag{A.2}$$

$$\rho(V_t + UV_X + VV_Y) = -P_Y + \mu(V_{XX} + V_{YY}) + \rho[Y\omega^2 + 2\lambda\omega U - \lambda g\sin(\omega t)], \tag{A.3}$$

$$\rho c_p(T_t + UT_X + VT_Y) = K_f(T_{XX} + T_{YY}) + 2\mu(U_X^2 + V_Y^2) + \mu(U_Y + V_X)^2, \tag{A.4}$$

where subscripts t, X, and Y denote the partial differentiations with respect to these variables, and λ=-1 or +1 for the trailing and leading sides of the fin, respectively.

In laminar-free-convection problems of incompressible flow, the temperature difference is usually regarded as the only significant cause of the variation in density and, also, this variation is assumed to be small. In other words, if β is the coefficient of volume expansion and subscript "∞" indicates a convenient steady state of reference, the density

of the fluid at temperature T is taken as

$$\rho = \rho_\infty[1 - \beta(T-T_\infty)] \tag{A.5}$$

where

$$\beta(T-T_\infty) \ll 1 \tag{A.6}$$

is the necessary condition.

When the problem is steady, a conventional assumption is often applied; namely, the density ρ is regarded as a constant in all terms of the governing equations except those terms associated with body forces. This is because the body forces usually have larger magnitudes than the others (such as inertia force) in free-convection problems, the product of the small density change and these body force terms can not, then, be ignored in spite of the condition (A.6). In fact, this product is the primary factor driving the free-convection phenomena. However, the feasibility of applying this Oberbeck-Boussinesq approximation to an unsteady free-convection problem needs some further consideration.

When the unsteadiness is due to the loss of equilibrium from a steady state such as in transient problems, the transient terms in the governing equations can be small in comparison with the body force terms. The application of the Oberbeck-Boussinesq approximation is then essentially the same as in the steady problems. In the present study, the unsteadiness is caused by the

periodically varying effect of the gravitational force. If the rotating speed of the system is relatively high but not high enough to abate the gravitational force effect, the transient terms may not be small and, on the contrary, may even be of the same order of magnitude as body force terms. Hence, it is possible that changes in fluid density can produce a significant effect in periodic convection problems through not only the body force but the transient terms. Therefore, substitution of approximation (A.5) into equations (A.1)-(A.4) gives, respectively:

$$U_X + V_Y = \beta(T_t + UT_X + VT_Y)/[1 + \beta(T-T_\infty)] \tag{A.7}$$

$$[1 - \beta(T-T_\infty)](U_t + UU_X + VU_Y) = -\frac{1}{\rho_\infty}P_X + \nu(U_{XX} + U_{YY}) - [1 - \beta(T-T_\infty)][(R-X)\omega^2 + 2\lambda\omega V + g\cos(\omega t)], \tag{A.8}$$

$$[1 - \beta(T-T_\infty)](V_t + UV_X + VV_Y) = \frac{-1}{\rho_\infty}P_Y + \nu(V_{XX} + V_{YY}) + [1 - \beta(T-T_\infty)][Y\omega^2 + 2\lambda\omega U - \lambda g\sin(\omega t)], \tag{A.9}$$

$$[1 - \beta(T-T_\infty)](T_t + UT_X + VT_Y) = \kappa_f(T_{XX} + T_{YY}) + \frac{2\nu}{c_p}(U_X^2 + V_Y^2) + \frac{\nu}{c_p}(U_Y + V_X)^2. \tag{A.10}$$

For convenience, the temperature of the fluid "infinitely" far from the fin can be chosen to be the reference temperature of the system; in addition, it is also desirable to set

$$P = P_\infty + \underline{P} \tag{A.11}$$

where $\underline{P}$ is the pressure departure from the reference pressure distribution P_∞ satisfying

$$\frac{\partial P_\infty}{\partial X} = -\rho_\infty[(R-X)\omega^2 + g\cos(\omega t)] \tag{A.12}$$

and

$$\frac{\partial P_\infty}{\partial Y} = \rho_\infty[Y\omega^2 - \lambda g\sin(\omega t)]. \tag{A.13}$$

In other words, P_∞ is the pressure distribution when the whole system is at a uniform temperature T_∞ (i.e. neither heating nor cooling at the root of the fin) and is rotating at a constant angular velocity ω about a fixed horizontal axis.

With the help of equations (A.11)-(A.13) and the condition (A.6), the governing equations (A.7)-(A.10) are simplified to be

$$U_X + V_Y = \beta(T_t + UT_X + VT_Y), \tag{A.14}$$

$$U_t + UU_X + VU_Y = -\frac{1}{\rho_\infty}\underline{P}_X + \nu(U_{XX} + U_{YY}) - 2\lambda\omega V + \beta[(R-X)\omega^2 + g\cos(\omega t)](T-T_\infty), \tag{A.15}$$

$$V_t + UV_X + VV_Y = -\frac{1}{\rho_\infty}\underline{P}_Y + \nu(V_{XX} + V_{YY}) + 2\lambda\omega U - \beta[Y\omega^2 - \lambda g\sin(\omega t)](T-T_\infty), \tag{A.16}$$

and

$$T_t + UT_X + VT_Y = \kappa_f(T_{XX} + T_{YY}) + \frac{2\nu}{c_p}(U_X^2 + V_Y^2) + \frac{\nu}{c_p}(U_Y + V_X)^2. \tag{A.17}$$

These are the boundary layer equations used in the present study. It is worth mentioning that owing to condition (A.6), the buoyancy effect of the Coriolis force is suppressed in the equations of motion by comparing it to the Coriolis force itself.

APPENDIX B

NORMALIZATION

The method for separation of equations, described in section 2.4, can be used to split the governing equations (A.14)-(A.17) into a steady state set:

$$U^S_X + V^S_Y = \beta(U^S\theta^S_X + V^S\theta^S_Y), \tag{B.1}$$

$$U^S U^S_X + V^S U^S_Y = \frac{-1}{\rho_\infty} P^S_X + \nu(U^S_{XX} + U^S_{YY}) - 2\lambda\omega V^S + \beta\omega^2(R-X)\theta^S, \tag{B.2}$$

$$U^S V^S_X + V^S V^S_Y = \frac{-1}{\rho_\infty} P^S_Y + \nu(V^S_{XX} + V^S_{YY}) + 2\lambda\omega U^S - \beta\omega^2 Y\theta^S, \tag{B.3}$$

$$U^S\theta^S_X + V^S\theta^S_Y = \kappa_f(\theta^S_{XX} + \theta^S_{YY}) + \frac{2\nu}{c_p}[(U^S_X)^2 + (V^S_Y)^2] + \frac{\nu}{c_p}(U^S_Y + V^S_X)^2 \tag{B.4}$$

and a periodic set:

$$U^P_X + V^P_Y = \beta[\theta^P_t + U^S\theta^P_X + V^S\theta^P_Y + U^P\theta^S_X + V^P\theta^S_Y + U^P\theta^P_X + V^P\theta^P_Y], \tag{B.5}$$

$$U^P_t + U^S U^P_X + V^S U^P_Y + U^P U^S_X + V^P U^S_Y + U^P U^P_X + V^P U^P_Y = \frac{-1}{\rho_\infty} P^P_X + \nu(U^P_{XX} + U^P_{YY}) - 2\lambda\omega V^P + \beta\omega^2(R-X)\theta^P + \beta g\cos(\omega t)\theta^S + \beta g\cos(\omega t)\theta^P, \tag{B.6}$$

$$v^p_t + u^s v^p_x + v^s v^p_y + u^p v^s_x + v^p v^s_y + u^p v^p_x + v^p v^p_y$$

$$= \frac{-1}{\rho_\infty} p^p_y + \nu(v^p_{xx} + v^p_{yy}) + 2\lambda\omega u^p - \beta\omega^2 y\theta^p$$

$$+ \lambda\beta g \sin(\omega t)\theta^s + \lambda\beta g \sin(\omega t)\theta^p, \qquad (B.7)$$

$$\theta^p_t + u^s\theta^p_x + v^s\theta^p_y + u^p\theta^s_x + v^p\theta^s_y + u^p\theta^p_x + v^p\theta^p_y$$

$$= \kappa_f(\theta^p_{xx} + \theta^p_{yy}) + \frac{2\nu}{c_p}[2u^s_x u^p_x + (u^p_x)^2 + 2v^s_y v^p_y + (v^p_y)^2]$$

$$+ \frac{\nu}{c_p}[(u^p_y)^2 + (v^p_x)^2 + 2(u^s_y u^p_y + u^s_y v^p_x + v^s_x u^p_y$$

$$+ u^p_y v^p_x + v^s_x v^p_x)]. \qquad (B.8)$$

Splitting the boundary conditions in the same manner, one can first analyze the steady problem separately; and then, based on the steady results, study the periodic part of the problem.

B.1 STEADY EQUATIONS

Since the problem approaches quasi-steady state when the rotating speed of the system becomes very high, it is reasonable to expect that the steady solutions are those of references [27,28]. Accordingly, the same normalization procedure can be applied to the present problem.

Upon using the following normalized variables [27]

$$x = X/L \qquad y = YRa^{1/4}/L$$

$$u^s = U^s L/\kappa_f Ra^{1/2} \qquad v^s = V^s L/\kappa_f Ra^{1/4} \qquad (B.9)$$

$$p^s = p^s/\rho\kappa\omega Ra^{1/4} \qquad \phi = \theta/\theta_r = (T-T_\infty)/(T_r-T_\infty),$$

equations (B.1)-(B.4) can be normalized:

$$u^s_x + v^s_y = \beta\theta_r(u^s\theta^s_x + v^s\theta^s_y) \tag{B.10}$$

$$\frac{1}{Pr}(u^s u^s_x + v^s u^s_y) - u^s_{yy} - (1-\gamma x)\phi^s = -[Ek^{-1}Ra^{-3/4}](p^s_x + 2\lambda v^s) + [Ra^{-1/2}]u^s_{xx}, \tag{B.11}$$

$$[Ek^{-1}Ra^{-1/2}](p^s_y - 2\lambda u^s) = [Ra^{-3/4}]v^s_{xx} + [Ra^{-1/4}](v^s_{yy} - y\phi) - [Ra^{-1/4}](u^s v^s_x + v^s v^s_y), \tag{B.12}$$

and

$$u^s\phi^s_x + v^s\phi^s_y - \phi^s_{yy} = [Ra^{-1/2}]\phi^s_{xx} + [Os](u^s_y)^2 + 2[OsRa^{-1/2}](u^s_x u^s_x + u^s_y v^s_x + v^s_y v^s_y) + [OsRa^{-1}](v^s_x)^2 \tag{B.13}$$

When air is the fluid, Prandtl number is of order one and the conditions that $Ra^{-1/4}$, $\beta\theta_r$, and Os are all much less than unity, all the right hand sides of equations (B.10)-(B.13) are negligible. The following boundary layer equations are, therefore, derived:

$$u^s_x + v^s_y = 0, \tag{B.14}$$

$$\frac{1}{Pr}(u^s u^s_x + v^s u^s_y) = u^s_{yy} + (1-\gamma x)\phi^s, \tag{B.15}$$

$$p^s_y = 2\lambda u^s \tag{B.16}$$

and

$$u^s\phi^s_x + v^s\phi^s_y = \phi^s_{yy} \tag{B.17}$$

As an example, for a 6-inch aluminum fin, 12 inches from the center of rotation, rotating synchronously with its ambient air 300 rpm, if $\Theta_r = T_r - T_\infty$ is 10°F, one will have $\beta\Theta_r \approx 0.019$, $Os \approx 2.2 \times 10^{-4}$, $Ra^{-1/4} \approx 0.011$, and $Ek^{-1}Ra^{-3/4} \approx 0.06$.

Equations (B.14)-(B.17) imply that in the boundary layers:

(1) the viscous force and the buoyancy force due to the centrifugal acceleration are of the same order of magnitude;

(2) the inertia force has a comparable magnitude to the above two forces if Prandtl number is of order one;

(3) the inertia force is negligible if Prandtl number is much greater than one;

(4) the Coriolis force induces the lateral pressure variation;

(5) conduction and advection are equally important; and

(6) disregarding the pressure distribution, the problem is symmetric about the X-axis.

In a word, the nature of this quasi-steady problem is governed by the simultaneous equations (B.14), (B.15), and (B.17), and the pressure distribution can be calculated separately, if desired, after the velocity and temperature distributions have been obtained.

The normalized, boundary conditions associated with equations (B.14), (B.15) and (B.17) are

$$x = 0: \qquad u^s = 0, \qquad \phi^s = 0$$

$$y = 0 (1 \geq x \geq 0): \qquad u^s = 0, \quad v^s = 0, \quad \phi^s = \phi_o^s(x) \qquad (B.18)$$

$$y = \infty: \qquad u^s = 0, \qquad \phi^s = 0$$

where $\phi_o^s(x)$ is the steady temperature distribution along the fin surface.

B.2 PERIODIC EQUATIONS

In addition to the normalized variables (B.9) for steady solutions, the following variables can be introduced into the unsteady equations (B.5)-(B.8) of this periodic problem:

$$u^p = \frac{U^p}{U_c}, \quad v^p = \frac{V^p}{V_c}, \quad \underline{x} = \frac{X}{X_c}, \quad \underline{Y} = \frac{Y}{Y_c},$$

$$\tau = \frac{t}{t_c}, \quad p^p = \frac{P^p}{P_c}, \quad \text{and} \quad \phi^p = \frac{\theta^p}{\theta_c}, \qquad (B.19)$$

where subscript c indicates the undetermined characteristic values of the corresponding variables. The normalized equations, then, become

$$\left[\frac{U_c}{X_c}\right] u^p_{\underline{x}} + \left[\frac{V_c}{Y_c}\right] v^p_{\underline{Y}} = \left[\frac{\beta\theta_c}{t_c}\right] \phi^p_\tau + \left[\frac{\beta\theta_c \kappa_f Ra^{1/2}}{LX_c}\right] u^s \phi^p_{\underline{x}}$$

$$+ \left[\frac{\beta\theta_c \kappa_f Ra^{1/4}}{LY_c}\right] v^s \phi^p_{\underline{Y}} + \left[\frac{\beta\theta_r U_c}{L}\right] u^p \phi^s_x + \left[\frac{\beta\theta_r V_c Ra^{1/4}}{L}\right] v^p \phi^s_y$$

$$+ \left[\frac{\beta\theta_c U_c}{X_c}\right] u^p \phi^p_{\underline{x}} + \left[\frac{\beta\theta_c V_c}{Y_c}\right] v^p \phi^p_{\underline{Y}} \qquad (B.20)$$

$$\left[\frac{U_c}{t_c}\right]u^p_\tau + \left[\frac{U_c\kappa_f Ra^{1/2}}{LX_c}\right]u^s u^p_{\underline{x}} + \left[\frac{U_c\kappa_f Ra^{1/4}}{LY_c}\right]v^s u^p_{\underline{y}}$$

$$+ \left[\frac{U_c\kappa_f Ra^{1/2}}{L^2}\right]u^p u^s_x + \left[\frac{V_c\kappa_f Ra^{3/4}}{L^2}\right]v^p u^s_y + \left[\frac{U_c^2}{X_c}\right]u^p u^p_{\underline{x}}$$

$$+ \left[\frac{V_c U_c}{Y_c}\right]v^p u^p_{\underline{y}}$$

$$= -\left[\frac{P_c}{\rho_\infty X_c}\right]p^p_{\underline{x}} + \left[\frac{\nu U_c}{X_c^2}\right]u^p_{\underline{xx}} + \left[\frac{\nu U_c}{Y_c^2}\right]u^p_{\underline{yy}} - [\omega V_c]2\lambda v^p$$

$$+ [\beta\theta_c R\omega^2]\phi^p - [\beta\theta_c X_c\omega^2]\underline{x}\phi^p + [\beta\theta_r g]\phi^s\cos(\omega t_c\tau)$$

$$+ [\beta\theta_c g]\phi^p\cos(\omega t_c\tau), \qquad \text{(B.21)}$$

$$\left[\frac{V_c}{t_c}\right]v^p_\tau + \left[\frac{V_c\kappa_f Ra^{1/2}}{LX_c}\right]u^s v^p_{\underline{x}} + \left[\frac{V_c\kappa_f Ra^{1/4}}{LY_c}\right]v^s v^p_{\underline{y}}$$

$$+ \left[\frac{U_c\kappa_f Ra^{1/4}}{L^2}\right]u^p v^s_x + \left[\frac{V_c\kappa_f Ra^{1/2}}{L^2}\right]v^p f^s_y + \left[\frac{U_c V_c}{X_c}\right]u^p v^p_{\underline{x}}$$

$$+ \left[\frac{V_c^2}{Y_c}\right]v^p v^p_{\underline{y}}$$

$$= -\left[\frac{P_c}{\rho_\infty Y_c}\right]p^p_{\underline{y}} + \left[\frac{\nu V_c}{X_c^2}\right]v^p_{\underline{xx}} + \left[\frac{\nu V_c}{Y_c^2}\right]v^p_{\underline{yy}} + [\omega U_c]2\lambda u^p$$

$$- [\beta\theta_c Y_c\omega^2]\underline{y}\phi^p + [\beta\theta_r g]\lambda\phi^s\sin(\omega t_c\tau)$$

$$+ [\beta\theta_c g]\lambda\phi^p\sin(\omega t_c\tau), \qquad \text{(B.22)}$$

and

$$\left[\frac{G_c}{t_c}\right]\phi^p_\tau + \left[\frac{\theta_c \kappa_f Ra^{1/2}}{LX_c}\right]u^s\phi^p_{\underline{x}} + \left[\frac{\theta_c \kappa_f Ra^{1/4}}{LY_c}\right]v^s\phi^p_{\underline{y}} + \left[\frac{U_c \theta_r}{L}\right]u^p\phi^s_x$$

$$+ \left[\frac{V_c \theta_r Ra^{1/4}}{L}\right]v^p\phi^s_y + \left[\frac{U_c \theta_c}{X_c}\right]u^p\phi^p_{\underline{x}} + \left[\frac{V_c \theta_c}{Y_c}\right]v^p\phi^p_{\underline{y}}$$

$$= \left[\frac{\kappa_f \theta_c}{X_c^2}\right]\phi^p_{\underline{xx}} + \left[\frac{\kappa_f \theta_c}{Y_c^2}\right]\phi^p_{\underline{yy}} + \left[\frac{\nu U_c \kappa_f Ra^{1/2}}{c_p L^2 X_c}\right]4u^s_x u^p_{\underline{x}}$$

$$+\left[\frac{\nu U_c^2}{c_p X_c^2}\right]2(u^p_{\underline{x}})^2 + \left[\frac{\nu V_c \kappa_f Ra^{1/2}}{c_p LY_c}\right]4v^s_y v^p_{\underline{y}} + \left[\frac{\nu V_c^2}{c_p Y_c^2}\right]2(v^p_{\underline{y}})^2$$

$$+\left[\frac{\nu U_c^2}{c_p Y_c^2}\right](u^p_{\underline{y}})^2 + \left[\frac{\nu V_c^2}{c_p X_c^2}\right](v^p_{\underline{x}})^2 + \left[\frac{\nu U_c \kappa_f Ra^{3/4}}{c_p L^2 Y_c}\right]2u^s_y u^p_{\underline{y}}$$

$$+ \left[\frac{\nu V_c \kappa_f Ra^{3/4}}{c_p L^2 X_c}\right]2u^s_y v^p_{\underline{x}} + \left[\frac{\nu U_c \kappa_f Ra^{1/4}}{c_p L^2 Y_c}\right]2v^s_x u^p_{\underline{y}}$$

$$+\left[\frac{\nu U_c V_c}{c_p X_c Y_c}\right]2u^p_{\underline{y}} v^p_{\underline{x}} + \left[\frac{\nu V_c \kappa_f Ra^{1/4}}{c_p L^2 X_c}\right]2v^s_x v^p_{\underline{x}} \qquad \text{(B.23)}$$

In order to simplify these unsteady equations through normalization, one has to find the characteristic values of the periodic variables (B.19). The fin length is a convenient choice for X_c. Thus

$$X_c = L \qquad \text{(B.24)}$$

implies that

$$\underline{x} = x$$

When the angular velocity ω is decreasing from its very large value for the quasi-steady case, the periodic phenomenon gradually develops in the system. It is quite clear that this periodic character comes from the buoyancy force effect when gravity introduces its periodic influence, $g\cos(\omega t_c \tau)$ in the X-directional equation of motion, into the quasi-steady temperature field ϕ^s. In other words, this periodic driving force, $\beta g \phi^s \cos(\omega t_c \tau)$, is large in the vicinity of the solid fin because of higher temperature ϕ^s, decreases gradually across the thermal boundary layer, and eventually dies out with ϕ^s outside this steady thermal layer. Hence the Y-directional characteristic length of the steady problem can be chosen as Y_c, i.e.

$$Y_c = L/Ra^{1/4} \tag{B.25}$$

and thus

$$\underline{Y} = y \ .$$

A consequent question of interest is how the periodic buoyancy force, $\phi^s \cos(\omega t_c \tau)$, gives rise to the velocity fluctuations. Equation (B.21) shows that the fluctuation in u^p may be induced through inertia, viscous, or even transient terms. Consider the solid-fluid interface where the no-slip condition eliminates not only the transient and inertia terms but also the viscous term $u^p_{\underline{XX}}$ of equation (B.21). One can presume that the driving buoyance $\phi^s \cos(\omega t_c \tau)$

is balanced by the viscous force $u^p_{\underline{YY}}$ in the vicinity of the interface and set

$$\beta\theta_c g = \nu U_c / Y_c^2 \quad .$$

which yields

$$U_c = \frac{\kappa_f Ra^{1/2}}{LFr} \qquad (B.26)$$

There are two possible ways the periodic velocity u^p can introduce the fluctuation into the temperature field; one through the continuity equation (B.20) and the other through the energy equation (B.22). In the continuity equation, if the $u^p_{\underline{X}}$ term is the main "source" of the fluctuation and, hence, possesses the highest order of magnitude, it must be balanced by the ϕ^p_τ, $u^s\phi^p_{\underline{X}}$, or $v^s\phi^p_{\underline{Y}}$ terms. The fact that the last two terms are of the same magnitude leads to the necessary comparison of the magnitudes of the first two terms. To find their ratio, $L^2/t_c\kappa_f Ra^{1/2}$, one should first determine the characteristic time, t_c, of this problem.

It is evident that the period of the gravitational effect, $g\cos(\omega t)$, which generates the whole periodic phenomena, is a reasonalbe time scale, t_c. Therefore,

$$t_c = \frac{2\pi}{\omega} \qquad (B.27)$$

indicates that the aforementioned ratio becomes

$$\frac{\omega L^2}{2\pi\kappa_f Ra^{1/2}} = \frac{1}{2\pi}\left(\frac{Pr\gamma}{\beta\theta_r}\right)^{1/2} \quad .$$

If the ambient fluid is air at room temperature and θ_r is $10^{\circ}F$, the order of this ratio approaches $O\ \gamma^{1/2} \leq O[1]$. Hence in equation (B.20), both $u^p_{\underline{x}}$ and $u^s\phi^p_{\underline{x}}$ should have the same order of magnitude if the temperature fluctuation was produced through this equation. By setting

$$\frac{U_c}{X_c} = \frac{\beta\theta_c\kappa_f Ra^{1/2}}{LX_c}$$

one can define

$$\theta_c = \frac{1}{\beta Fr}$$

Substitution of this θ_c value into the transient term θ^p_τ in the energy equation (B.23) yields

$$\frac{\theta_c}{t_c} = \frac{\omega}{2\pi\beta Fr}$$

Obviously, this should never be greater than the order of magnitude of $u^p\phi^s_x$, which is the "source" of the fluctuation in this energy equation. However, the ratio of the magnitude of $u^p\phi^s_x$ to ϕ^p_τ reveals a contradiction:

$$\frac{U_c\theta_r t_c}{L\theta_c} = 2\pi\left(\frac{\beta^3\theta_r^3}{Pr\gamma}\right)^{1/2} \leq O[1]$$

when air is the fluid at room temperature.

This conflict indicates that the temperature fluctuation does not come directly from the continuity equation. Nevertheless, one does find that the transient term ϕ^p_τ is not as significant as $u^p_{\underline{x}}$ in the equation of continuity.

It is then reasonalbe by equating $u^p_{\underline{x}}$ and $v^p_{\underline{y}}$ to get

$$V_c = \frac{\kappa_f Ra^{1/4}}{LFr} \tag{B.28}$$

With the aid of characteristic values (B.24)-(B.28), the energy equation (B.23) can be rewritten as

$$\left[\frac{1}{DRa^{1/2}}\right]\phi^p_\tau + u^s\phi^p_x + v^s\phi^p_y + \left[\frac{\theta_r}{Fr\theta_c}\right](u^p\phi^s_x + v^p\phi^s_y)$$

$$+ \left[\frac{1}{Fr}\right](u^p\phi^p_x + v^p\phi^p_y)$$

$$= \left[\frac{1}{Ra^{1/2}}\right]\phi^p_{xx} + \phi^p_{yy} + \left[\frac{\theta_r Os}{\theta_c Fr}\right]\left[\frac{1}{Ra^{1/2}}\right](4u^s_x u^p_x + 4v^s_y v^p_y + 2u^s_y v^p_x + 2v^s_x u^p_y)$$

$$+ \left[\frac{1}{FrRa^{1/2}}\right]\left\{\left[2(u^p_x)^2 + 2(v^p_y)^2 + 2u^p_y v^p_x\right] + \left[\frac{1}{Fr}\right](u^p_y)^2\right.$$

$$\left. + \left[\frac{1}{FrRa}\right](v^p_x)^2 + 2u^s_y u^p_y + \left[\frac{1}{Ra}\right]2v^s_x f^p_x\right\} \tag{B.23a}$$

where parameter D is the dimensionless period for the fluid flow, and is equal to $2\pi\kappa_f/\omega L^2$. As mentioned before, if the temperature at the root of the fin is 10°F higher than that of its ambient air, i.e. θ_r=10°F, then

$$\frac{1}{DRa^{1/2}} = \frac{1}{2\pi}\left[\frac{Pr\gamma}{\beta\theta_r}\right]^{1/2}$$

$$= O[\gamma^{1/2}]$$

Since the parameter γ is always less than unity, it is apparent that if $A=DRa^{1/2}$

$$\frac{1}{A} = \frac{1}{DRa^{1/2}} \leq O[1].$$

In general, if $Ra^{-1/2}$ and Os are much less than order one, all the viscous dissipation terms in energy equation become negligible in comparison with the driving terms, $u^p\phi^s_x + v^p\phi^s_y$, of the temperature fluctuation. As a matter of fact, the whole energy equation may be normalized by setting

$$\frac{\theta_r}{Fr\theta_c} = 1,$$

therefore the characteristic value of θ_c is found

$$\theta_c = \frac{\theta_r}{Fr} . \qquad (B.29)$$

Substituting characteristic values (B.24)-(B.29) into the continuity equation (B.20), one obtains

$$u^p_x + v^p_y = \left[\frac{\beta\theta_r}{A}\right]\phi^p + [\beta\theta_r](u^s\phi^p_x + v^s\phi^p_y + u^p\phi^s_x + v^p\phi^s_y)$$

$$+\left[\frac{\beta\theta_r}{Fr}\right](u^p\phi^p_x + v^p\phi^p_y) . \qquad (B.20a)$$

No contradiction takes place by choosing the definition (B.29) for θ_c.

In order to determine p_c, one again introduces the obtained characteristic values into, and then normalizes, the Y-directional equation of motion. Equation (B.22) becomes

$$\left[\frac{S_1}{2\pi Ra^{1/4}}\right]v^p_\tau + \left[\frac{S_2}{PrRa^{1/4}}\right](u^s v^p_x + v^s v^p_y + u^p v^s_x + v^p v^s_y)$$

$$+\left[\frac{S_2}{PrFrRa^{1/4}}\right](u^p v^p_x + v^p v^p_y) = -p^p_y + \left[\frac{S_2}{Ra^{3/4}}\right]v^p_{xx} + \left[\frac{S_2}{Ra^{1/4}}\right]v^p_{yy}$$

$$+ [S_1]2\lambda u^p - \left[\frac{S_2\gamma}{Ra^{1/4}}\right]y\phi^p + [S_2]\lambda\phi^s \sin(2\pi\tau) + \left[\frac{S_2\gamma}{FrRa^{1/4}}\right]\lambda\phi^p \sin(2\pi\tau),$$

(B.22a)

Comparison of the magnitudes of parameters

$$S_1 = \frac{\rho_\infty \kappa_f \, Ra^{1/4}}{2\pi P_c Fr}$$

and

$$S_2 = \frac{\rho_\infty \beta \theta_r g L}{P_c Ra^{1/4}}$$

will indicate whether the Coriolis or the gravitational force causes the pressure fluctuation. The ratio of S_1 to S_2 is defined by

$$S = \frac{S_1}{S_2} = \frac{1}{2\pi}\left(\frac{\gamma}{Pr\beta\theta_r}\right)^{1/2} ,$$

If S>O[1], setting

$$P_c = \rho_\infty \kappa_f \omega Ra^{1/4}/2\pi Fr \qquad (B.30)$$

into equation (B.22a) gives

$$p_y^p = 2\lambda u^p + [\tfrac{1}{S}]\lambda\phi^s \sin(2\pi\tau) \qquad (B.22b)$$

and if S<O[1], setting

$$P_c = \rho_\infty \beta \theta_r g L/Ra^{1/4} \qquad (B.30a)$$

into equation (B.22a) gives

$$p_y^p = \lambda\phi^s \sin(2\pi\tau) + [S]2\lambda u^p \; ; \qquad (B.22c)$$

for S=O[1]. Both definitions (B.30) and (B.30a) are proper.

In fact, no matter which definition of P_c is chosen, the X-directional momentum equation (B.21) can be normalized

into

$$\frac{1}{Pr}\left[\left[\frac{1}{A}\right]u^p_\tau + u^s u^p_x + u^p u^s_x + v^s u^p_y + v^p u^s_y + \left[\frac{1}{Fr}\right](u^p u^p_x + v^p u^p_y)\right]$$

$$= u^p_{yy} + \phi^s \cos(2\pi\tau) + (1-\gamma x)\phi^p + \left[\frac{1}{Fr}\right]\phi^p \cos(2\pi\tau)$$

$$+ O[Ra^{1/4}, Ek^{-1}Ra^{-3/4}] \qquad \text{(B.21a)}$$

With the help of the example illustrated in section B.1, it is easy to show that the velocity and temperature fluctuations are governed by

$$u^p_x + v^p_y = 0, \qquad \text{(B.20b)}$$

$$\frac{1}{Pr}\left[\left[\frac{1}{A}\right]u^p_\tau + u^s u^p_x + u^p u^s_x + v^s u^p_y + v^p u^s_y + \left[\frac{1}{Fr}\right](u^p u^p_x + v^p u^p_y)\right]$$

$$= u^p_{yy} + \phi^s \cos(2\pi\tau) + (1-\gamma x)\phi^p + \left[\frac{1}{Fr}\right]\phi^p \cos(2\pi\tau), \qquad \text{(B.21b)}$$

and

$$\left[\frac{1}{A}\right]\phi^p_\tau + u^s \phi^p_x + v^s \phi^p_y + u^p \phi^s_x + v^p \phi^s_y + \left[\frac{1}{Fr}\right](u^p \phi^p_x + v^p \phi^p_y)$$

$$= \phi^p_{yy}, \qquad \text{(B.23b)}$$

subject to the boundary conditions

$$\begin{aligned} &x = 0: && u^p = 0, && \phi^p = 0 \\ &y = 0 \ (x \geq 0): && u^p = 0, && v^p = 0, \quad \phi^p = \phi^p_o(x,\tau) \\ &y = \infty: && u^p = 0, && \phi^p = 0 \end{aligned} \qquad \text{(B.31)}$$

The pressure fluctuation p^p can be obtained separately from either equation (B.22b) or (B.22c) depending on the magnitude of parameter S.

From this normalization, equation (2.8) can be re-written as:

$$u(x,y,\tau) = u^s(x,y) + [\frac{1}{Fr}]u^p(x,y,\tau),$$

$$v(x,y,\tau) = v^s(x,y) + [\frac{1}{Fr}]v^p(x,y,\tau), \qquad (B.32)$$

and $$\phi(x,y,\tau) = \phi^s(x,y) + [\frac{1}{Fr}]\phi^p(x,y,\tau),$$

where $$u = UL/\kappa_f Ra^{1/4}$$

$$v = VL/\kappa_f Ra^{1/4}$$

and $$\phi = \theta/\theta_r = (T-T_\infty)/(T_r-T_\infty)$$

are the normalized solutions of the complete problem. Accordingly, the normalized forms of equations (A.14)-(A.17) are

$$u_x + v_y = 0, \qquad (B.34)$$

$$\frac{1}{Pr}\left[[\frac{1}{A}]u_\tau + uu_x + vu_y\right] = u_{yy} + (1-\gamma x)\phi + [\frac{1}{Fr}]\phi\cos(2\pi\tau), \qquad (B.35)$$

$$p_y = 2\lambda u, \qquad (B.36)$$

and

$$[\frac{1}{A}]\phi_\tau + u\phi_x + v\phi_y = \phi_{yy}\,. \qquad (B.37)$$

It should be pointed out that in the above equations, u_τ and ϕ_τ are not normalized quantities if the magnitude of 1/Fr is not of order one since from the equalities (B.32)

$$u_\tau = \frac{1}{Fr}\,u^p_\tau \qquad \text{and} \qquad \phi_\tau = \frac{1}{Fr}\,\phi^p_\tau$$

where quantities u_τ^p and ϕ_τ^p instead of u_τ and ϕ_τ , are actually normalized. This fact would not be revealed if equations (B.34)-(B.37) were obtained from the direct normalization of equations (A.14)-(A.17). In other words, when the Froude number Fr in equation (B.35) decreases with the angular velocity ω of the system from very high magnitude, this equation (B.35) can not provide sufficient information about the point where the transient term starts introducing a comparatively significant effect on the problem. From equation (B.21b), it is very clear that the parameter A is the determining factor of this.

If the temperature at the fin root is 10°F above the ambient temperature and the Prandtl number of the fluid is of order one, the magnitude

$$\frac{1}{A} = \frac{1}{2\pi}\left(\frac{Pr}{\beta\theta_r}\right)^{1/2} = O[\gamma^{1/2}] \qquad (B.38)$$

indicates that the transient effect is negligible when the geometric ratio γ approaches the limiting case of $\gamma=0$ [27,35]. In general, $0<\gamma<1$ implies

$$\frac{1}{A} \leq O[1],$$

hence it is proper to keep the transient terms in equations (B.35) and (B.37), provided that the Froude number is not much greater than unity.

APPENDIX C

LOCAL SIMILARITY TRANSFORMATION

In order to solve three simultaneous boundary layer equations (B.34), (B.35) and (B.37), a stream function $\psi(x,y)$ defind by

$$u = \frac{\partial \psi}{\partial y} \qquad \text{and} \qquad v = -\frac{\partial \psi}{\partial x} ,$$

is introduced. Since the continuity equation (B.34) is satisfied completely, this boundary layer problem is then governed by only two simultaneous equations:

$$Pr\psi_{yyy} + \psi_x\psi_{yy} - \psi_y\psi_{xy} + Pr\left[(1-\gamma x) + [\frac{1}{Fr}]\cos(2\pi\tau)\right]\phi - [\frac{1}{A}]\psi_{y\tau} = 0 \qquad (C.1)$$

$$\phi_{yy} + \psi_x\phi_y - \psi_y\phi_x - [\frac{1}{A}]\phi_\tau = 0 \qquad (C.2)$$

The associated coundary conditions are:

$x = 0;$ $\quad \psi_y = 0,$ $\quad \phi = 0$

$y = 0 (1 \geq x \geq 0);$ $\quad \psi = 0,$ $\quad \psi_y = 0,$ $\quad \phi = \phi_o(x),$

$y = \infty;$ $\quad \psi_y = 0,$ $\quad \phi = 0.$

The follow-up effort is in finding a suitable transformation to:

(1) lessen the dependence of the solutions in the streamwise direction and thus decrease the error introduced by any finite difference formula on approximating streamwise derivatives of the governing equations;

(2) alleviate the possible singularity problem at the leading edge; that is,

$$\lim_{x\to 0}\phi_o(x) \neq \lim_{y\to 0}\phi(0,y) = 0$$

(3) reduce the importance of the Prandtl number in the resulting problem and thus remove the need to determine separate solutions for a large number of Pr.

A transformation is assumed to take the following form:

$$\xi = L(x), \quad \eta = F(Pr)N(x)I(y), \quad \Phi(\xi,\eta) = \phi(x,y), \text{ and } \quad f(\xi,\eta) = \psi(x,y)/G(Pr)M(x), \tag{C.3}$$

where $\Phi(\xi,\eta)$ and $f(\xi,\eta)$ are two dependent variables in the new coordinate system, and correspond to original temperature function $\phi(x,y)$ and stream function $\psi(x,y)$ respectively. Six unknown functions, L(x), M(x), I(y), F(Pr) and G(Pr), are disclosed after the substitution of this transformation into equations (C.1) and (C.2). That is,

$$\begin{aligned}&\left[(PrF^3GMN^3I_y^3)f_{\eta\eta\eta} + 3(PrF^2GMN^2I_yI_{yy})f_{\eta\eta} + (PrFGMNI_{yyy})f_\eta\right] \\ &+ \left[(F^2G^2MN^2M_xI_y^2)ff_{\eta\eta} + (F^2G^2M^2NN_xII_{yy} - F^2G^2MN^2M_xI_y^2 \right. \\ &\left. - F^2G^2M^2NN_xI_y^2)f_\eta^2\right] + \left[(Pr)\left(1 - \gamma x + \frac{1}{Fr}\cos(2\pi\tau)\right)\Phi\right] \\ &= \left[(F^2G^2M^2N^2L_xI_y^2)(f_\eta f_{\eta\xi} - f_{\eta\eta}f_\xi) - (FG^2M^2NL_xI_{yy})f_\eta f_\xi\right] \\ &+ \left[\frac{1}{A}(FGMNI_y)f_{\eta\tau}\right]\end{aligned} \tag{C.4}$$

and

$$\begin{aligned}&\left[(F^2N^2I_y^2)\Phi_{\eta\eta} + (FNI_{yy})\Phi_\eta\right] + \left[(FGNM_xI_y)f\Phi_\eta\right] \\ &= \left[(FGMNL_xI_y)(f_\eta\Phi_\xi - \Phi_\eta f_\xi)\right] + \left[\frac{1}{A}\Phi_\tau\right]\end{aligned} \tag{C.5}$$

With the purpose constructing a basis for "local similarity", terms containing only the η-derivatives are kept on the left-hand-sides of the equations. In addition, terms for the same physical effect are square-bracketed into one group. For instance, the first three groups on the left-hand-side of equation (C.4) are, in a sequential order, related to viscous, inertia and buoyancy forces while the first and the second square-bracketed groups on the right-hand-side correspond to the variation of the inertia force along ξ-direction and the transient effect. Similarly, the first and the second groups on the left-hnad-side of equation (C.5) represent advection and conduction heat transfer while the first and the second right-hand-side groups indicate the variation of conduction in the ξ-direction and the transient effect, respectively.

It is assumed at this stage and is later substantiated by the normalized equations that the highest order derivative term in each square-bracketed group should never be suppressed by other terms in the same group. Hence, only the coefficient of highest order term in a group is employed below to determine the aforesaid six unknown functions whenever the group is considered to be physically significant.

Since advection and conduction are equally important in the thermal boundary layer, it is reasonable to equate

their parenthesized coefficients in equation (C.5). That is, $F^2N^2I_y^2 = FGNM_xI_y$

or by rearrangement,

$$\frac{N(x)}{M_x(x)I_y(y)} = \frac{G(Pr)}{F(Pr)} = C_1$$

where C_1 is an undefined constant because the left-hand-side of the above equality is a function of x and y while the right-hand-side is a function of Pr only. Similarly,

$$\frac{N(x)}{M_x(x)} = C_1I_y(y) = C_2;$$

that is, the function I(y) takes the form

$$I(y) = \frac{C_2}{C_1}y + C_3.$$

For convenience and without loss of generality, one can define $C_1=C_2=1$ and $C_3=0$ and obtain

$$F(Pr) = G(Pr) \qquad (C.6)$$

$$I(y) = y \qquad (C.7)$$

$$N(x) = M_x(x) \qquad (C.8)$$

In order to find F(Pr) or G(Pr), consideration should be given to the momentum equation (C.4) where the buoyancy force term, ϕ, is always dominant. However, the inertia force term, $ff_{\eta\eta}$, and the viscous force term, $f_{\eta\eta\eta}$, vary inversely in significance as the Prandtl number changes. When Pr is of order one, both inertia and viscous forces play important roles in balancing the buoyancy force.

Therefore from equation (C.4) and equalities (C.6)-(C.8),

$$[F^3GMN^3I_y^3]_{Pr=O[1]} = O[1]$$

yields

$$MM_x^3[F^4]_{Pr=O[1]} = O[1] \tag{C.9}$$

and

$$\left[\frac{F^2G^2MN^2M_xI_y^2}{Pr}\right]_{Pr=O[1]} = O[1]$$

yields

$$MM_x^3\left[\frac{F^4}{Pr}\right]_{Pr=O[1]} = O[1]. \tag{C.10}$$

When Pr approaches infinity, the inertia force is negligibly small but the viscous effect remains significant. That is,

$$MM_x^3 \lim_{Pr\to\infty} [F^4] = O[1] \tag{C.11}$$

and

$$MM_x^3 \lim_{Pr\to\infty} \frac{F^4}{Pr} = 0. \tag{C.12}$$

On the other hand, the viscous force can be dominated by the inertia force at very small Pr. Thus,

$$MM_x^3 \lim_{Pr\to 0} [F^4] = 0 \tag{C.13}$$

and

$$MM_x^3 \lim_{Pr\to 0} \left[\frac{F^4}{Pr}\right] = O[1]. \tag{C.14}$$

Apparently, functions F(Pr) and M(x) must be defined in such a manner that the above six conditions (C.9)-(C.14)

are completely satisfied. This can be fulfilled by setting

$$MM_x^3 = 1, \qquad \text{and} \qquad F^4 + \frac{F^4}{Pr} = 1.$$

Hence,

$$M(x) = \left(\frac{4}{3}x + C_4\right)^{3/4}$$

and

$$F(Pr) = \left(\frac{Pr}{1+Pr}\right)^{1/4} \tag{C.15}$$

also from (C.8)

$$N(x) \equiv M_x(x) = \left(\frac{4}{3}x + C_4\right)^{-1/4};$$

Since in transformation (C.3),

$$\eta = F(Pr)N(x)I(y) = \left[\frac{Pr}{1+Pr}\right]^{1/4}\left(\frac{4}{3}x + C_4\right)^{-1/4}y,$$

the possible singularity at the leading edge of the fin,

i.e. $\lim_{x\to 0} \phi_o(x) > 0$

and $\lim_{y\to 0} \phi(0,y) = 0,$

can be removed by setting $C_4=0$ to get

$$\eta = \left[\frac{Pr}{1+Pr}\right]^{1/4}\left(\frac{4}{3}x\right)^{-1/4}y.$$

In other words, the singular point (0,0) in the x-y plane is "stretched" into a line in the new ξ-η plane so that the discontinuity of temperature at this singular point is smoothed out along the line.

In order to define a proper function for L(x), one can substitute the following functions:

$$I(y) = y, \qquad M(x) = \left(\frac{4}{3}x\right)^{3/4}, \qquad N(x) = \left(\frac{4}{3}x\right)^{-1/4},$$

and

$$F(Pr) = G(Pr) = \left(\frac{Pr}{1+Pr}\right)^{1/4},$$

into equations (C.4) and (C.5) to get

$$Prf_{\eta\eta\eta} + ff_{\eta} - \frac{2}{3} f_{\eta}^2 + (1+Pr)\left(1 + \cos(2\pi\tau)/Fr\right)\Phi$$

$$= \frac{4}{3}[xL_x](f_{\eta}f_{\eta\xi} - f_{\eta\eta}f_{\xi}) + [\gamma x](1+Pr)\Phi$$

$$+ \frac{1}{A}\left(\frac{4}{3}\frac{1+Pr}{Pr}\right)^{1/2}[x^{1/2}]f_{\eta\tau} \qquad (C.16)$$

and

$$\Phi_{\eta\eta} + f\Phi_{\eta} = \frac{4}{3}[xL_x](f_{\eta}\Phi_{\xi} - \Phi_{\eta}f_{\xi}) + \frac{1}{A}\left(\frac{4}{3}\frac{1+Pr}{Pr}\right)^{1/2}[x^{1/2}]\Phi_{\tau}\,. \qquad (C.17)$$

To complete the transformation from the x-y domain into the ξ-η domain, all the square-bracketed terms in the above two equations should be either a function of ξ or constant. Assuming

$$L_x(x) = \gamma$$

yields

$$\xi = L(x) = \gamma x$$

where the arbitrary constant of integration is set to be zero for the sake of convenience. To sum up, the governing equations (C.1) and (C.2) are transformed into

$$Prf_{\eta\eta\eta} + ff_{\eta\eta} - \frac{2}{3} f_{\eta}^2 + (1+Pr)\left(1 + \cos(2\pi\tau)/Fr\right)\Phi$$

$$= \xi\left(\frac{4}{3}(f_{\eta}f_{\eta\xi} - f_{\eta\eta}f_{\xi}) + (1+Pr)\Phi\right) + (K_1/2\pi)\xi^{1/2}f_{\eta\tau} \qquad (C.18)$$

and

$$\Phi_{\eta\eta} + f\Phi_{\eta} = \frac{4}{3}\xi(f_{\eta}\Phi_{\xi} - \Phi_{\eta}f_{\xi}) + (K_1/2\pi)\xi^{1/2}\Phi_{\tau} \qquad (C.19)$$

by the local similarity transformation:

$$\xi = \gamma x, \qquad \eta = \left(\frac{Pr}{1+Pr}\right)^{1/3}\left(\frac{4x}{3}\right)^{-1/3} y,$$

$$\Phi(\xi,\eta) = \phi(x,y), \qquad (C.20)$$

and $$f(\xi,\eta) = \left(\frac{Pr}{1+Pr}\right)^{-1/3}\left(\frac{4x}{3}\right)^{-1/3}\psi(x,y).$$

The associated boundary conditions for the above equations are

$$\eta = 0; \quad f = 0, \quad f' = 0, \quad \Phi_o(\xi) = \Phi(\xi,0) \qquad (C.21)$$

$$\eta = \infty; \quad f' = 0, \quad \Phi = 0.$$

APPENDIX D

PERTURBATION EXPANSION

The purpose of adopting this technique in the present study is not only to expand the solutions $f(\xi,\eta,\tau)$ and $\Phi(\xi,\eta,\tau)$ of equations (3.17)-(3.19) in a perturbation series of 1/Fr, but also to remove the time function from the perturbed equations so that less computation time is required to solve the remaining two-dimensional problem. To accomplish this, one seeks solutions in the form:

$$f(\xi,\eta,\tau) = f^s(\xi,\eta) + \frac{1}{Fr}[\tilde{f}(\xi,\eta)\cos(2\pi\tau) + \hat{f}(\xi,\eta)\sin(2\pi\tau)] + \frac{1}{Fr^2}[\bar{f}(\xi,\eta) + \tilde{\tilde{f}}(\xi,\eta)\cos(4\pi\tau) + \hat{\hat{f}}(\xi,\eta)\sin(4\pi\tau)] + O[\frac{1}{Fr^3}] \quad (D.1)$$

and

$$\Phi(\xi,\eta,\tau) = \Phi^s(\xi,\eta) + \frac{1}{Fr}[\tilde{\Phi}(\xi,\eta)\cos(2\pi\tau) + \hat{\Phi}(\xi,\eta)\sin(2\pi\tau)] + \frac{1}{Fr^2}[\bar{\Phi}(\xi,\eta) + \tilde{\tilde{\Phi}}(\xi,\eta)\cos(4\pi\tau) + \hat{\hat{\Phi}}(\xi,\eta)\sin(4\pi\tau)] + O[\frac{1}{Fr^3}] \quad (D.2)$$

where f^s and Φ^s, the quasi-steady solutions when $Fr=\infty$, satisfy the zeroth order equations:

$$Pr\, f^s_{\eta\eta\eta} + f^s f^s_{\eta\eta} - \frac{2}{3}(f^s_\eta)^2 + (1+Pr)\Phi^s = \xi[\frac{4}{3}(f^s_\eta f^s_{\eta\xi} - f^s_{\eta\eta} f^s_\xi) + (1+Pr)\Phi^s], \quad (D.3)$$

$$\Phi^s_{\eta\eta} + f^s\Phi^s_\eta = \frac{4}{3}\xi(f^s_\eta\Phi^s_\xi - \Phi^s_\eta f^s_\xi), \tag{D.4}$$

$$\xi\frac{d^2\Phi^s_o}{d\xi^2} + \frac{d\Phi^s_o}{d\xi} + K_3\xi^{-1/4}\Phi^s_\eta(\xi,0) = 0, \tag{D.5}$$

and the boundary conditions:

$$\begin{aligned} &\eta = 0: \quad \Phi^s = \Phi^s_o(\xi), \quad f^s = f^s_\eta = 0 \\ &\eta = \infty: \quad f^s_\eta = \Phi^s = 0 \\ &\xi = 0: \quad \xi\frac{d\Phi^s_o}{d\xi} = 0 \\ &\xi = \gamma: \quad \Phi^s_o = 1. \end{aligned} \tag{D.6}$$

The first order perturbation solutions $\tilde{f}(\xi,\eta)$, $\hat{f}(\xi,\eta)$, $\tilde{\Phi}(\xi,\eta)$, and $\hat{\Phi}(\xi,\eta)$ etc. can be obtained from the following simultaneous equations:

$$\begin{aligned} &Pr\ \tilde{f}_{\eta\eta\eta} + (1+Pr)(\tilde{\Phi}+\Phi^s) - \frac{4}{3}f^s_\eta\tilde{f}_\eta + f^s_{\eta\eta}\tilde{f} + f^s\tilde{f}_{\eta\eta} \\ &= K_1\xi^{1/2}\hat{f} + \frac{4}{3}\xi(f^s_{\eta\xi}\tilde{f}_\eta - f^s_\xi\tilde{f}_{\eta\eta} + f^s_\eta\tilde{f}_{\eta\xi} - f^s_{\eta\eta}\tilde{f}_\xi) + (1+Pr)\xi\tilde{\Phi} \end{aligned} \tag{D.7}$$

$$\tilde{\Phi}_{\eta\eta} + f^s\tilde{\Phi}_\eta + \Phi^s\tilde{f}_\eta = K_1\xi^{1/2}\hat{\Phi} + \frac{4}{3}\xi(\Phi^s_\xi\tilde{f}_\eta + f^s_\eta\tilde{\Phi}_\xi - \Phi^s_\eta\tilde{f}_\xi - f^s_\xi\tilde{\Phi}_\eta) \tag{D.8}$$

$$K_2\xi\hat{\Phi}_o + \xi\frac{d^2\tilde{\Phi}_o}{d\xi^2} + \frac{d\tilde{\Phi}_o}{d\xi} + K_3\xi^{-1/4}\tilde{\Phi}_\eta(\xi,0) = 0 \tag{D.9}$$

$$\begin{aligned} &Pr\ \hat{f}_{\eta\eta\eta} + (1+Pr)\hat{\Phi} - \frac{4}{3}f^s_\eta\hat{f}_\eta + f^s_{\eta\eta}\hat{f} + f^s\hat{f}_{\eta\eta} \\ &= -K_1\xi^{1/2}\tilde{f}_\eta + \frac{4}{3}\xi(f^s_{\eta\xi}\hat{f}_\eta - f^s_\xi\hat{f}_{\eta\eta} + f^s_\eta\hat{f}_{\eta\xi} - f^s_{\eta\eta}\hat{f}_\xi) \\ &\quad + (1+Pr)\xi\hat{\Phi} \end{aligned} \tag{D.10}$$

$$\hat{\Phi}_{\eta\eta} + \Phi_\eta^s \hat{f} + f^s \hat{\Phi}_\eta = -K_1 \xi^{1/2} \tilde{\Phi} + \frac{4}{3}\xi (\Phi_\xi^s \hat{f}_\eta + f_\eta^s \hat{\Phi}_\xi - \Phi_\eta^s \hat{f}_\xi - f_\xi^s \hat{\Phi}_\eta) \tag{D.11}$$

$$-K_2 \xi \tilde{\Phi} + \xi \frac{d^2 \hat{\Phi}_o}{d\xi^2} + \frac{d\hat{\Phi}_o}{d\xi} + K_3 \xi^{-1/4} \hat{\Phi}_\eta(\xi,0) = 0 \tag{D.12}$$

and the associated boundary conditions:

$$\begin{aligned}
&\eta = 0: \quad \tilde{f} = \hat{f} = \tilde{f}_\eta = \hat{f}_\eta = 0, \quad \tilde{\Phi} = \tilde{\Phi}_o(\xi), \quad \hat{\Phi} = \hat{\Phi}_o(\xi) \\
&\eta = \infty: \quad \tilde{f}_\eta = \hat{f}_\eta = \tilde{\Phi} = \hat{\Phi} = 0 \\
&\xi = 0: \quad \xi \frac{d\tilde{\Phi}_o}{d\xi} = \xi \frac{d\hat{\Phi}_o}{d\xi} = 0 \\
&\xi = \gamma: \quad \tilde{\Phi} = \hat{\Phi} = 0.
\end{aligned} \tag{D.13}$$

Similarly, once the zeroth and the first order perturbation solutions are obtained, the second order corrections can be found from the $(\frac{1}{Fr})^2$-order equations. First, the integration of equations:

$$\begin{aligned}
&Pr\ \bar{f}_{\eta\eta\eta} + (1+Pr)(\bar{\Phi} + \tfrac{1}{2}\tilde{\Phi}) + f^s \bar{f}_{\eta\eta} + f_{\eta\eta}^s \bar{f} - \tfrac{4}{3} f_\eta^s \bar{f}_\eta \\
&\quad + \tfrac{1}{2}(\tilde{f}\tilde{f}_{\eta\eta} + \hat{f}\hat{f}_{\eta\eta}) - \tfrac{1}{3}(\tilde{f}_\eta)^2 - \tfrac{1}{3}(\hat{f}_\eta)^2 \\
&= \xi[(1+Pr)\bar{\Phi} + \tfrac{4}{3}(f_{\eta\xi}^s \bar{f}_\eta + f_\eta^s \bar{f}_{\eta\xi} - f_\xi^s \bar{f}_{\eta\eta} - f_{\eta\eta}^s \bar{f}_\xi) \\
&\quad + \tfrac{2}{3}(\tilde{f}_\eta \tilde{f}_{\eta\xi} + \hat{f}_\eta \hat{f}_{\eta\xi} - \tilde{f}_{\eta\eta}\tilde{f}_\xi - \hat{f}_{\eta\eta}\hat{f}_\xi)],
\end{aligned} \tag{D.14}$$

$$\begin{aligned}
&\bar{\Phi}_{\eta\eta} + f^s \bar{\Phi}_\eta + \Phi_\eta^s \bar{f} + \tfrac{1}{2}(\tilde{\Phi}_\eta \tilde{f} + \hat{\Phi}_\eta \hat{f}) \\
&= \tfrac{4}{3}\xi(f_\eta^s \bar{\Phi}_\xi + \Phi_\xi^s \bar{f}_\eta - f_\xi^s \bar{\Phi}_\eta - \Phi_\eta^s \bar{f}_\xi) \\
&\quad + \tfrac{2}{3}\xi(\tilde{f}_\eta \tilde{\Phi}_\xi + \hat{f}_\eta \hat{\Phi}_\xi - \tilde{\Phi}_\eta \tilde{f}_\xi - \hat{\Phi}_\eta \hat{f}_\xi),
\end{aligned} \tag{D.15}$$

and

$$\frac{d}{d\xi}\left(\xi\frac{d\bar{\Phi}_o}{d\xi}\right) + K_3\xi^{-1/4}\bar{\Phi}_\eta(\xi,0) = 0, \tag{D.16}$$

with the corresponding boundary conditions

$$\begin{aligned}
&\eta = 0: \quad \bar{f} = \bar{f}_\eta = 0, \quad \bar{\Phi} = \bar{\Phi}_o(\xi)\\
&\eta = \infty: \quad \bar{f}_\eta = \bar{\Phi} = 0\\
&\xi = 0: \quad \xi\frac{d\bar{\Phi}_o}{d\xi} = 0\\
&\xi = \gamma: \quad \bar{\Phi}_o = 0
\end{aligned} \tag{D.17}$$

yields solutions $\bar{f}$ and $\bar{\Phi}$, etc.

The second order perturbation solutions $\tilde{\tilde{f}}$, $\tilde{\tilde{\Phi}}$, $\hat{\hat{f}}$, and $\hat{\hat{\Phi}}$ etc. should satisfy the following simultaneous equations:

$$\begin{aligned}
&\mathrm{Pr}\,\tilde{\tilde{f}}_{\eta\eta\eta} - \frac{4}{3}f^s_\eta\tilde{\tilde{f}}_\eta + f^s\tilde{\tilde{f}}_{\eta\eta} + f^s_{\eta\eta}\tilde{\tilde{f}} + \frac{1}{3}(\hat{\tilde{f}}^2_\eta - \tilde{\tilde{f}}^2_\eta) + \frac{1}{2}(\tilde{\tilde{f}}\tilde{\tilde{f}}_{\eta\eta} - \hat{\tilde{f}}\hat{\tilde{f}}_{\eta\eta})\\
&+ (1+\mathrm{Pr})(\tfrac{1}{2}\tilde{\tilde{\Phi}} + \tilde{\tilde{\Phi}})\\
&\quad = 2K_1\xi^{1/2}\hat{\hat{f}}_\eta + \frac{4}{3}\xi[f^s_\eta\tilde{\tilde{f}}_{\eta\xi} - \tilde{\tilde{f}}_{\eta\eta}f^s_\xi + \tilde{\tilde{f}}_\eta f^s_{\eta\xi} - f^s_{\eta\eta}\tilde{\tilde{f}}_\xi\\
&\qquad + \frac{1}{2}(\tilde{f}_\eta\tilde{f}_{\eta\xi} - \tilde{f}_{\eta\eta}\tilde{f}_\xi + \hat{f}_{\eta\eta}\hat{f}_\xi - \hat{f}_\eta\hat{f}_{\eta\xi})] + (1+\mathrm{Pr})\xi\tilde{\tilde{\Phi}},
\end{aligned} \tag{D.18}$$

$$\begin{aligned}
&\tilde{\tilde{\Phi}}_{\eta\eta} + f^s\tilde{\tilde{\Phi}}_\eta + \Phi^s_\eta\tilde{\tilde{f}} + \frac{1}{2}(\tilde{\tilde{f}}\tilde{\tilde{\Phi}}_\eta - \hat{\tilde{f}}\hat{\tilde{\Phi}}_\eta)\\
&\quad = 2K_1\xi^{1/2}\hat{\hat{\Phi}} + \frac{4}{3}\xi[f^s_\eta\tilde{\tilde{\Phi}}_\xi - \tilde{\tilde{\Phi}}_\eta f^s_\xi + \tilde{\tilde{f}}_\eta\Phi^s_\xi - \Phi^s_\eta\tilde{\tilde{f}}_\xi\\
&\qquad + \frac{1}{2}(\tilde{f}_\eta\tilde{\Phi}_\xi - \tilde{\Phi}_\eta\tilde{f}_\xi + \hat{\Phi}_\eta\hat{f}_\xi - \hat{f}_\eta\hat{\Phi}_\xi)],
\end{aligned} \tag{D.19}$$

$$2K_2\xi\hat{\tilde{\Phi}}_o + \frac{d}{d\xi}(\xi\frac{d\tilde{\tilde{\Phi}}_o}{d\xi}) + K_3\xi^{-1/4}\tilde{\tilde{\Phi}}_\eta(\xi,0) = 0 \qquad (D.20)$$

and

$$\Pr \hat{\tilde{f}}_{\eta\eta\eta} - \frac{4}{3}f^s_\eta\hat{\tilde{f}}_\eta + f^s\hat{\tilde{f}}_{\eta\eta} + f^s_{\eta\eta}\hat{\tilde{f}} - \frac{2}{3}\tilde{f}_\eta\hat{f}_\eta + \frac{1}{2}(\hat{f}\tilde{f}_{\eta\eta} + \tilde{f}\hat{f}_{\eta\eta})$$

$$+ (1+\Pr)(\frac{1}{2}\hat{\Phi} + \hat{\tilde{\Phi}})$$

$$= -2K_1\xi^{1/2}\tilde{\tilde{f}} + \frac{4}{3}\xi(f^s_\eta\hat{\tilde{f}}_{\eta\xi} - \hat{\tilde{f}}_{\eta\eta}f^s_\xi + \hat{\tilde{f}}_\eta f^s_{\eta\xi} - f^s_{\eta\eta}\hat{\tilde{f}}_\xi$$

$$+ \frac{1}{2}(\tilde{f}_\eta\hat{f}_{\eta\xi} - \hat{f}_{\eta\eta}\tilde{f}_\xi + \hat{f}_\eta\tilde{f}_{\eta\xi} - \tilde{f}_{\eta\eta}\hat{f}_\xi)] + (1+\Pr)\xi\hat{\tilde{\Phi}}, \qquad (D.21)$$

$$\hat{\tilde{\Phi}}_{\eta\eta} + f^s\hat{\tilde{\Phi}}_\eta + \Phi^s_\eta\hat{\tilde{f}} + \frac{1}{2}(\tilde{f}\hat{\Phi}_\eta + \hat{f}\tilde{\Phi}_\eta)$$

$$= -2K_1\xi^{1/2}\tilde{\tilde{\Phi}} + \frac{4}{3}\xi[f^s_\eta\hat{\tilde{\Phi}}_\xi - \hat{\tilde{\Phi}}_\eta f^s_\xi + \hat{\tilde{f}}_\eta\Phi^s_\xi - \Phi^s_\eta\hat{\tilde{f}}_\xi$$

$$+ \frac{1}{2}(\tilde{f}_\eta\hat{\Phi}_\xi - \hat{\Phi}_\eta\tilde{f}_\xi + \hat{f}_\eta\tilde{\Phi}_\xi - \tilde{\Phi}_\eta\hat{f}_\xi)], \qquad (D.22)$$

$$-2K_2\xi\tilde{\tilde{\Phi}}_o + \frac{d}{d\xi}(\xi\frac{d\hat{\tilde{\Phi}}_o}{d\xi}) + K_3\xi^{-1/4}\hat{\tilde{\Phi}}(\xi,0) = 0, \qquad (D.23)$$

The associated boundary conditions of the above equations are

$$\eta = 0: \quad \tilde{\tilde{f}} = \tilde{\tilde{f}}_\eta = \hat{\tilde{f}} = \hat{\tilde{f}}_\eta = 0, \quad \tilde{\tilde{\Phi}} = \tilde{\tilde{\Phi}}_o, \quad \hat{\tilde{\Phi}} = \hat{\tilde{\Phi}}_o,$$

$$\eta = \infty: \quad \tilde{\tilde{f}}_\eta = \hat{\tilde{f}}_\eta = \tilde{\tilde{\Phi}} = \hat{\tilde{\Phi}} = 0,$$

$$\xi = 0: \quad \xi\frac{d\tilde{\tilde{\Phi}}_o}{d\xi} = \xi\frac{d\hat{\tilde{\Phi}}_o}{d\xi} = 0,$$

$$\xi = \gamma: \quad \tilde{\tilde{\Phi}}_o = \hat{\tilde{\Phi}}_o = 0.$$

It is clear that the time variable has been removed from the problem. As a result, difficulty in predicting accurate initial conditions (at every single point on the

ξ-η surface) to assure fast convergence of the periodic solutions is avoided and excessive computation caused by time-wise iteration is effectively eliminated. In spite of the fact that this approximation technique will inevitably become tedious and less reliable when much higher-order perturbation solutions are required (for the small Froude number cases) its lower-order solutions alone still provide some extremely valuable information and hints in solving the problem for small Froude number (section 3.2.2).

APPENDIX E

A SIMPLE TIME DEPENDENT SOLUTION

When the thermal inertia effect on the phase behavior of solutions is neglected, the Nusselt number (Nu) for laminar free convection around the heated rotating fin, depicted in figure (2.1), can be estimated by a simple engineering approach. At first, the following relation is assumed:

$$Nu \propto Ra_{eff}^{1/4} \tag{E.1}$$

where the effective Rayleigh number, Ra_{eff}, is defined by

$$Ra_{eff} = \frac{\beta g_{eff} \theta_r L^3}{\nu \kappa_f} \tag{E.2}$$

If the streamwise acceleration at a point on the fin surface L/n feet ($n \geq 1$) from the fin tip equals the effective acceleration g_{eff} for the entire fin, then

$$g_{eff} = (R-L/n)\omega^2 + g\cos(\omega t). \tag{E.3}$$

By using $\gamma = L/R$ and $Fr = R\omega^2$, equation (E.3) becomes

$$g_{eff} = (1-\gamma/n)R\omega^2 + g\cos(\omega t) \tag{E.4}$$

or $$g_{eff} = [(1-\gamma/n)Fr + \cos(\omega t)]g. \tag{E.5}$$

Furthermore, combination of equations (E.2) and (E.5) yields

$$Ra_{eff} = \frac{\beta[(1-\gamma/n)Fr + \cos(\omega t)]\, g\theta_r L^3}{\nu\kappa_f} \qquad (E.6)$$

or

$$Ra_{eff} = [(1-\gamma/n)Fr + \cos(\omega t)]\, Ra_s, \qquad (E.7)$$

where

$$Ra_s = \frac{\beta g\theta_r L^3}{\nu\kappa_f} \quad . \qquad (E.8)$$

From equation (E.7), relation (E.1) can be rewritten as

$$Nu \propto [(1-\gamma/n)Fr + \cos(\omega t)]^{1/4} Ra_s^{1/4} \qquad (E.9)$$

or more specifically,

$$Nu = m\,[(1-\gamma/n)Fr + \cos(\omega t)]^{1/4} Ra_s^{1/4} \qquad (E.10)$$

where m is an empirical constant.

The value of m can be estimated by considering the Nusselt number at the fin root for the quasi-steady case of the problem. When the effective acceleration g_{eff} in equation (E.2) is replaced by the streamwise acceleration at the fin root (n=1), equation (E.2) can be used to calculate the associated local Rayleigh number; that is,

$$Ra_r(t) = \frac{\beta\,[(R-L)\omega^2 + g\cos(\omega t)]\,\theta_r L^3}{\nu\kappa_f} \qquad (E.11)$$

Consequently, the local Nusselt number at the fin root can

be expressed by substituting n=1 into equation (E.10); namely

$$Nu_r(t) = m\left[(1-\gamma)Fr + \cos(\omega t)\right]^{1/4} Ra_s^{1/4} . \qquad (E.12)$$

When the problem is in the quasi-steady state, the Froude number (Fr) in equation (E.12) is so large that the $\cos(\omega t)$ term can be neglected. Therefore, equation (E.12) becomes

$$\bar{Nu}^s = m\left[(1-\gamma)Fr\right]^{1/4} Ra_s^{1/4} = m(1-\gamma)^{1/4}(FrRa_s)^{1/4}$$

or
$$\bar{Nu}^s = m(1-\gamma)^{1/4} Ra^{1/4} , \qquad (E.13)$$

where
$$Ra = \frac{\beta R\omega^2 \Theta_r L^3}{\nu K_f} .$$

By using the series expansion:

$$(1-\gamma)^{1/4} = 1 - \frac{1}{4}\gamma - \frac{3}{32}\gamma^2 + \frac{7}{128}\gamma^3 - \ldots$$

$$= 1 - \frac{1}{4}\gamma\left(1+\frac{3}{8}\gamma-\frac{7}{128}\gamma^2+ \ldots\right) ,$$

equation (E.13) is rewritten as

$$\bar{Nu}^s \simeq m\left(1-\frac{b}{4}\gamma\right)Ra^{1/4} , \qquad (E.14)$$

where constant b is used to account for the error of approximation.

It is worth pointing out that equation (E.14) is in the identical form as the empirical equation (4.9):

$$\bar{Nu}^s = (F_1' - F_2'\gamma)Ra^{1/4}, \qquad (4.9)$$

which has obtained independently in section 4.1.3-2 by applying a least-squares curve fitting technique to the quasi-steady-state solutions. Comparison between equations (4.9) and (E.14) suggests that

$$m = F_1' \qquad \text{(E.15)}$$

Values of F_1' are tabulated in Table (4.4) for various levels of parameter C, which represents the degree of coupling between the conduction and convection heat transfer problems.

Once the value of m is known, the time dependent Nusselt number for the rotating fin problem can be determined by equation (E.10) provided that the thermal inertia effect on the total heat transfer rate is negligibly small. For a sample problem of C=0.01, γ=0.1, and Fr=2, Table (4.4) and equation (E.15) yield

$$m = 0.39 \ ,$$

and equation (E.10) becomes

$$Nu = 0.39[2(1-0.1/n) + \cos(\omega t)]^{1/4} Ra_s^{1/4} \qquad \text{(E.16)}$$

If the streamwise acceleration at the middle point (n=2) of the fin surface is chosen as the effective acceleration g_{eff} for the entire fin, the time dependent Nusselt number is then expressed as

$$Nu = 0.39[1.9 + \cos(\omega t)]^{1/4} Ra_s^{1/4} \ . \qquad \text{(E.17)}$$

The reliability of the above approach can be checked as follow. The maximum and minimum values of the Nusselt number, corresponding to t=0 and t=π/ω respectively in equation (E.17), are

$$Nu_{max} = 0.5089\ Ra_s^{1/4}$$

and

$$Nu_{min} = 0.3799\ Ra_s^{1/4}\ ;$$

the ratio between these two extreme values is

$$\frac{Nu_{max}}{Nu_{min}} = 1.340 \qquad \text{(E.18)}$$

The dimensionless total heat transfer rate based on the theoretical solutions for the same example is shown in figure (4.27), where the additional parameters K_1 and K_2 regulating the thermal inertia effect are set to 1 and 100 respectively. The fact that the maximum and minimum values in figure (4.27) also appear at t=0($\alpha=0^o$) and t=π/ω($\alpha=180^o$), indicates a negligible thermal inertia effect on the total heat transfer rate; that is, solutions are in phase with the periodic acceleration gcos(ωt) for this sample problem. Despite the thermal inertia effect, the ratio of the maximum to the minimum total heat transfer rates presented in figure (4.27) is

$$\frac{0.0543}{0.0414} = 1.312 \qquad \text{(E.19)}$$

Now, because the total heat transfer rate is proportional to the Nusselt number, the ratio obtained in (E.19) on the basis of the theoretical solutions can be compared to the ratio estimated in (E.18) by using this practical approach; a difference of 2% is found between these two ratios. This observation suggests that equation (E.10) and Table (4.4) can be used as the practical means to estimate the total heat transfer rate for a heated rotating fin problem.